STUDIES OF GAS-PHASE ION/MOLECULE REACTIONS IN RELATION TO A PROPOSED IONIC MECHANISM OF SOOT FORMATION

BY

FEZA ÖZTÜRK

A DISSERTATION PRESENTED TO THE GRADUATE SCHOOL
OF THE UNIVERSITY OF FLORIDA IN
PARTIAL FULFILLMENT OF THE REQUIREMENTS
FOR THE DEGREE OF DOCTOR OF PHILOSOPHY

UNIVERSITY OF FLORIDA

1988

TO ELIF

ACKNOWLEDGEMENTS

This work is the final product of the efforts and encouragement of many. First, I must thank my colleagues, Bryan Hearn, Dr. Cliff Watson and Dr. Steve Bach, in the Eyler group, including Dr. GÖkhan Baykut and Dr. Mehdi Moini who are no longer with the group, for their help and suggestions. Each one deserves particular thanks for their special efforts and friendship throughout these last years. I have greatly benefitted particularly from their technical experience and skills whenever questions and difficulties arose in the lab.

Next, I wish to acknowledge my research advisor, Dr. John Eyler, whose guidance and encouragement has enabled me to experience the intellectual satisfaction and enjoyment of scientific research. With his research funds, I had the opportunity to spend my time exclusively doing research and attend the annual meetings of the American Society of Mass Spectrometry which provided the best setting for scientific communication. I also would like to mention his editing skills which have always assisted me and had a major role in putting this manuscript to its final form.

I would like to acknowledge Dr. Floyd Wiseman from the Environics Division of Tyndall Air Force Base for his interest and efforts in this research project. His contribution to the work by the kinetic modeling study deserves an important credit for providing a better understanding of experimental results.

Special thanks are extended to Dr. William Weltner, Dr. Robert Hanrahan, Dr. Merle Battiste, Dr. Willis Person and Dr. Charles Proctor for serving as committee members. I particularly wish to thank Dr. Calvin VanderWerf, Dr. Robert Hanrahan, Dr. Kathryn Williams, and Dr. William Weltner for their efforts and willingness to be supportive in every way throughout these long years.

Another special person deserving particular thanks is my friend, Zekiye Onsan. She has been an endless source of encouragement and never failed to give her help whenever needed. I also wish to thank Taghi Alizadeh Yekani for sharing the difficult times with me with patience and sincerity in my earlier years of study.

Finally, there is my five-year old, Elif. She made it worhwhile by just being there for me.

TABLE OF CONTENTS

Abstract of Dissertation Presented to the Graduate School of the University of Florida in Partial Fulfillment of the Requirements for the Degree of Doctor of Philosophy

STUDIES OF GAS-PHASE ION/MOLECULE REACTIONS IN RELATION TO A PROPOSED IONIC MECHANISM OF SOOT FORMATION

By

FEZA ÖZTÜRK

August, 1988

Chairman: John R. Eyler
Major Department: Chemistry

The reactions of small hydrocarbon ions such as $C_3H_3^+$, $C_5H_3^+$, $C_5H_5^+$, and $C_7H_7^+$ with acetylene and diacetylene have been investigated using Fourier Transform Ion Cyclotron Resonance (FTICR) mass spectrometry to provide qualitative and quantitative information about a proposed ionic mechanism of soot formation. Ion/molecule reaction pathways and rate coefficients have been determined for several isomers of each of the ions listed above, formed from a variety of precursors, and reacting with precursors, acetylene and diacetylene. Further understanding of reaction mechanisms of some of the reactions proposed experimentally was obtained from kinetic modeling studies.

All of the small hydrocarbon ions studied reacted with diacetylene extensively while almost no production of larger

ions was observed with acetylene. Linear $C_3H_3^+$ was formed by charge transfer ionization of propargyl iodide using Xe^+, and was found to isomerize to the cyclic form of $C_3H_3^+$ in reactions with both acetylene and diacetylene. The isomerization was shown to take place via a long-lived $C_5H_5^{+*}$ complex by isotope exchange reactions between linear $C_3H_3^+$ and deuterated acetylene. The reaction rate coefficients for the reaction of $C_3H_3^+$ with deuterated acetylene and diacetylene were $(4.5 \pm 1.9) \times 10^{-10}$ cm^3/s and $(1.4 \pm 0.7) \times 10^{-9}$ cm^3/s, respectively.

While different structures could be attributed to $C_3H_3^+$, $C_5H_3^+$, and $C_7H_7^+$ ions produced from different precursors on the basis of reactivity, this could not be done for $C_5H_5^+$ ions, whose reactivity with acetylene and diacetylene was similar within experimental error regardless of precursor. Presence of two structural isomers of $C_5H_3^+$ was determined using different precursors and several structures for these isomers were proposed. The reactive isomer was observed to react with diacetylene with a rate constant of $(5.6 \pm 1.7) \times 10^{-10}$ cm^3/s. Rate coefficients for the ion/molecule reactions of $C_7H_7^+$ were found to be different when it was formed from various precursors, which implied the involvement of different $C_7H_7^+$ structures. All experimental results are discussed in relation to theoretical work involving structures of the ions studied and a proposed ionic route to soot formation.

CHAPTER 1
INTRODUCTION

Soot is a combustion product which has undesirable effects both on human health and on the efficiency of fuel-powered engines due to increased heat transfer to critical engine components. Considering the fact that the use of alternative fuels such as shale or coal-derived gas in the near future would lead to increased soot emissions, search for an effective way to reduce soot has been going on for a long time. The design and development of advanced engines to achieve soot suppression requires a sufficient fundamental understanding of the mechanisms governing soot formation. Soot formation in hydrocarbon flames involves a succession of fast processes that occur within a few milliseconds during the combustion of the hydrocarbon. Although many investigations have been undertaken in relation to the process of soot formation in fuel-rich hydrocarbon flames, understanding of this process is still limited. Experimental techniques such as mass spectrometry (Calcote, 1963; Michaud et al., 1981), laser-light scattering (Kent et al., 1981; D'Alessio et al., 1977), laser induced ionization (Smith and Mallard, 1981), and laser induced fluorescence (DiLorenzo et al., 1981) have

been used to study the molecular species and particles in flames.

Soot collected from flames consists of chainlike aggregates of spherical units having diameters of 10-50 nm with a carbon/hydrogen atom ratio in the range 8:1-12:1 (Calcote, 1981). Three distinct steps of soot formation have been recognized over many years of research (Calcote, 1981):

1. Nucleation- a phase change from molecular species where chemical reactions dominate to incipient soot particles where physical processes dominate;
2. Growth to spherical particles of 10-50 nm in diameter; and
3. Aggregation or agglomeration of the spherical units to form chains.

Among these, the first step, nucleation, is the least understood in the process. Although many diverse theories have been put forward to explain the nucleation process, only two of these have received quantitative support:

1. Mechanisms involving neutral and free radical species; and
2. Ionic mechanisms.

Neutral and Free Radical Mechanisms. A large number of neutral and free radical mechanisms have been proposed to describe the transition from molecular species to soot

(Palmer and Cullis, 1965; Lahaye and Prado, 1978; Gaydon and Wolfhard, 1979).

One of the proposed paths involves polyacetylenes where acetylene reacts to form higher species (Bonne et al., 1965).

$$C_2H_2 \xrightarrow{C_2H_2} C_4H_2 \xrightarrow{-H} C_4H_3 \ (+H) \xrightarrow{C_2H_2} C_6H_2 \xrightarrow{-H} C_6H_3 \ (+H_2) \xrightarrow{C_2H_2} C_8H_2 \xrightarrow{-H} C_8H_3 \ (+H_2)$$

It was suggested that the continuation of this series leads to larger radicals which further react with each other and with higher polyacetylenes forming even larger molecules. However, because this mechanism leads to formation of a giant chain molecule instead of a polycyclic carbon structure, it was not accepted as being responsible for soot formation (Homann, 1967). To account for the problem of ring formation, Homann and Wagner (1967, 1968) suggested that radicals such as C_2H attack the polyacetylenic species forming side chains which lead to branched polymerization, and presumably ring closures. The experimental support of this scheme comes from the observation that in the oxidation region of the flame, the concentration of polyacetylenes decreases while that of the polycyclic aromatics increases. But the growth of polyacetylenes was considered too slow by Calcote (1981), to

account for the rapid formation of soot particles. Furthermore, as pointed out by Bonne et al. (1965), Thomas (1965) and Cullis (1976), the rearrangement of a polyacetylene to an aromatic graphite-like structure would also be a slow process.

Another hypothesis proposed by Glassman (1980) emphasized the importance of strongly conjugated molecules such as butadiene in the formation of ring structures with side chains to which butadiene-type molecules keep adding. This mechanism did not receive much support on the basis of concentration profiles in which the butadiene concentration is observed to fall very rapidly even before the initiation of soot formation (Calcote,1981).

Some models considered C_2, C_2H and C_3 radicals as initial nuclei for soot formation which undergo condensation reactions with each other or with acetylene (Jensen, 1974; Smith, 1940; Carbannes, 1956). The main objection to these mechanisms based on C_2 and C_3 condensation reactions was the presence of a very strong C_2 radiation in rich cyanogen-oxygen flames which do not form soot.

Finally, direct condensation of aromatic rings was proposed as being the most favored thermodynamic path to soot formation (Bonne et al., 1965; Graham et al., 1975; Stein, 1978). However, by a detailed analysis of the concentration and the flux profiles of the species, Bittner and Howard (1981a, 1981b) were able to show that soot is

produced via nonaromatic hydrocarbon intermediates rather than via intact aromatic rings. But after a consideration of many species, only a few intermediates were found to favor the rearrangement to a ring structure over other decomposition channels.

To conclude the discussion above, it is clear that all the proposed neutral species mechanisms for soot formation have serious problems with the nucleation step, and thus none can be considered completely satisfactory in understanding the soot formation process. Particularly it is difficult in any of the proposed neutral schemes to produce small cyclic and polycyclic species with a sufficiently high rate to model the quite rapid soot formation seen in flames. Recently, however, a neutral/radical soot formation model has been proposed which contains many steps and incorporates quite recently obtained shock tube kinetic data (Frenklach et al., 1985). This model is capable of yielding small ring compounds at a higher rate than previously suggested radical mechanisms, although there is some question as to the correct rate constant for one or two of the crucial steps in formation of the first ring.

Ionic Mechanisms. A number of experimental observations in flames have led to a consideration of the

importance of ions in soot formation. Such observations in flames include (Olson and Calcote, 1981a; Calcote, 1981):

1. Presence of a unit charge on soot particles;
2. A positive correlation between the growth of large ions and the appearance of soot;
3. The increase both in the concentration of large ions and the onset of soot formation by the addition of electrophilic molecules;
4. Identical location for the peak concentrations of molecular ions and soot precursors;
5. Production of larger particles by an increase in the residence time of the positive ions; and
6. High ion concentrations in hydrocarbon pyrolysis.

As a consequence of the above observations, several ionic mechanisms have been suggested (for references, see Calcote, 1981). The postulated general growth of soot particles from primary ions is shown in Figure 1.1. Calcote (1962) proposed the chemiionization reactions (1.1) and (1.2) for the formation of primary ions:

$$CH + O \text{ ----> } CHO^+ + e^- \qquad (1.1)$$

$$CH^* + C_2H_2 \text{ ----> } C_3H_3^+ + e- \qquad (1.2)$$

The $C_3H_3^+$ ion is the dominant ion observed in fuel-rich flames (Knewstubb and Sugden, 1959; Goodings et al., 1979; Olson and Calcote, 1981b; Michaud et al., 1981) and its

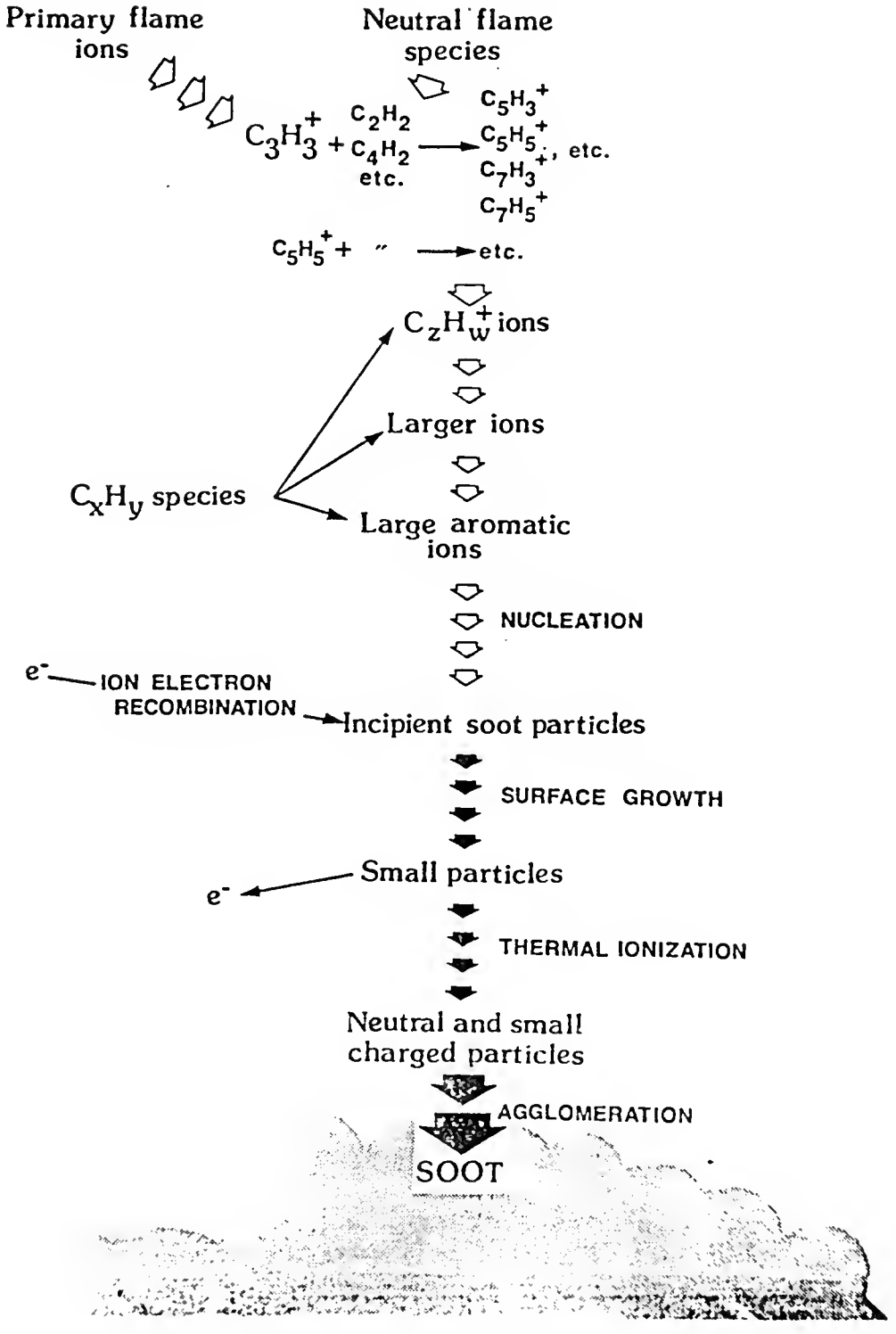

Figure 1-1. Growth of Soot Particles from Primary Molecular Species.

concentration falls very rapidly at the critical equivalence ratio of soot formation where the concentration of the larger ions starts to increase (see Figure 1.2) (Calcote, 1981). Unfortunately, the mechanism of $C_3H_3^+$ formation is still not clear. An alternative mechanism (Calcote, 1972) for $C_3H_3^+$ formation is shown by reactions (1.3) and (1.4):

$$CHO^+ + C_2H_2O \text{ ----> } C_2H_3O^+ + CO \qquad (1.3)$$

$$C_2H_3O^+ + C_2H_2 \text{ ----> } C_3H_3^+ + CH_2O \qquad (1.4)$$

Reaction (1.5) is postulated (Calcote, 1972) to account for the dominant H_3O^+ observed in near stoichiometric and lean flames:

$$CHO^+ + H_2O \text{ ----> } H_3O^+ + CO \qquad (1.5)$$

The $C_2H_3^+$ ion was also considered as a possible nucleating center for soot formation in flames and its formation is shown by reaction (1.6) as proposed by Vinckier et al. (1977).

$$CHO^+ + C_2H_2 \text{ ----> } C_2H_3^+ + CO \qquad (1.6)$$

The primary ions mentioned above are proposed to react with C_xH_y molecules by fast ion/molecule reactions (Calcote,

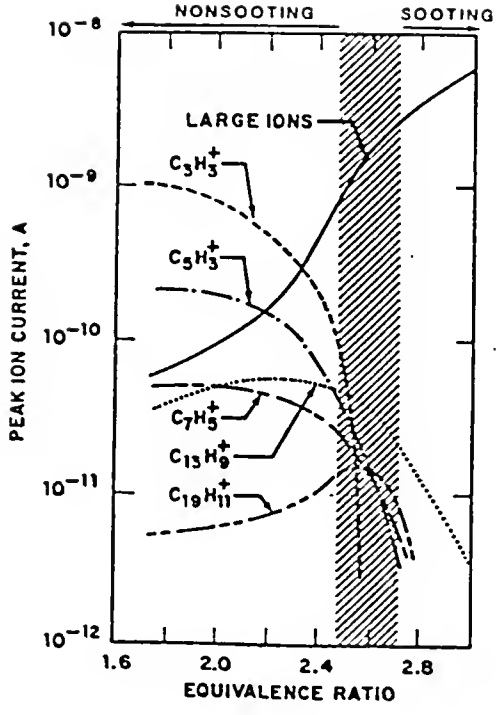

Figure 1.2. Effect of Equivalence Ratio on Peak Ion Currents for 2.0 kPa Acetylene-Oxygen Flames. The shaded area indicates the minimum equivalence ratio for soot formation.

1981; Olson and Calcote, 1981a). The typical set of reactions for $C_3H_3^+$ are shown below:

$$C_3H_3^+ + C_2H_2 \longrightarrow C_5H_3^+ + H_2 \quad (1.7)$$

$$C_3H_3^+ + C_2H_2 \longrightarrow C_5H_5^+ \quad (1.8)$$

$$C_3H_3^+ + C_2H \longrightarrow C_5H_3^+ + H \quad (1.9)$$

$$C_3H_3^+ + C_4H_2 \longrightarrow C_5H_3^+ + C_2H_2 \quad (1.10)$$

$$C_3H_3^+ + C_4H_2 \longrightarrow C_7H_5^+ \quad (1.11)$$

The next step is the further addition of neutral building blocks, acetylene and diacetylene to the product ions producing larger ions with increased C:H ratio. Following are a few reactions representative of this step.

$$C_5H_3^+ + C_2H_2 \longrightarrow C_7H_5^+ \quad (1.12)$$

$$C_5H_3^+ + C_4H_2 \longrightarrow C_9H_5^+ \quad (1.13)$$

$$C_7H_5^+ + C_4H_2 \longrightarrow C_9H_5^+ + C_2H_2 \quad (1.14)$$

This series of reactions is suggested to lead to the formation of polycyclic structures such as $C_{13}H_9^+$ and $C_{19}H_{11}^+$.

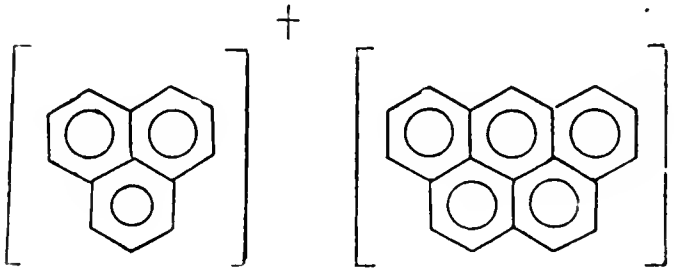

$C_{13}H_9^+$ $C_{19}H_{11}^+$

The problem of rearrangement of linear structures to polycyclic structures encountered in the neutral mechanism is overcome in the ionic mechanism because of the general observation that gaseous ions usually rearrange upon formation to their most stable structure (Calcote, 1981).

Michaud et al. (1981) have made an alternate suggestion that direct reactions of $C_3H_3^+$ with aromatic neutrals such as benzene, toluene, naphthalene, methylnaphthalenes, and indene may be more important in forming polycyclic ions than sequential reactions involving acetylene and diacetylene. In fact, recent ion cyclotron resonance (ICR) studies of reactions of $C_3H_3^+$ with aromatic neutrals showed (Baykut et al., 1986) that these reactions are fast enough to be considered as possible bypass channels in ionic soot formation pathways.

The main objection to the ionic mechanism is the lower concentration of ions in flames compared to that of neutral species. Figure 1.3 (Calcote, 1981) shows the concentration profiles of primary neutrals and ions observed in flames as a function of distance above the burner. One of the most important features of the figure is that the soot concentration is lower than that of the large positive ions which implies that there are probably enough of these large ions to produce the observed levels of soot. Several orders of magnitude higher concentrations of neutral species compared to those of ions in flames can be explained as a

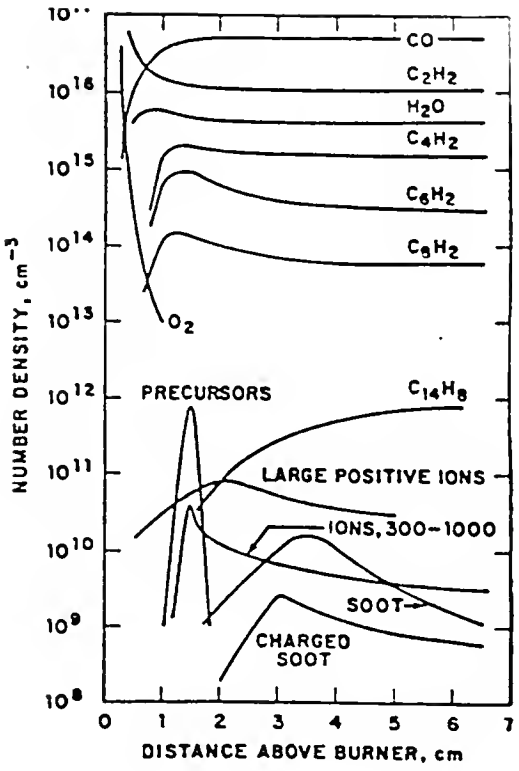

Figure 1.3. Number Densities of Neutral and Ionic Species Found within Flames.

requirement for the ion/molecule reactions to proceed fast enough to account for the rapid formation of soot.

In this study, the reactions of primary ions with flame neutrals have been investigated to identify different reactant ion structures, reaction products and mechanisms. One of the goals of this study was to determine how fast these ion/molecule reactions proceed under laboratory conditions, which hopefully leads to a better understanding of the complex phenomena occurring under flame conditions. Fourier Transform Ion Cyclotron Resonance (FTICR) mass spectrometry, used in this study, is well suited to investigate ion/molecule reactions due to its inherent qualities which differ from other mass spectrometers. These qualities include very clean isolation of the mass of interest from a complicated reaction mixture and accurate rate constant measurements along with reaction mechanism and branching ratio studies. The basics of this technique are discussed in Chapter 2 along with an explanation of the determination of some experimental pressure measurement parameters such as Baratron factors and the system factor inherent to the instrument. The use of FTICR mass spectrometry for studying ion/molecule reactions is discussed in Chapter 3 along with some theoretical models developed for ion-molecule reactions. The main body of the experimental work, reported in Chapters 4-7, deals with proposed nucleation steps of the ionic mechanism of soot

formation. An overall conclusion of the experimental results is included in Chapter 8.

CHAPTER 2
INSTRUMENTATION

Fourier Transform Ion Cyclotron Resonance (FTICR) Mass Spectrometry was introduced in the mid-1970s by Comisarow and Marshall (1974a, 1974b, 1974c, 1975). It involves the application of Fourier multiplex concepts (Griffiths, 1978; Marshall, 1982) to ICR mass spectrometry. High speed, high sensitivity, computerization, ultra-high mass resolution, and wide mass range are some of the advantages of Fourier Transform over continuous-wave spectrometry (Marshall, 1985). Basic principles and the vast applications of this relative newcomer to mass spectrometry are summarized in several recent review articles (Johlman et al., 1983; Gross and Rempel, 1984; Comisarow, 1985; Marshall, 1985; Baykut and Eyler, 1986; Laude et al.,1986). In this chapter, the basic theory of operation of ICR which led to the concepts and development of the FTICR technique will first be discussed. Following that is a description of the instrument along with typical experimental parameters and the general sequence of operation.

Theory. An ion of charge, q, moving at velocity, v when put in a uniform magnetic field, B, is subject to the Lorentz force,

$$\vec{F} = m\vec{a} = q\,(\vec{v} \times \vec{B}) \qquad (2.1)$$

which acts perpendicular to the direction of ion motion. Under the influence of this force, the ion follows a helical path (Lawrence and Livingston, 1932) which, when projected into a plane perpendicular to the magnetic field gives a circle with a radius, r proportional to the velocity of the ion, as shown in Figure 2.1. Substitution of the centripetal acceleration in terms of angular frequency, ω, into equation (2.1) gives

$$|\vec{F}| = m|\vec{a}| = mv^2/r = mr\omega^2 = q\omega rB \qquad (2.2)$$

and

$$\omega = qB/m \text{ (mks units)} \qquad (2.3)$$

which relates the ion's characteristic cyclotron frequency to its q/m (charge/mass). Equation (2.3) is called the cyclotron equation and provides the basic principle of mass measurement in terms of cyclotron frequency in the ICR mass spectrometer. For a magnetic field of 3.0 Tesla, singly charged ions with masses in the range of 18-5000 a.m.u. have cyclotron frequencies in the radiofrequency range (10 kHz-2.6 MHz), within which frequency can be measured with high precision.

Operation. A schematic representation of the commercial Nicolet FTMS-1000 mass spectrometer with a superconducting solenoid magnet (3 Tesla) is shown in Figure

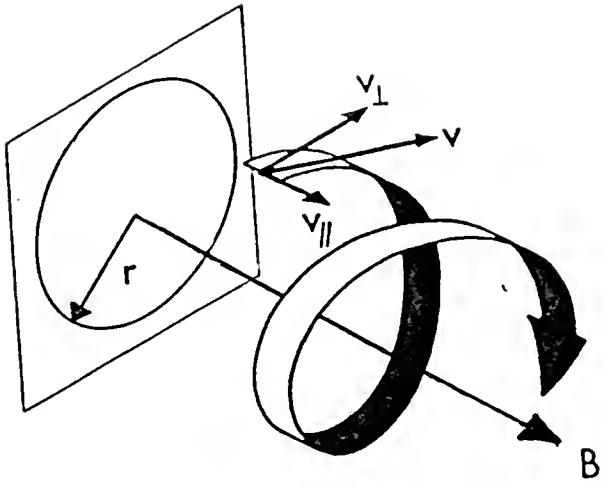

Figure 2.1. Motion of an Ion with Initial Velocity v in a Magnetic Field B.

2.2. All data acquisition and processing and the selection of various experimental parameters (except emission current) are under computer control. Figure 2.3 shows a simplified block diagram of an FTICR mass spectrometer. The simplicity of operation results from the ability to form, excite, react and detect ions in the same 1-inch cubic stainless steel cell shown in Figure 2.4. This analyzer cell is located in the center of a vacuum chamber which passes through the bore of the magnet. The background pressure of 10^{-9} torr is achieved by the use of a four-inch diameter oil diffusion pump and by baking out the system at 250°C for several hours each night.

An inlet system which is evacuated with a three-inch diameter diffusion pump permits the introduction of gas and liquid samples into the high vacuum through precision leak valves. The liquid samples are used after multiple freeze-pump-thaw cycles to remove non-condensible gases. A solids insertion probe is used for the introduction of solid samples into the vacuum chamber and can be heated up to 250°C to promote sublimation of the solid.

Ion formation is typically achieved in 5 ms by collisions of electrons accelerated to 10-70 eV with neutrals leaked into the vacuum chamber. The number of ions is controlled by monitoring the emission current, measured by means of an electron collector located behind the trap plate opposite to the filament. When ions are formed, they

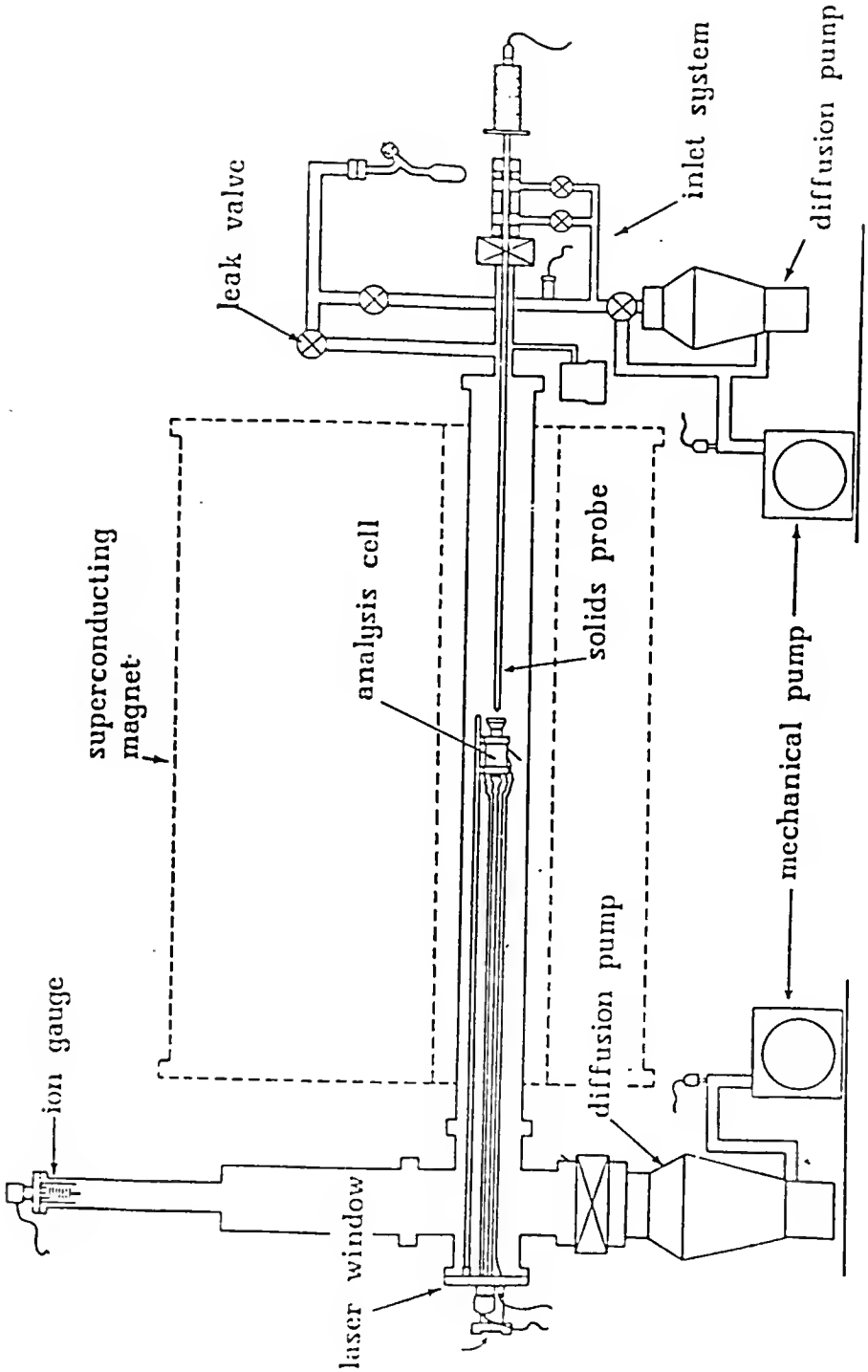

Figure 2.2. Schematic Diagram of FTICR-1000 Mass Spectrometer.

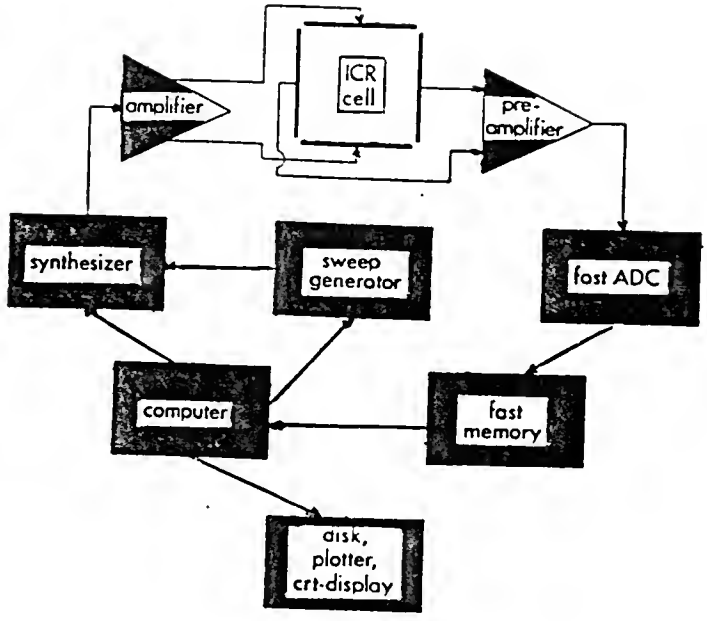

Figure 2.3. Simplified Block Diagram of an FTICR Mass Spectrometer.

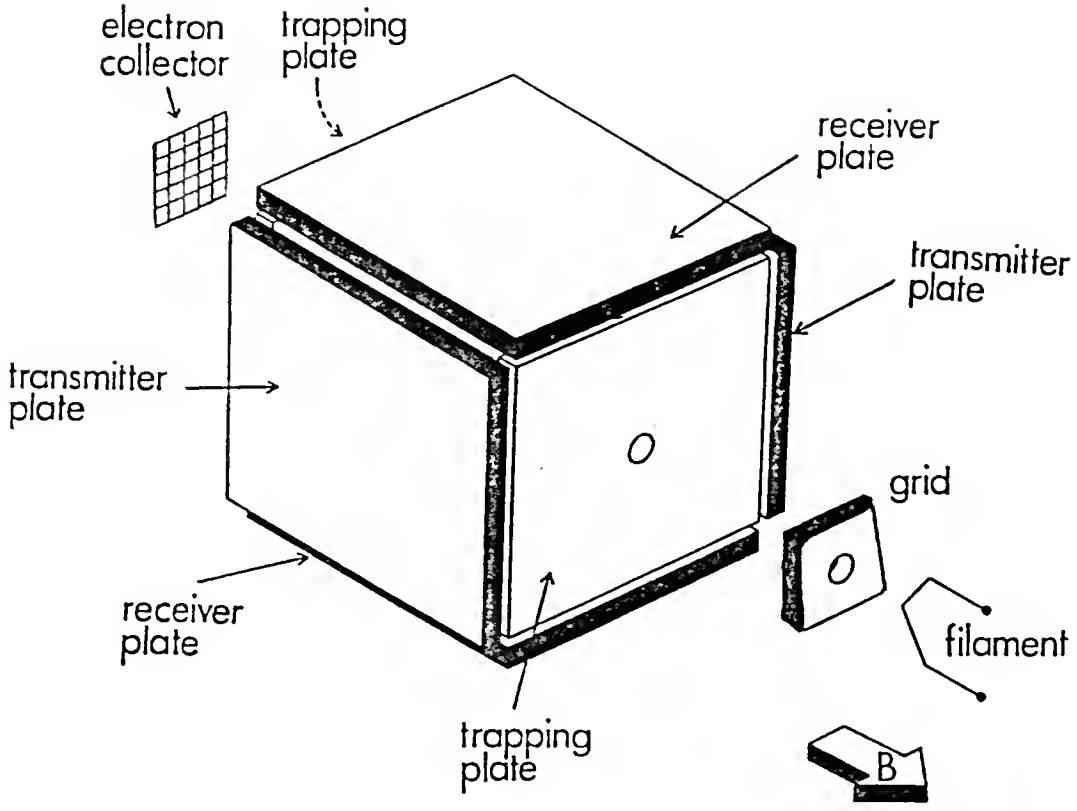

Figure 2.4. Cubic FTICR Cell.

start cyclotron motion at their characteristic frequency with a random phase. The trapping plates shown in Figure 2.4 constrain the ion motion in the direction parallel to magnetic field lines. Positive and negative ions are trapped by the application of, typically, positive and negative 1 volt potentials to the trapping plates, respectively.

To detect the ions, a fast sweep of oscillating voltage in the radiofrequency range is applied to the transmitter plates shown in Figure 2.4. Ions absorb energy at their cyclotron frequency and are driven into coherent motion with a larger radius, thus inducing an image current oscillating at the frequency of their cyclotron motion on the receiver plates (see Figure 2.5). The image current is amplified, digitized and stored in the computer's memory as a time-domain signal which contains the superimposed frequency information of all the ions with different masses in the analyzer cell. A fast Fourier Transform (Cooley and Tukey, 1965) is applied to the time-domain data to produce the frequency-domain spectrum which can be plotted in terms of the ion masses. Figure 2.6a shows a time-domain spectrum of two superimposed sine waves of frequencies ω_1 and ω_2. The decay of the signal results from the dephasing of ions due to collisions with the neutral molecules. Fourier transformation of this spectrum gives the mass-domain spectrum shown in Figure 2.6b. In this procedure, the lowest mass detected is limited by the sampling frequency of

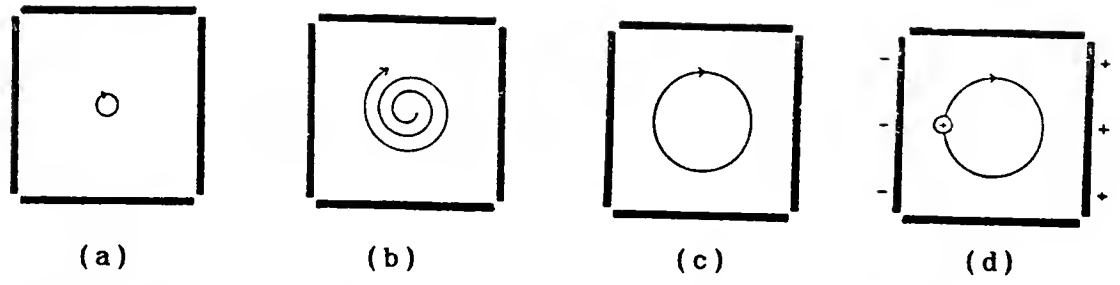

Figure 2.5. Excitation and Detection of Ion Motion. (a) Ion motion in magnetic field only, (b) motion during radio-frequency pulse applied to the transmitter plates, (c) larger radius of ion motion after excitation, and (d) generation of an image current in the receiver plates by a rotating ion "clump".

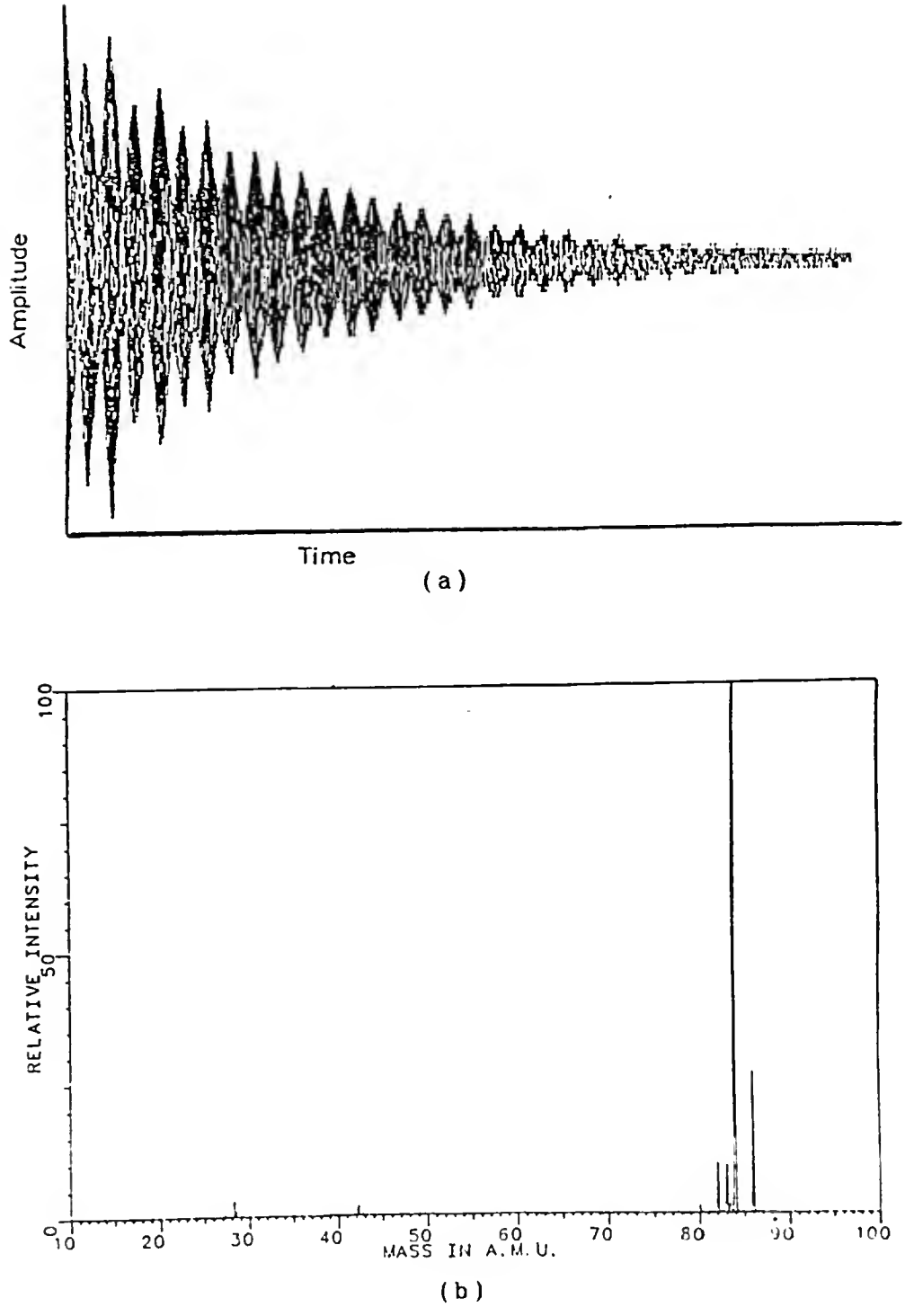

Figure 2.6. Ion Detection by Fourier Transform. (a) Time-domain spectrum (Abscissa is time; ordinate is ion signal). (b) Frequency-Domain Spectrum after Fast Fourier Transform of the time-domain data (Abscissa is frequency; ordinate is ion signal).

the analog-to-digital converter, which should be twice the signal frequency according to the Nyquist criterion. Since the highest cyclotron frequency detected is one-half the ADC frequency, for a magnetic field of 3 Tesla used in this work, the singly charged ion mass corresponding to this frequency is 18 a.m.u., which sets the low mass limit.

A typical experimental sequence is shown in Figure 2.7. Ions can be manipulated in various ways between the formation and the excitation pulses. Ion ejection is used to clean the cell of all ions except one of interest. Ions are ejected by the same principle as excitation. The only difference is that a higher amplitute of excitation voltage is used. In this way ions achieve large enough radii to strike the cell walls and be neutralized. Application of either a single ejection pulse at a single cyclotron frequency or a swept pulse covering a range of frequencies is determined according to the user's purpose.

After selection of the ion of interest, different kinds of ion chemistry can be performed. Among these, ion/molecule reactions, collisionally activated dissociation, and photodissociation are the most commonly used processes in characterization of ion structures. Since the number of stages of ion ejection and manipulation is not limited by hardware or software, $(MS)^n$ (multiple stages of mass selection and manipulation) experiments can be performed by repeating the same processes for the various generations of

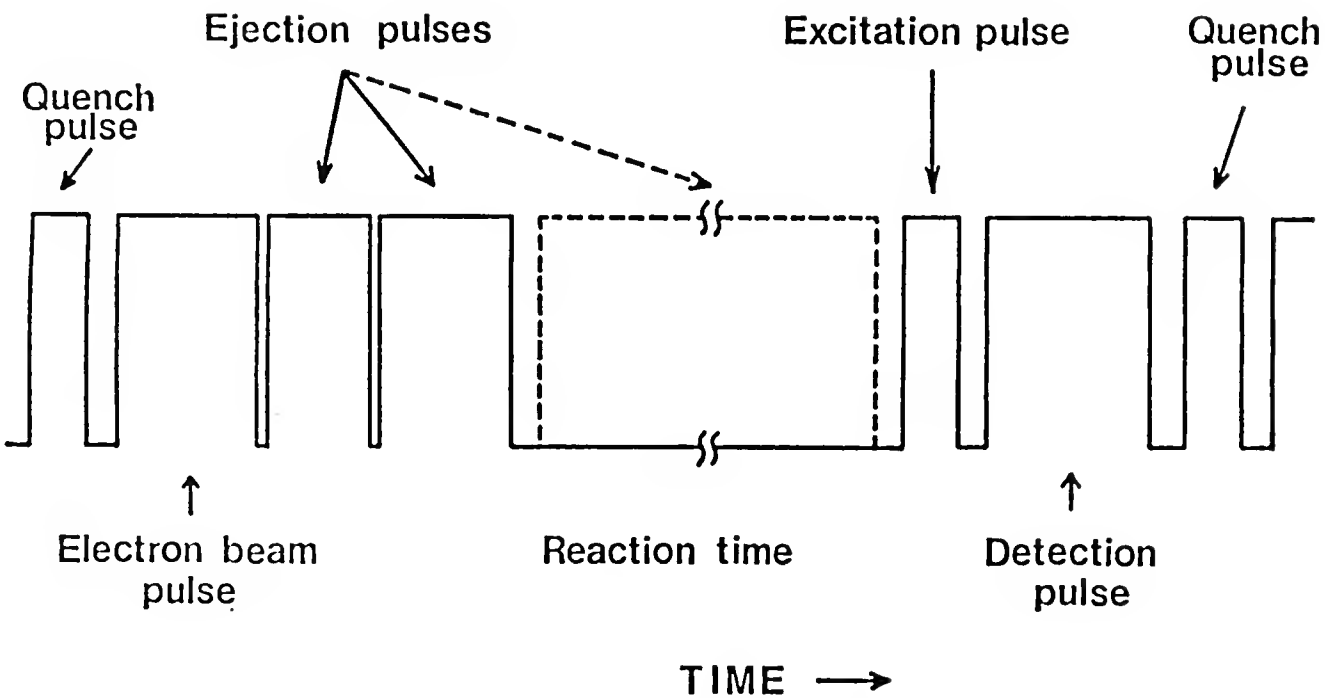

Figure 2.7. A Typical Experimental Sequence in the FTICR Cell.

offspring ions. Laser desorption of solid samples and laser ionization are other techniques used in conjuction with FTICR.

Experimental Parameters. In this study, the FTICR technique was used mainly to determine ion/molecule reaction rates and mechanisms. Ion formation was accomplished by dissociative ionization using various charge transfer agents instead of electron impact ionization, in order to form the ions with well-defined internal energies. Reaction pathways were delineated by using the ejection capabilities of FTICR which make it possible to eject one ion from a complicated reaction mixture to determine its contribution to the mass spectrum of all the other ions.

Reaction rate coefficients were determined by monitoring the intensity of the reactant ion as a function of time (typically for at least 2s) after ejection of all other ions from the analyzer cell. Neutral gas pressures were measured with an ionizing gauge. Ionization gauge readings were then corrected by constructing calibration curves of ionization gauge vs. capacitance manometer (MKS-Baratron) readings in the 1×10^{-6} to 1×10^{-4} Torr range. In order to correct for the fact that the ionization gauge and capacitance manometer were located at different points on the vacuum system, somewhat removed from the FTICR analyzer cell, a correction factor was required. This was

obtained by determining the rate coefficient of a well-studied reaction ($C_2H_4^+ + C_2H_4$ ----> products), where the ionization gauge pressure readings were corrected by using the capacitance manometer. This experimentally determined rate coefficient was then compared with the average of published values, $k_{av} = (1.0 \pm 0.3) \times 10^{-9}$ cm^3/s (Herod and Harrison, 1970; Gross and Norbeck, 1971; Sieck and Ausloos, 1972; Warneck, 1972; Le Breton et al., 1975) and the ratio of the measured value to the published, which was 0.3 ± 0.1, was used as a correction factor. This factor was used in calculating the absolute rate coefficients reported in this work. The large uncertainities (95% confidence limits) reported for the correction factor and rate coefficients calculated using it are primarily due to the wide range of reported values for the $C_2H_4^+ + C_2H_4$ reaction used to determine the correction factor. The even more widely studied "standard" calibration reaction of CH_4^+ with CH_4 could not be employed because of the lowest accessible mass limit in the FTICR instrument mentioned earlier. All calculations of rate coefficients and 95% confidence limits were performed with a menu-driven Fortran computer program (given in Appendix I).

CHAPTER 3
ION/MOLECULE REACTIONS

In this chapter the various theoretical models which have been developed for ion/molecule reactions will first be discussed. Then follows a description of practical aspects of studying such reactions by the use of FTICR mass spectrometry.

Theory of Ion/Molecule Reactions

A number of both classical and statistical ion/molecule collision theories have been introduced during the last two decades to provide an adequate model explaining the experimental observations of ion/molecule reactions. Classical treatments mainly include the pure polarization (ion-induced dipole) theory first developed by Langevin (1905) and the various ion-dipole theories.

A. Pure Polarization Theory. Detailed discussions of this model can be found in a number of articles (Gioumousis and Stevenson, 1958; McDaniel, 1964; Futrell and Tiernan, 1968; Henglein, 1970). Langevin's model assumes that the neutral has no permanent dipole moment, and that both the ion and the neutral molecule are point particles with no internal energy. The classical charge-induced dipole potential at an ion-molecule separation r is

$$V(r) = - \alpha q^2/2r^4 \qquad (3.1)$$

where q is the charge on the ion and α is the polarizability of the neutral. Since the energy of relative rotation, $E_{rot}(r)$ of the particles is associated with an outwardly directed centrifugal force, the effective potential of the ion/molecule system can be given by

$$V_{eff}(r) = V(r) + E_{rot}(r) \qquad (3.2)$$

or

$$V_{eff}(r) = -(q^2\alpha/2r^4) + (L^2/2\mu r^2) \qquad (3.3)$$

where L is the classical orbiting angular momentum of the two particles and μ is the reduced mass. The total relative energy of the system is a sum of the translational energy and the effective potential energy.

$$E_r = E_{trans}(r) + V_{eff}(r) \qquad (3.4)$$

Figure 3.1 shows a plot of $V_{eff}(r)$ versus r at constant E_r for three different values of the impact parameter, b. When b=0, since there is no centrifugal potential energy, the effective potential is attractive at all ion/molecule separations leading to a collision between two particles. For b > 0, there is a critical value of the impact

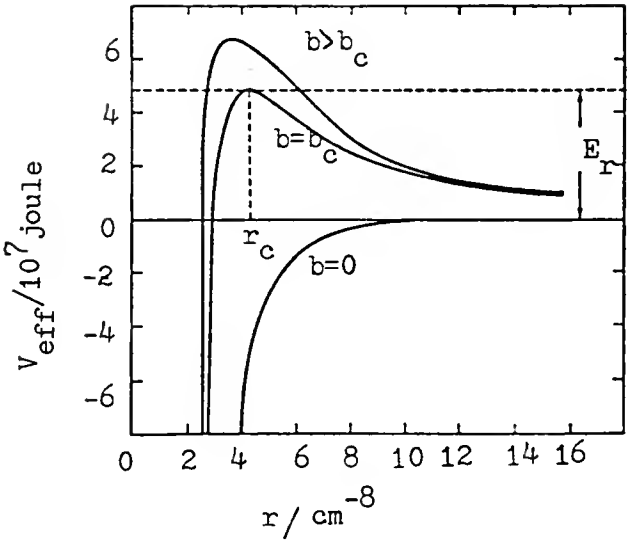

Figure 3.1. Plot of V_{eff} vs r from Equation (3.3) for N_2 Colliding with N_2.

paramater, b_c at which the particles orbit around the scattering center with a constant radius, r_c. At this ion/molecule separation, there is no contribution from the attractive potential and V_{eff} is equal to centrifugal energy which creates a "centrifugal barrier" to a capture collision. For all $b < b_c$, a capture collision occurs, whereas it is precluded by the centrifugal barrier for all $b > b_c$.

Capture cross section is defined as the area of a circle with radius b_c perpendicular to the line of collision at infinite ion/molecule separation and a capture collision occurs for all the ions that pass through the circle when approaching the neutral molecule. Capture cross section can be derived for a given relative velocity in terms of the charge of ion, q, polarizability of the neutral, α, and the reduced mass, μ as shown in equation (3.5).

$$\sigma_c(v) = 2\pi q(\alpha/\mu)^{1/2}/v \qquad (3.5)$$

Thus the collision rate constant is given by

$$k_c = v\sigma_c = 2\pi q(\alpha/\mu)^{1/2} \qquad (3.6)$$

The rate coefficients obtained from this expression are generally good for some simple low energy ion/molecule

reactions but underestimate the rate constants of most ion/polar molecule collisions.

B. Ion/Dipole Theory. Several different models were proposed to describe the theory of ion/dipole collisions. Among these are "The Locked Dipole Approximation" (Moran and Hamill, 1963), "The Frozen Rotor Approximation" (Dugan and Magee, 1966), "Ion/Dipole Trajectory Calculations" (Dugan and Magee, 1967), "The Average Dipole Orientation (ADO) Theory" (Bowers and Laudenslager, 1972), "Barker-Ridge (BR) Model" (Barker and Ridge, 1976) and "The Average Dipole Orientation Theory with Conservation of Angular Momentum (AADO)" (Su et al., 1978).

Both the "Locked Dipole" and "The Frozen Rotor" approximations assume that the polar molecule is fixed at angle θ (θ = 0 for the "Locked Dipole" model) with respect to the line of centers of the collision. The resulting rate constants provide upper limits to the ion/dipole capture collisions and overestimate the dipole effect (Su and Bowers, 1973).

Ion/Dipole Trajectory Calculations provide numerical solutions for the equations of motion for the collision of an ion with a rotating polar molecule. As a result of these calculations, the numerical capture cross section was found to depend on relative translational energy. When compared with experimental results, this numerical approach seems to

be useful in the investigation of nonreactive ion/dipole phenomena such as energy transfer, but does not give a good estimation of capture collision rates.

ADO theory assumes that there exists an overall average orientation of the dipole with respect to the ion and the extent of locking of the dipole increases as the dipole moment of the molecule increases. Su and Bowers (1973) have parametrized the ADO theory to calculate the ADO capture rate constants. The results indicate that the ADO theory gives the best prediction of rate constants in most cases with respect to the other theories.

BR theory uses a simple statistical approach to study the ion/dipole collisions and is based on the Langevin model. BR results overestimate the dipole effect by almost a factor of 2 for charge transfer and proton transfer as well as momentum transfer reactions.

Su et al. (1978) modified the ADO theory by the application of the conservation of angular momentum with the assumption that there is no net angular momentum transfer between the rotating molecule and the ion/molecule orbital motion. This modified version of ADO theory is termed the AADO theory. The capture rate constants obtained from AADO model are larger than the ADO predictions, providing better agreement between theory and experiment.

C. Ion/Quadrupole Theory. This theory makes theoretical predictions of ion/quadrupole interactions for the molecules having D_∞ symmetries. Similar to ADO theory, the average quadrupole orientation theory, AQO, was developed by Su and Bowers (1975). This model predicts significant quadrupole effects for molecules with high quadrupole moments and improves the agreement between theory and experiment.

Statistical Treatments of ion/molecule reactions include the statistical theory and the orbiting transition state theory. Statistical Theory is divided into three categories according to the type of reaction dynamics as shown in Figure 3.2.

A. Transition State Theory. This theory is developed for direct bimolecular reactions (Pelzer and Wigner, 1932; Evans and Polanyi, 1935; Eyring, 1935). This method was later refined by Pechukas and McLafferty (1972) and by Miller (1974). The microcanonical rate constant is given by

$$k(E) = W^{\dagger}(E-E_0)/h\rho(E) \qquad (3.7)$$

where $W^{\dagger}(E-E_0)$ is the total sum of states (vibrational and rotational) of the transition state complex with nonfixed energy less than or equal to $E-E_0$, where E is the total

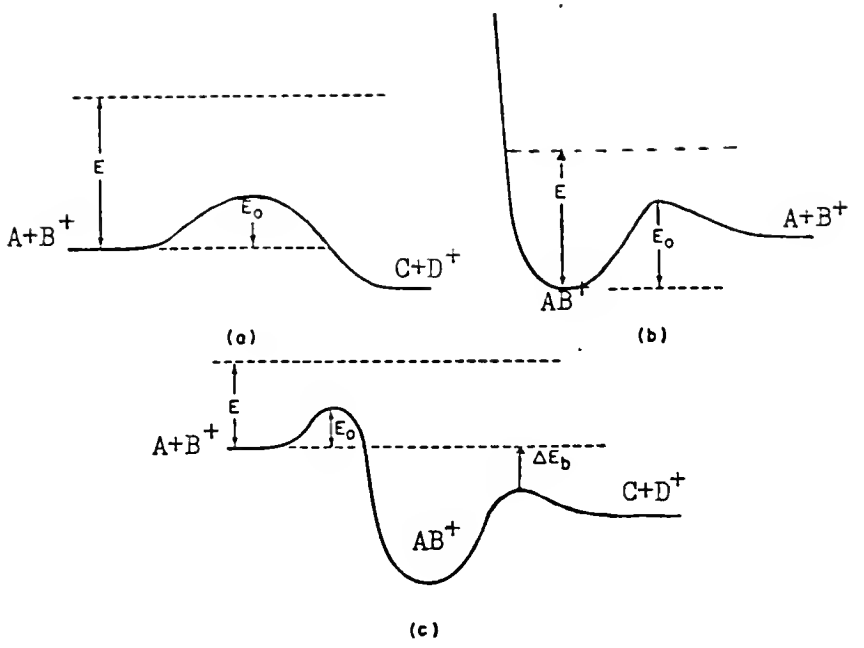

Figure 3.2. Schematic Potential Surfaces for Various Ion/Molecule Reactions. (a) Direct bimolecular, (b) Unimolecular, and (c) Complex formation reactions.

system energy, and $\rho(E)$ is the total density of states of the reactants. For a given potential surface, transition state theory provides a rigorous upper limit to the true rate constant.

B. Unimolecular Theory. This theory involves two approaches, RRKM and QET (quasi-equilibrium theory) which arrive at similar results for the unimolecular reaction of an isolated energized molecule. These methods were developed independently by Marcus and Rice (1951) using the assumptions of transition state theory and by Rosenstock et al. (1952) using the quasi-equilibrium hypothesis. Experimental evidence suggests that most unimolecular systems appear to behave according to the quasi-equilibrium hypothesis which assumes a random distribution of excess energy independent of the pattern of initial energization prior to unimolecular decomposition.

C. Complex Formation Theory. This theory involves the statistical treatment of reactions which form a long-lived complex assuming quasi-equilibrium for the intermediate complex (Keck, 1958; Light, 1967). Thus, the rate constant for decomposition to each available channel is assumed to be proportional to the flux through the transition state for that channel.

The Orbiting Transition State Theory is developed to overcome the problem of determining the energy distribution of reactants that leads to the formation of a given transition state complex. In this method the transition state is located at the maximum of the long range effective potential where the reactants retain their original identity. The orbiting rate constants for both bimolecular reactions (Miller, 1976; Light, 1967), and unimolecular reactions (Chesnavich and Bowers, 1977) can be obtained as a function of translational, rotational, and vibrational energy of the reacting system. Comparison with experiment in general reveals that orbiting unimolecular rate constants are unrealistically high while the orbiting bimolecular rate constants are similar to experimental results at thermal energies. This model also predicts the probability of a given translational energy release (Chesnavich and Bowers, 1976) which in most cases is in good agreement with experimental results for reactions with no reverse activation energy.

Experimental Study of Ion/Molecule Reactions Using FTICR

Rate Coefficients. ICR techniques cannot be used for experimental tests of statistical theories since the application of statistical models requires a detailed knowledge of energy states of the system, which cannot be

obtained from ICR. On the other hand, theoretical bimolecular rate constants using Langevin's model are usually found to agree with the experimental results obtained for low energy ion/molecule reactions using ICR technique. Reactant ions with energies close to thermal can be prepared by charge transfer ionization of a precursor molecule followed by collisional relaxation of the ions by inert gas molecules. Thus, this method provides the determination of thermal bimolecular rate constants which can be used to test the basic assumptions of the Pure Polarization method.

The first step in the experimental determination of rate coefficients by FTICR involves the ejection of all ions except the one of interest from the analyzer cell following charge transfer ionization. Next the decay of the ion signal is monitored as a function of time long enough to permit the ion of interest to react away completely.

Method of Data Analysis. The ion/molecule reactions studied in FTICR most often involve bimolecular collisions and follow second order kinetics. The rate expression for a simple second order reaction is given by

$$-d[I]/dt = k_2[I][R] \qquad (3.8)$$

where I is the ion and R is the reactant neutral. Since the ion number density created in the FTICR instrument is at

least three orders of magnitude lower than the neutral number density, a "pseudo-first order" rate coefficient, k_1' can be substituted for the term $k_2[R]$ in equation (3.8).

$$-d[I]/dt = k_1'[I] \qquad (3.9)$$

After integration, the rate expression giving the number density of the reactant at any given time is obtained:

$$[I](t) = [I](0)\ \exp(-k_1't) \qquad (3.10)$$

where [I](0) is the initial number of ions present. Thus, k_1' can be determined from the slope of the simple ln(ion signal) vs time plot. The true rate coefficient, k_2 can then be obtained from k_1' by dividing k_1' by the number density of the reactant neutral. The number density of the neutral is determined using the expression, $(n/V) = P/RT$, where V and T are the volume and the temperature of the analyzer cell respectively, and P is the pressure of the reactant neutral measured by a capacitance manometer.

In an experimental situation, there is often a second neutral present in the cell, which is the precursor neutral of the ion of interest. Thus, the decay of the ion signal includes ion/molecule reactions with both the precursor and the neutral molecules of interest. In this case the rate expression becomes

$$-d[I]/dt = (k_2[R] + k_3[P])[I] \qquad (3.11)$$

where k_3 is the bimolecular rate coefficient for the reaction of the ion with the precursor molecule, P. The integrated form is

$$[I](t) = [I](0) \exp [-(k_2[R] + k_3[P])t] \qquad (3.12)$$

In order to determine the rate coefficient of reactions of the ion with the neutral reactant, it is necessary first to monitor the reactions of the ion with precursor neutral with no reactant neutral present in the analyzer cell and then to subtract the rate coefficient for this reaction from the total rate coefficient observed in the presence of both the precursor neutral and the reactant of interest. If the precursor neutral pressure is kept constant for the two cases, only the pseudo-first order rate constants are used in the subtraction step.

When two or more isomers of a particular ion are formed from the same parent neutral, a single ion signal is observed in the mass spectrometer whose intensity is the sum of the intensities of all the isomers. For a simple case of only two ion structures,

$$[I](t) = [A](t) + [B](t) \qquad (3.13)$$

Thus, the integrated form of the rate expression is given by

$$[I](t) = [A](0)\ \exp[-(k_2[R] + k_3[P])t] + [B](0)\ \exp[-(k_2'[R] + k_3'[P])t] \qquad (3.14)$$

where A and B are the isomers of ion I. Consequently, the decay curve of the ion signal is composed of segments with two different exponential time constants, each slope corresponding to the reaction rate of a different ion structure. The sum of the rate coefficients (for reactions with precursor and reactant neutrals) of the slower reacting structure is calculated from the tail of the double decay curve while that of the faster reacting structure is determined by subtracting the amount of the slow reacting isomer at each point in the initial part of the curve using Equation (3.14). Often, one of the structures is completely unreactive, while the other is reactive as shown in Figure 3.3, simplifying the data analysis for structure identification.

Reaction Mechanisms. Reaction pathways leading to final product ions from a ion/molecule reactant system can be studied using the ejection capabilities of FTICR. The

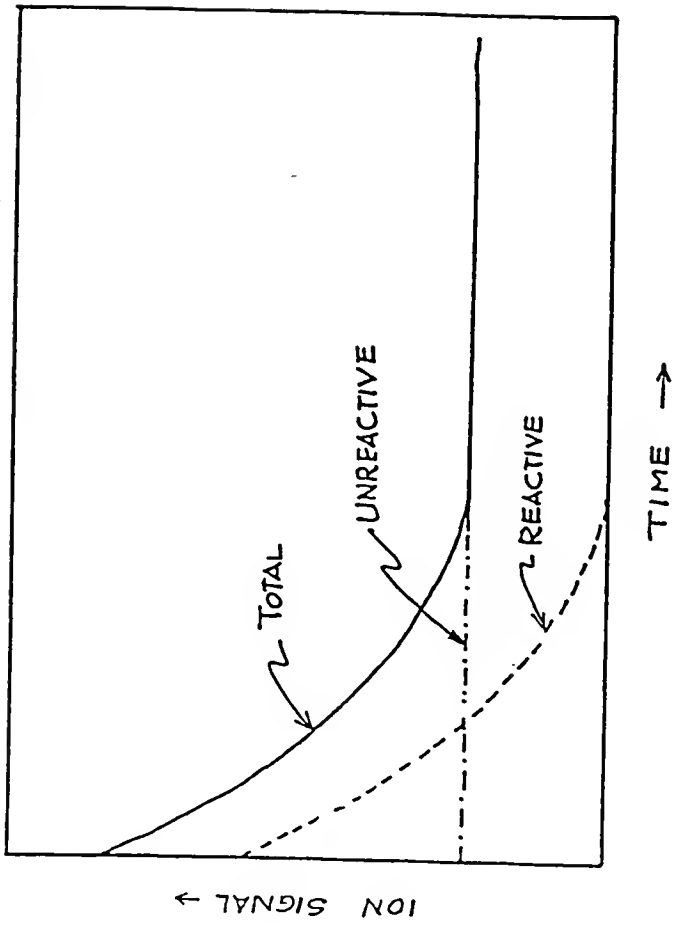

Figure 3.3. Ion Decay Curve with Reactive and Unreactive Components.

method involves the ejection of each first generation product ion continuously during the reaction time to see its effect on the intensity distribution of the mass spectrum of the final product ions. This method also can be used to calculate the branching ratios for the product ions. Studying reaction pathways and branching ratios of the ions produced in different ways (either from different precursors or different methods of ionization) provides an alternative means to rate coefficient determination for the differentiation of structural isomers of the ion of interest.

CHAPTER 4
REACTIONS OF $C_3H_3^+$ WITH ACETYLENE AND DIACETYLENE IN THE GAS PHASE

Introduction

The $C_3H_3^+$ ion has received considerable attention in recent years as a possible soot precursor because it is found in quite high abundance in fuel-rich and sooting flames (Goodings et al, 1979; Olson and Calcote, 1981b; Michaud et al., 1981). Although substantial uncertainty remains as to $C_3H_3^+$ formation mechanisms in flames (Calcote, 1981), the ion is postulated (Calcote, 1981; Olson and Calcote, 1981a) to react with neutrals such as acetylene, diacetylene, and C_2H in rapid, sequential condensation and condensation/elimination reactions, forming successively larger ions, which can rearrange to cyclic species during the ion/molecule reaction chain.

Two isomeric structures of $C_3H_3^+$ shown in Figure 4.1 are important in discussing the role of $C_3H_3^+$ in ion/molecule reaction mechanisms. The first is the cyclopropenylium ion, recognized as the most stable isomer, which has a theoretically calculated heat of formation of 253 kcal/mol (Radom et al., 1976), in quite good agreement with the 256 kcal/mol determined by experiment (Lossing, 1972). A second and potentially more important $C_3H_3^+$

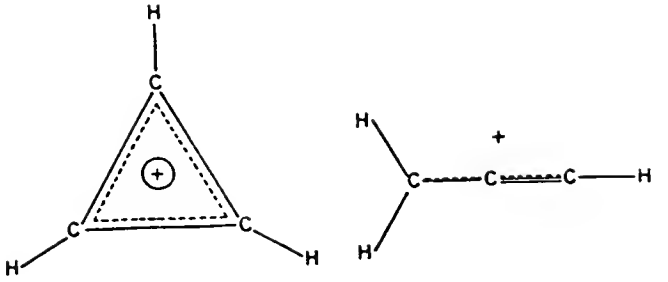

(4.1) (4.2)

Figure 4.1. The Most Stable $C_3H_3^+$ Structures: Cyclopropenylium (4.1) and Propargylium (4.2).

structure is that of the linear propargylium ion with a calculated (Radom et al., 1976) heat of formation 31 to 34 kcal/mol higher than that of the cyclopropenylium ion, in fair agreement with the 25 kcal/mol difference found experimentally by Lossing (1972). Recent calculations have shown several other stable isomeric structures of the $C_3H_3^+$ ion with higher heats of formation relative to the cyclopropenylium and propargylium ions.

The importance of different precursors in affecting the reactivity of $C_3H_3^+$ ions was reported in a thermochemical study by Holmes and Lossing (1979). In an ICR study of $C_3H_3^+$ reactions, Ausloos and Lias (1981) showed that significant fractions of the linear isomer can be produced by charge transfer reactions of small ions (Ar^+, Xe^+, CO^+, Ne^+, etc.) with propargyl chloride and bromide. Later it was reported (Baykut et al., 1986) that even higher proportions of the propargylium isomer relative to the cyclopropenylium isomer can be obtained with propargyl iodide either by electron impact or charge exchange using Xe^+.

A study by Smyth et al.(1982) demonstrated that the cyclopropenylium ion was relatively unreactive toward simple hydrocarbon fuels whereas the linear, propargylium ion was quite reactive. In particular, reaction of propargylium ions with acetylene was reported to produce $C_5H_3^+$ and $C_5H_5^+$ ions with an overall $C_3H_3^+$ disappearance rate coefficient of

1×10^{-9} cm^3/s. In the work discussed in this chapter, results substantially different from those reported earlier were found and the research was thus expanded to investigate possible production of $C_5H_5^+$ ions from ionic sources other than $C_3H_3^+$ present in the reaction media using the ejection capabilities of Fourier transform ion cyclotron resonance (FTICR) mass spectrometry. Reactions of propargylium ions with C_2D_2 were also studied in order to delineate further a proposed mechanism for the $C_3H_3^+$/acetylene interaction.

Diacetylene is another important flame neutral which has been postulated to react with $C_3H_3^+$ ions in an ion/molecule soot formation mechanism (Olson and Calcote, 1981a). Reaction pathways and the rate coefficient for the reaction of propargylium ions with diacetylene near room temperature were thus also investigated. In this chapter, results for the reactions of $C_3H_3^+$ ions with acetylene, deuterated acetylene, and diacetylene are reported and discussed in relation to previous work involving $C_3H_3^+$ reactions (Ausloos and Lias, 1981; Smyth et al., 1982; Baykut et al.,1986).

Experimental

Reactive and non-reactive $C_3H_3^+$ ions were produced by charge transfer reactions of various precursors with Xe^+, formed with an electron beam pulse of 5 ms duration at an ionizing electron energy of ca. 15 eV. Propargyl iodide was

used as a precursor for $C_3H_3^+$ in studies of the reaction of this ion with acetylene, deuterated acetylene, and diacetylene, while a number of different precursors (propargyl iodide, propargyl bromide, propargyl chloride, propyne and allene) were used to investigate the reaction mechanisms leading to $C_5H_5^+$ ion formation. In some studies $C_3H_3^+$ ions were produced directly from the above-mentioned precursors by electron impact to compare the effect of ionization technique on the ratio of reactive to unreactive isomers.

Propargyl iodide was prepared from propargyl chloride by a halogen exchange reaction (March, 1977). The details of purification are given elsewhere (Baykut et al., 1986). Propargyl chloride, propargyl bromide, allene, propyne and acetylene were obtained commercially and their purity was checked by obtaining wide mass range spectra. In the case of acetylene, some production of protonated acetone was observed at long delay times indicating the presence of a small amount of acetone as an impurity. Propargyl bromide was distilled before use in order to remove toluene which was present as a stabilizing agent. Deuterated acetylene was prepared from D_2O and CaC_2. Diacetylene was prepared by the method of dehydrochlorination of 1,4-dichloro-3-butyne in aqueous potassium hydroxide/dioxane solution (Snow, 1985). All the samples were used after multiple freeze-pump-thaw cycles.

Results

$C_3H_3^+$ Reactions with Acetylene. Despite an earlier report (Smyth et al., 1982) that $C_3H_3^+$ is quite reactive with acetylene, only very low intensities of $C_5H_3^+$ and $C_5H_5^+$ produced via this reaction could be found in this work. Experimental conditions of the earlier study were duplicated as closely as possible, and then varied substantially with respect to relative pressures of neutrals (from 1:1 to 8:1 C_2H_2:C_3H_3I) and overall system pressure (from 5 X 10^{-7} to 3 x 10^{-5} torr). The $C_3H_3^+$ ions were formed from propargyl chloride, bromide, and iodide by both charge transfer using Xe^+ and electron impact. In order to determine other possible sources of $C_5H_5^+$ observed under the earlier reaction conditions, binary mixtures of acetylene and one of the $C_3H_3^+$ precursors reported (Ausloos and Lias, 1981; Smyth et al., 1982; Baykut et al., 1986) earlier were used. Intensities of $C_5H_5^+$ and $C_5H_3^+$ were first measured after a 125 ms reaction time. Then the parent ion, $C_2H_2^+$, and $C_3H_3^+$ were each ejected separately during the 125 ms reaction period to assess their contribution to $C_5H_5^+$ and $C_5H_3^+$ formation.

For each different neutral precursor, the sources and amounts of $C_5H_5^+$ ions produced were found to be different. Propyne and allene were similar in producing large amounts of $C_5H_5^+$ and no $C_5H_3^+$ ion. However, the $C_3H_3^+$ + C_2H_2

reaction was <u>not</u> responsible for $C_5H_5^+$ formation. The main reactions leading to $C_5H_5^+$ were

$$C_2H_2^+ + C_3H_4 \text{ ----> } C_5H_5^+ + H \qquad (4.1)$$

$$C_3H_4^+ + C_2H_2 \text{ ----> } C_5H_5^+ + H \qquad (4.2)$$

in both cases. On the other hand, when propargyl iodide, propargyl bromide and propargyl chloride were used as precursors, relatively smaller amounts of $C_5H_5^+$ ion formation were observed along with $C_5H_3^+$ ion production. In the propargyl chloride case

$$C_3H_3Cl^+ + C_2H_2 \text{ ----> } C_5H_5^+ + Cl \qquad (4.3)$$

$$C_2H_2^+ + C_3H_3Cl \text{ ----> } C_5H_5^+ + Cl \qquad (4.4)$$

were the major reactions leading to $C_5H_5^+$ formation. For propargyl bromide the

$$C_3H_3Br^+ + C_2H_2 \text{ ----> } C_5H_5^+ + Br \qquad (4.5)$$

reaction was the only source of $C_5H_5^+$ ions observed. Any contribution to $C_5H_5^+$ formation from linear $C_3H_3^+$ was less than the experimental uncertainty. Finally, very little (almost negligible) amounts of $C_5H_5^+$ ions were observed when propargyl iodide was used as a precursor and the reactions

$$C_2H_2^+ + C_3H_3I \text{ ----> } C_5H_5^+ + I \qquad (4.6)$$

$$C_3H_3^+ + C_2H_2 \text{ ----> } C_5H_5^+ \qquad (4.7)$$

were the major contributors in this case. An upper limit for the rate constant, k, for reaction (4.7) was estimated as 5 X 10^{-12} cm^3/s by assuming that the very small $C_5H_5^+$ signal observed resulted from this reaction, and using the expression $[C_3H_3^+](t) = [C_3H_3^+](0) - [C_5H_5^+](t) = [C_3H_3^+](0)e^{-nkt}$, where n is the C_2H_2 number density. Overall results for the production of $C_5H_5^+$ and $C_5H_3^+$ ions in mixtures of acetylene and various neutrals used as the precursors of $C_3H_3^+$ are summarized in Table 4.1.

Because propargyl iodide was shown to produce the highest reactive/unreactive ratio of $C_3H_3^+$ ions both in earlier (Baykut et al., 1986; Holmes and Lossing, 1979) and the present work (see Table 4.2), it was used as a precursor for $C_3H_3^+$ ions in these reaction kinetics studies. Since the precursor neutral molecule was always present in the FTICR analyzer cell, it was a competitor with the reactant neutral of interest in ion/molecule reactions involving $C_3H_3^+$. In order to determine the rate coefficient of reactions of $C_3H_3^+$ with the neutral reactant, it was necessary first to monitor the reactions of this ion with C_3H_3I and then to subtract the rate coefficient for this reaction from the total rate coefficient observed in the presence of both the precursor neutral and the reactant of

TABLE 4.1

Production of $C_5H_5^+$ and $C_5H_3^+$ Ions in Mixtures of Various Neutrals and Acetylene[a].

Neutral	Ionic sources[b] of $C_5H_5^+$ after Xe^+ charge transfer ionization of a mixture of the neutral and acetylene	Ratio of $C_5H_5^+$ prod. relative to that in allene case[c]	Ionic sources[b] of $C_5H_3^+$	Intensity of $C_5H_5^+$ vs. $C_5H_3^+$	Percent reactive $C_3H_3^+$ ions
Allene	$C_2H_2^+$(40%) $C_3H_4^+$(60%)	1.0	-	-	<5
Propyne	$C_2H_2^+$(40%) $C_3H_4^+$(60%)	0.75	-	-	30
Propargyl chloride	$C_2H_2^+$(40-50%) $C_3H_3Cl^+$(50-60%)	0.25	$C_3H_3Cl^+$(20%) $C_3H_3^+$(20%) $C_2H_2^+$(60%)	3.0	15
Propargyl bromide	$C_3H_3Br^+$(90-100%)	0.08	$C_2H_2^+$(70%) [$C_3H_3^+$ + $C_3H_3Br^+$](30%)	2.0	85
Propargyl iodide	$C_2H_2^+$(40%) $C_3H_3^+$(60%)	<0.02	$C_2H_2^+$(50%) $C_3H_3^+$(50%)	1.7	90

[a] All ions were produced by chemical ionization charge transfer from Xe^+.
[b] Percentages show the relative contributions to $C_5H_5^+$ and $C_5H_3^+$ production as determined by double resonance experiments and have an estimated uncertainty of ±10%.
[c] Neutral reactants all had the same pressure (7×10^{-7} torr) as measured by the ionization gauge. Xenon and acetylene pressures were 5.6×10^{-6} and 1.8×10^{-6} torr, respectively.

TABLE 4.2 .

Percentages[a] of reactive $C_3H_3^+$ found from various precursors by various ionization techniques (monitored by observing reaction with the precursor neutral).

	precursor		
Ionizing Technique	Propargyl iodide	Propargyl bromide	Propargyl chloride
Electron impact (15eV)	90	40	10
Chemical ionization charge transfer with Xe^+	90	85	15

[a]Estimated error is $\pm$5%.

interest. Reactions of $C_3H_3^+$ with propargyl iodide were monitored as a function of time following charge transfer chemical ionization of C_3H_3I by Xe^+ and ejection of all ions but $C_3H_3^+$ from the analyzer cell. Results obtained were identical to $C_3H_3^+$ reaction channels with propargyl iodide which have been reported elsewhere (Baykut et al., 1986).

Isomerization of Linear $C_3H_3^+$. In addition to the absence of any significant $C_5H_3^+$ and $C_5H_5^+$ formed by reaction of linear $C_3H_3^+$ with C_2H_2, it was also observed that C_2H_2 led to the isomerization of linear $C_3H_3^+$ ions to their cyclic form, thus rendering them unreactive toward their parent neutral (C_3H_3I) as well as toward C_2H_2. This isomerization was followed as a function of C_2H_2 pressure and a direct pressure dependence was found, as can be seen in Figure 4.2.

$C_3H_3^+$ Reactions with C_2D_2. To achieve a better understanding of the isomerization of linear $C_3H_3^+$, C_2D_2 instead of C_2H_2 was used as the neutral reactant. The following isotope exchange reactions were observed:

$$C_3H_3^+ + C_2D_2 \text{ ----> } C_3H_2D^+ + C_2DH \qquad (4.8)$$

$$C_3H_3^+ + C_2D_2 \text{ ----> } C_3HD_2^+ + C_2H_2 \qquad (4.9)$$

$$C_3H_2D^+ + C_2D_2 \text{ ----> } C_3HD_2^+ + C_2DH \qquad (4.10)$$

$$C_3H_2D^+ + C_2D_2 \text{ ----> } C_3D_3^+ + C_2H_2 \qquad (4.11)$$

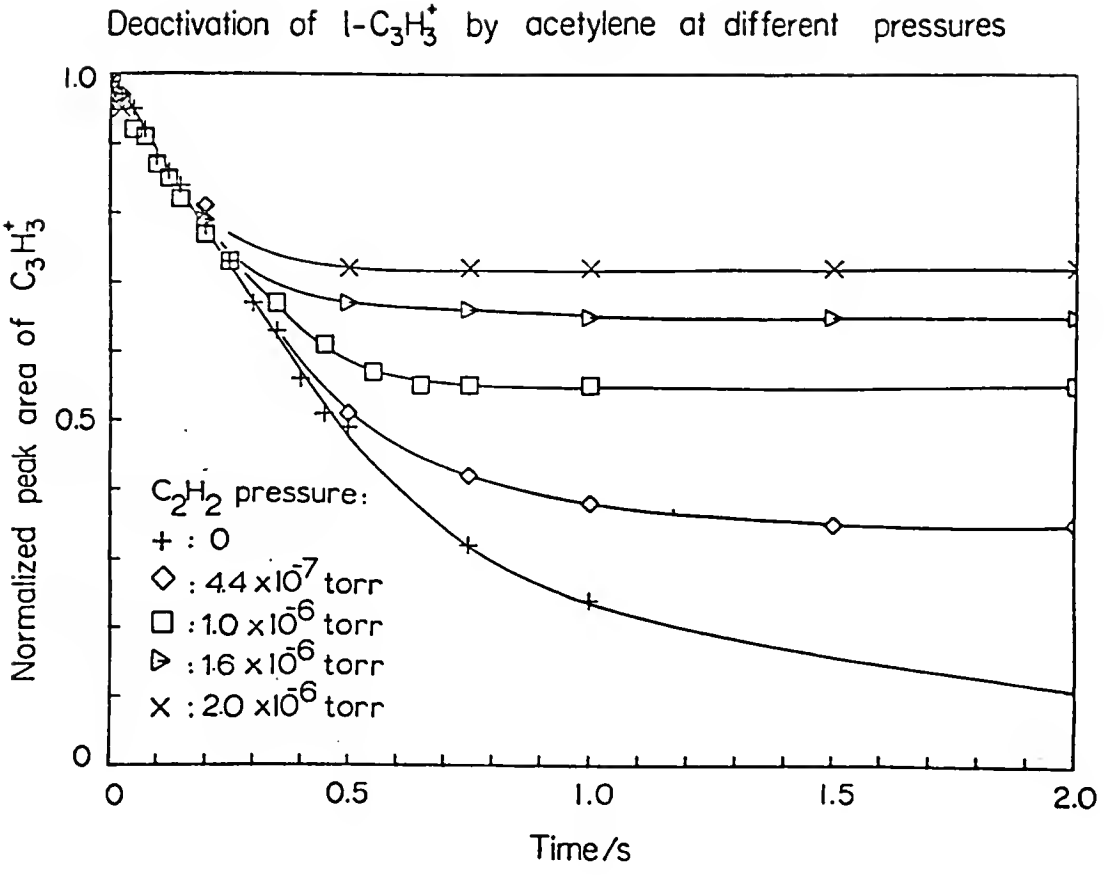

Figure 4.2. Isomerization of Linear $C_3H_3^+$ Ions at Different Pressures of C_2H_2. $C_3H_3^+$ ions were produced by charge transfer reactions with Xe^+. $p(C_3H_3I) = 1.1 \times 10^{-7}$ torr; p(Xe) was adjusted to maintain a constant total pressure of 2.6×10^{-6} torr as measured on the ionization gauge. (All pressures are capacitance-manometer corrected.)

$$C_3HD_2^+ + C_2D_2 \text{ ----> } C_3D_3^+ + C_2DH \qquad (4.12)$$

Using FTICR ejection capabilities, it was found that reactions (4.9) and (4.10) contribute equally to the production of $C_3HD_2^+$ while reaction (4.12) produces more of $C_3D_3^+$ (80%) than reaction (4.11) (20%).

Ion intensity vs. time curves for the $C_3H_3^+/C_2D_2$ reaction are shown in Figure 4.3. The overall rate coefficient for the disappearance of $C_3H_3^+$ was calculated by subtracting the observed rate coefficient for the reaction with propargyl iodide from the total observed rate coefficient in the presence of C_2D_2. This observed rate coefficient was then converted to the true rate coefficient using the corrected pressure of C_2D_2. A value of $(4.5\pm1.9) \times 10^{-10}$ cm^3/s was found at a cell temperature of 373 K for the disappearance of $C_3H_3^+$ (reactions (4.8) and (4.9)). In Figure 4.4, ion intensity vs. time curves of $C_3H_3^+$ are compared for reactions with and without C_2D_2.

<u>$C_3H_3^+$ Reactions with Diacetylene.</u> After ejection of all ions except $C_3H_3^+$ following charge transfer chemical ionization by Xe^+ of a mixture of diacetylene and propargyl iodide, the ion/molecule reactions as a function of time were monitored. Consecutive C_2 and C_4H_2 addition reactions were observed:

$$C_3H_3^+ + C_4H_2 \text{ ----> } C_7H_5^+ \qquad (4.13)$$

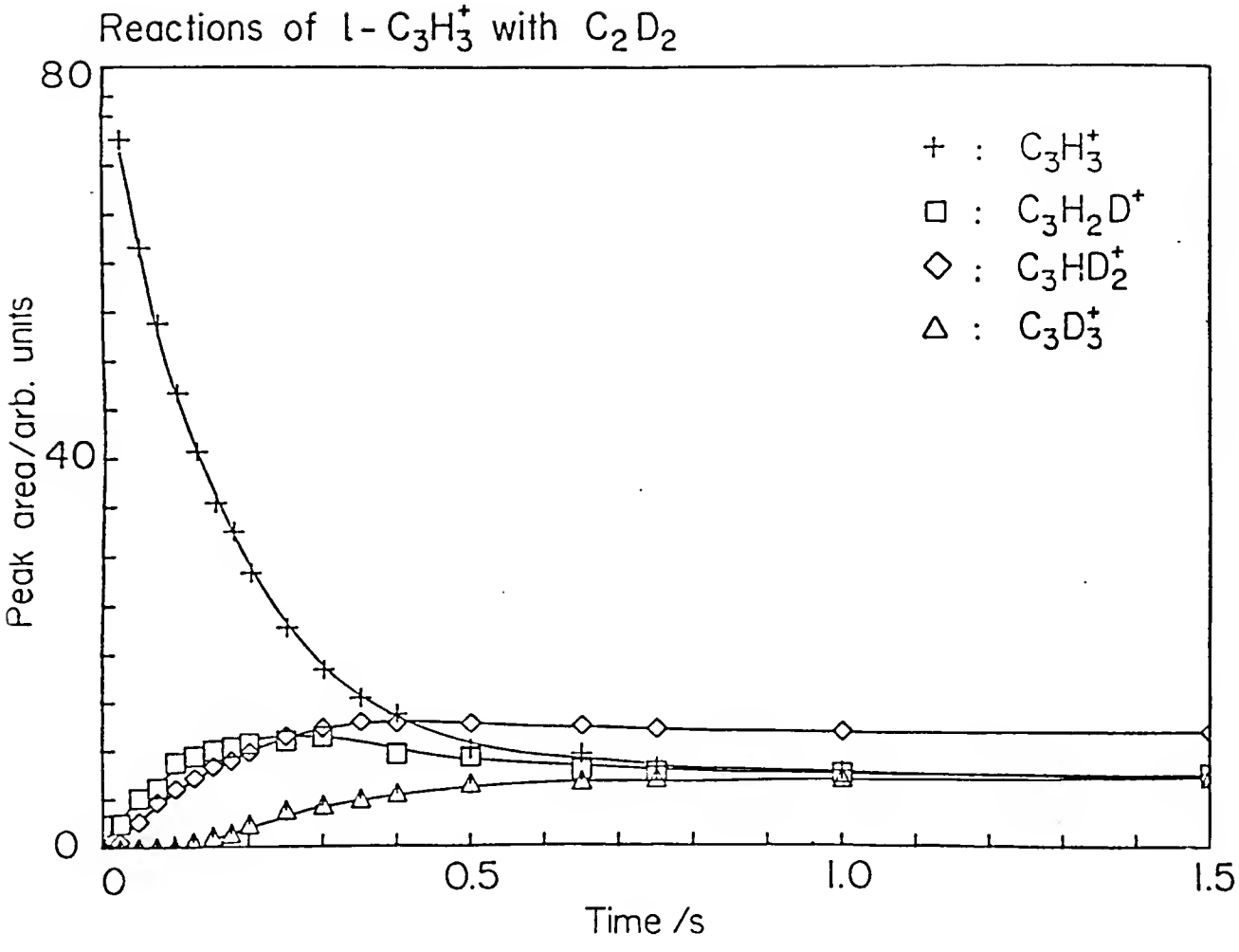

Figure 4.3. Isotope Exchange Reactions of $C_3H_3^+$ with C_2D_2. Disappearance of $C_3H_3^+$ ion includes reactions with propargyl iodide. Note that the sum of all isotopic forms of $C_3H_3^+$ remaining at the end of the reaction with C_2D_2 approximately equals the total unreactive $C_3H_3^+$ when C_2H_2 is used as a neutral reactant at the same pressure (see Fig. 4.2). $p(C_3H_3I) = 1.1 \times 10^{-7}$ torr; $p(C_2D_2) = 1.2 \times 10^{-6}$ torr; $p(Xe) = 6.2 \times 10^{-6}$ torr.

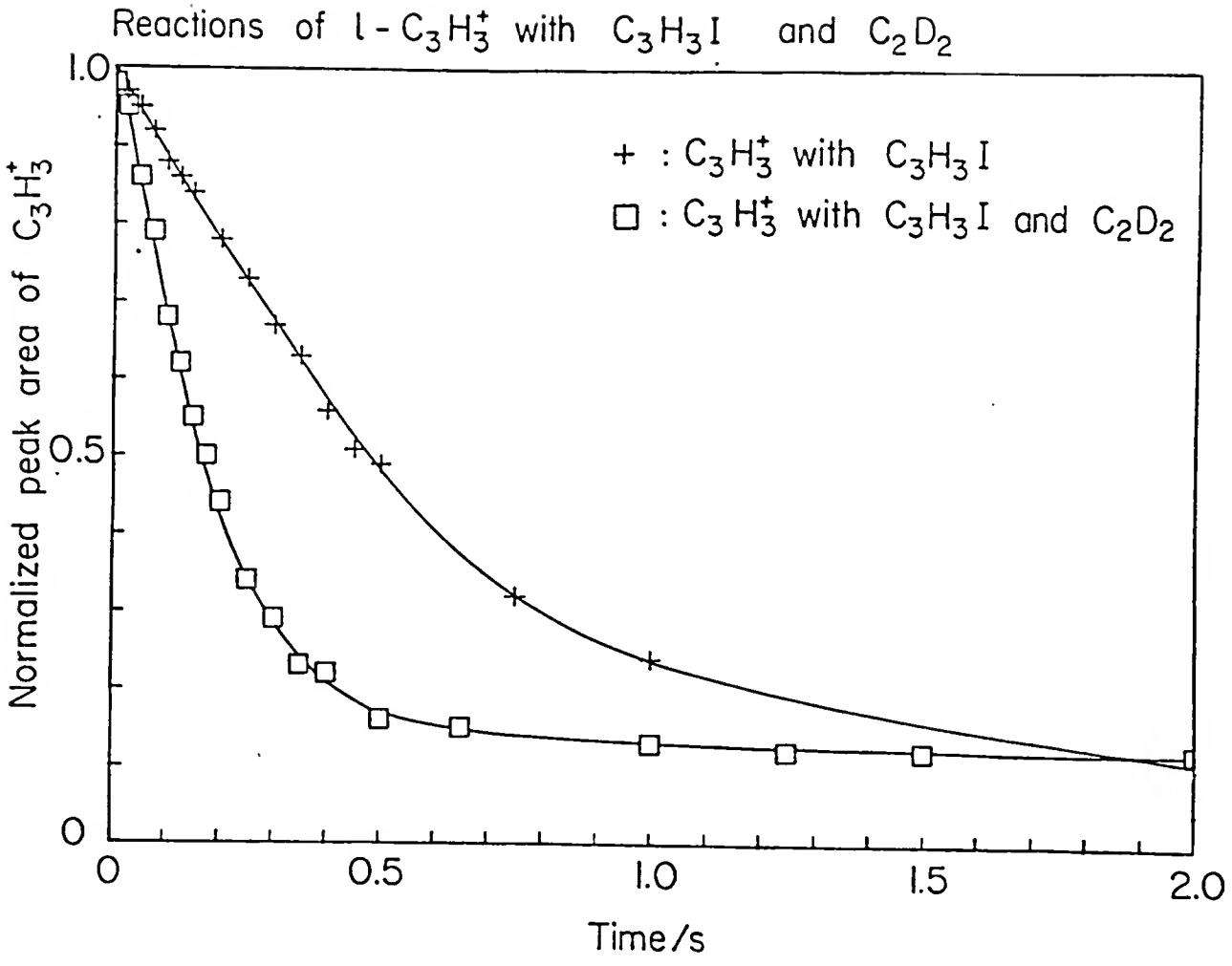

Figure 4.4. $C_3H_3^+$ Ion Decay Curves for Reaction with C_3H_3I and C_2D_2. (Pressures are the same as given for Fig. 4.3.)

$$C_3H_3^+ + C_4H_2 \text{ ----> } C_5H_3^+ + C_2H_2 \quad (4.14)$$

$$C_5H_3^+ + C_4H_2 \text{ ----> } C_9H_5^+ \quad (4.15)$$

$$C_5H_3^+ + C_4H_2 \text{ ----> } C_7H_3^+ + C_2H_2 \quad (4.16)$$

$$C_7H_3^+ + C_4H_2 \text{ ----> } C_{11}H_5^+ \quad (4.17)$$

$$C_9H_5^+ + C_4H_2 \text{ ----> } C_{11}H_5^+ + C_2H_2 \quad (4.18)$$

$$C_9H_5^+ + C_4H_2 \text{ ----> } C_{13}H_7^+ \quad (4.19)$$

Some of these product ions were seen to react further with propargyl iodide by displacement of atomic iodine:

$$C_5H_3^+ + C_3H_3I \text{ ----> } C_8H_6^+ + I \quad (4.20)$$

$$C_7H_3^+ + C_3H_3I \text{ ----> } C_{10}H_6^+ + I \quad (4.21)$$

$$C_7H_5^+ + C_3H_3I \text{ ----> } C_{10}H_8^+ + I \quad (4.22)$$

$$C_8H_6^+ + C_3H_3I \text{ ----> } C_{11}H_9^+ + I \quad (4.23)$$

$$C_9H_5^+ + C_3H_3I \text{ ----> } C_{12}H_8^+ + I \quad (4.24)$$

Ion intensity vs. time curves for the $C_3H_3^+/C_4H_2$ reaction are shown in Figure 4.5. The rate coefficient for the disappearance of $C_3H_3^+$ (reactions (4.13) and (4.14), Figure 4.6) was calculated as described earlier, and a value of $k = (1.4 \pm 0.7) \times 10^{-9}$ cm^3/s was found. Propargyl iodide, bromide, and chloride were all used as precursors of $C_3H_3^+$ in studying its reactions with diacetylene. For each precursor, both electron impact and charge transfer chemical ionization techniques were used. The percentages of reactive isomer in the reaction with diacetylene are shown

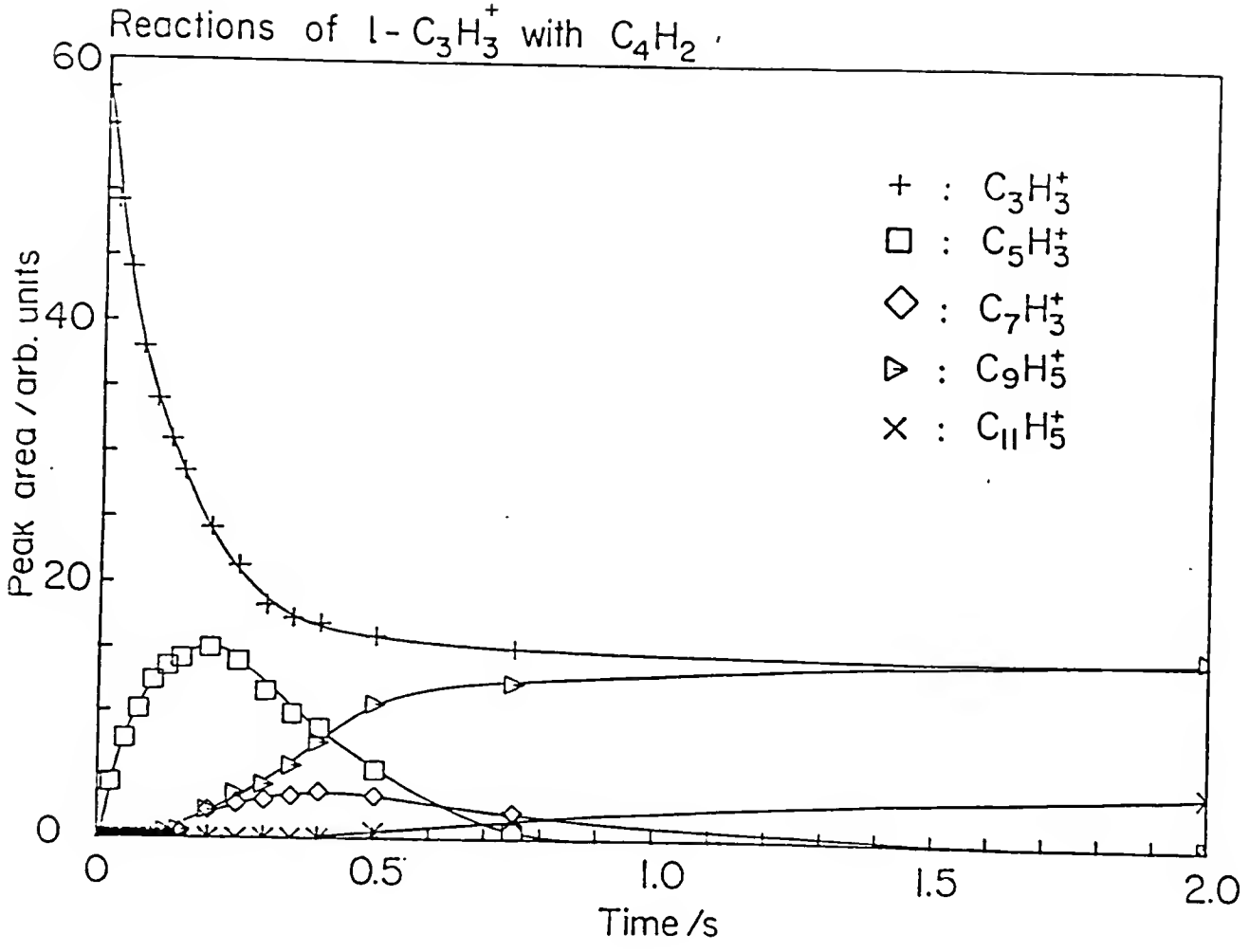

Figure 4.5. Reactions of $C_3H_3^+$ with C_4H_2. Disappearance of $C_3H_3^+$ and product ions include reactions with propargyl iodide. $p(C_3H_3I) = 1.1 \times 10^{-7}$ torr; $p(C_4H_2) = 4.8 \times 10^{-7}$ torr; $p(Xe) = 6.2 \times 10^{-6}$ torr. (All pressures are capacitance-manometer corrected.)

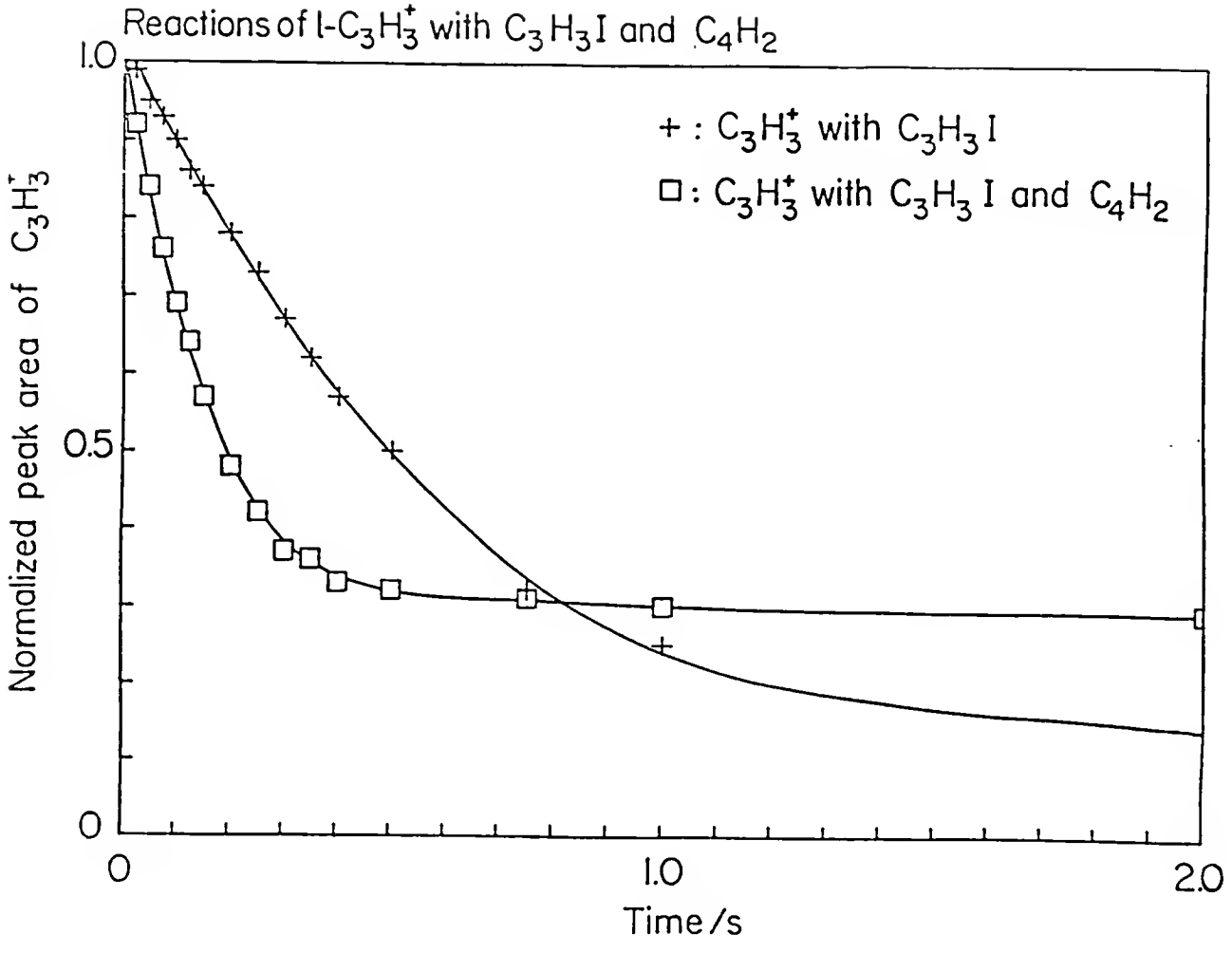

Figure 4.6. $C_3H_3^+$ Decay Curves for the Reactions with C_3H_3I and C_4H_2. (Pressures are the same as given for Fig. 4.5.)

TABLE 4.3

Percentages[a] of reactive $C_3H_3^+$ observed in the reaction with C_4H_2.[b]

Ionizing Technique	precursor: Propargyl iodide	Propargyl bromide	Propargyl chloride
Electron impact (15eV)	75	30	5
Chemical ionization charge transfer with Xe^+	75	65	5

[a]Estimated error is ±5% [b]$P(C_4H_2) = 4.8 \times 10^{-7}$ torr

in Table 4.3. When these percentages of reactive isomer were compared to those in the absence of C_4H_2 (see Table 4.2), it was clear that some isomerization of the reactive linear $C_3H_3^+$ ion, as well as reactions (4.13) and (4.14), had taken place (see also Fig. 4.6). This isomerization was followed as a function of C_4H_2 pressure and a direct pressure dependence was found, as can be seen in Table 4.4.

The reactions of $l\text{-}C_3H_3^+$ with propargyl iodide and with both acetylene and diacetylene have also been followed at several elevated temperatures up to 500 K. All the rate constants were found to be similar to their room temperature value within experimental error.

Discussion

Effect of Different Precursors. Different percentages of reactive $C_3H_3^+$ were found from three different precursors, propargyl iodide, propargyl bromide and propargyl chloride as shown in Table 4.2. To explain the differences observed in reactivity, schematic potential energy surfaces for these precursors are shown in Figure 4.7. Experimental thermochemical data reported by Holmes and Lossing (1978) were used in the generation of the potential surfaces. Reverse activation energies for $c\text{-}C_3H_3^+$ formation from propargyl bromide and chloride were determined by the difference between the experimental and the calculated appearance potentials. Since the appearance

TABLE 4.4

Changes in $C_3H_3^+$ reactivity[a] at different pressures of diacetylene.[b]

C_4H_2 pressure/10^{-7} Torr	% unreactive $C_3H_3^+$
0.8	16
1.6	17
4.8	25
7.2	32
8.0	35
9.6	40

[a] 1-$C_3H_3^+$ ions were produced from propargyl iodide by chemical ionization charge transfer with Xe^+. ($p(C_3H_3I)$ = 1.1 X 10^{-7} torr; p_{Xe} was adjusted to maintain a constant total pressure of 2.6 X 10^{-6} torr as read on the ionization gauge).
[b] All pressures are capacitance-manometer corrected.

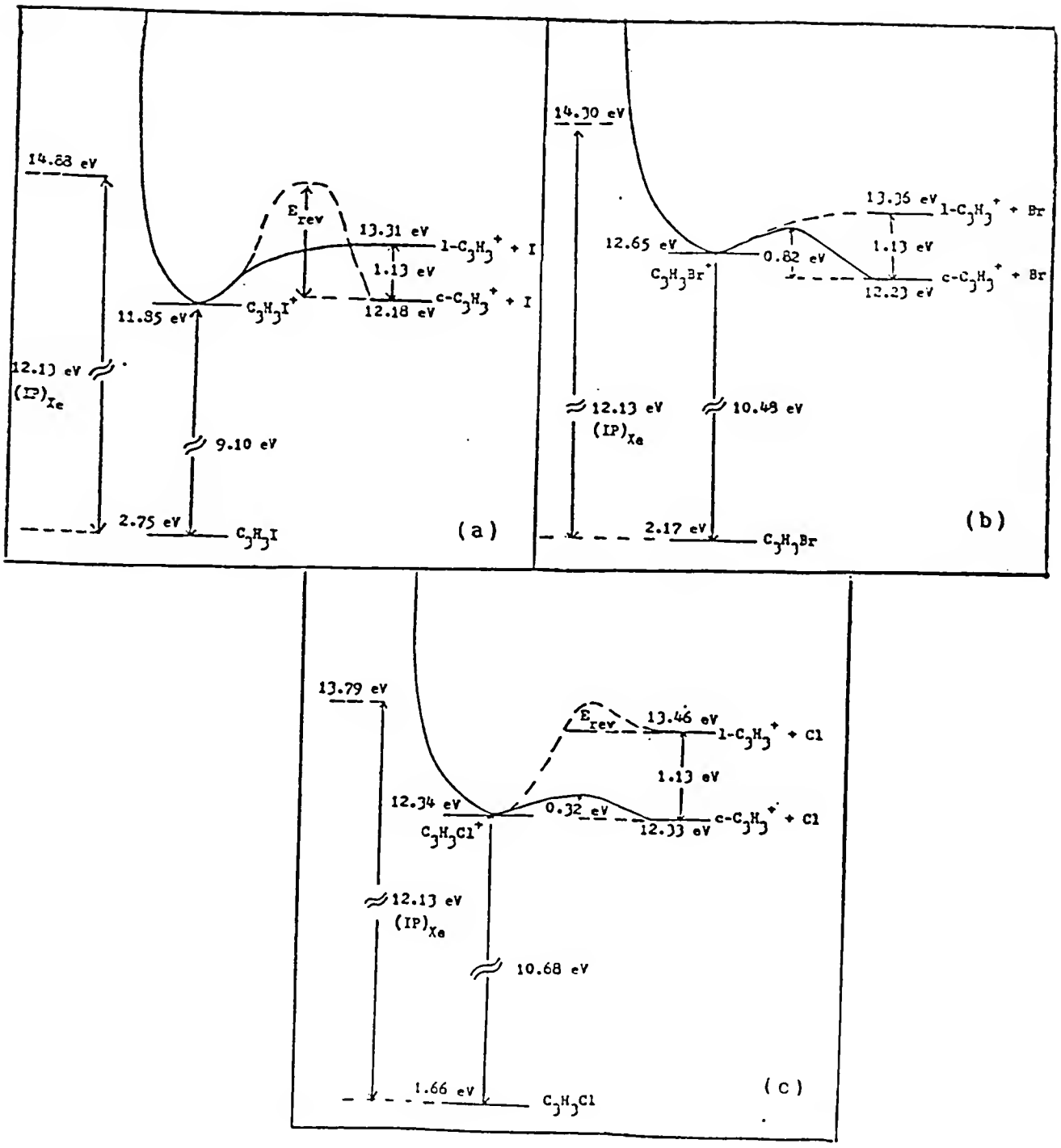

Figure 4.7. Schematic Potential Energy Surfaces for $C_3H_3^+/C_3H_3X^+$ System from Different Precursors. Propargyl Iodide (a), Propargyl Bromide (b), and Propargyl Chloride (c).

potential of $C_3H_3^+$ produced from propargyl iodide very closely corresponds to the calculated threshold for $l\text{-}C_3H_3^+$ rather than $c\text{-}C_3H_3^+$, the dissociation to the latter is assumed to have a significant energy barrier. Thus, reverse activation energy for the dissociation channel giving unreactive $c\text{-}C_3H_3^+$ decreases in the order $E_{iodo} > E_{bromo} > E_{chloro}$ as shown in the figure. Production of almost exclusively reactive $l\text{-}C_3H_3^+$ by both electron impact and Xe^+ charge transfer ionization from propargyl iodide suggests that E_{iodo} is so large that the fragmentation channel leading to $l\text{-}C_3H_3^+$ becomes the lowest energy channel. In the case of propargyl bromide, there is enough excess energy to dissociate to both $l\text{-}C_3H_3^+$ and $c\text{-}C_3H_3^+$. Production of 80% $l\text{-}C_3H_3^+$ by Xe^+ chemical ionization suggests no significant energy barrier for the $l\text{-}C_3H_3^+$ channel. It is interesting to note that dissociation to $l\text{-}C_3H_3^+$ reduces by a factor of two when electron impact ionization is used, which demonstrates the effect of a large distribution of electron energies from an electron impact ionization source on the relative abundances of two channels almost equally accessible energetically. The very small reactive $l\text{-}C_3H_3^+$ percentage produced from propargyl chloride by both electron impact and Xe^+ charge transfer ionization suggests at least a small energy barrier for this dissociation channel, as indicated schematically in Figure 4.7c.

Internal Energy of the Ions in Relation to Rate Coefficient Measurements. In studying reactions it is desirable to have knowledge of the internal energy distribution of the reactant ions. The reactions studied here are bimolecular addition reactions followed by unimolecular decomposition. As shown in Figure 4.7a, when $1\text{-}C_3H_3^+$ is formed from propargyl iodide by Xe^+ charge transfer chemical ionization, 1.5 eV of excess energy is available. Much of this excess energy will be converted into translational motion of the heavy Xe and I neutrals resulting from the charge transfer in the collision process. Under typical experimental conditions (ca. 2 - 3 x 10^{-6} torr total pressure), about 125 ms was allowed for the charge transfer process and for ejecting intermediates. For these conditions the $C_3H_3^+$ ions collided a number (10-15) of times with the excess Xe present in the FTICR cell, leading to near thermalization of internal energy before the ion/molecule reactions were monitored. Since the reaction time scale was on the order of seconds, it can be assumed that any slight initial deviation from Boltzmann behavior presents no serious error. On the other hand, the observation that the rate constants for the reactions of $1\text{-}C_3H_3^+$ with propargyl iodide and with both diacetylene and acetylene are temperature independent implies that thermalization of the ions is not complete under the conditions reported and there is still some internal energy

in 1-$C_3H_3^+$, which is comparable in magnitude to that contributed from the range of temperatures studied.

Reactivity of 1-$C_3H_3^+$ with Acetylene. Although the results of $C_3H_3^+ + C_2H_2$ reaction are not in agreement with the earlier report (Smyth et al., 1982) of $C_3H_3^+/C_2H_2$ reactivity, the discrepancy is most likely due to limitations of the older pulsed ICR (Smyth et al., 1982) instrumentation for studying ion/molecule reaction pathways in complicated systems when compared to newer FTICR capabilities. Facile ejection of all ions except the one whose ion/molecule reactions are being investigated offers a very clean monitoring opportunity for product-parent relationships even in complicated consecutive and competitive reaction systems. Various alternative pathways for the production of $C_5H_3^+$ and $C_5H_5^+$ which have been described above probably contributed significantly to the intensities of these ions seen in the earlier work. Additional support for the low reactivity of $C_3H_3^+$ with C_2H_2 is found in a recent report (Anicich et al., 1986) of the rate coefficient for this reaction as less than 0.01×10^{-9} cm^3/s, although the isomeric form of $C_3H_3^+$ was not given. It is also possible that the highest pressures used in this work did not reach those of the earlier study due to differences in the location of capacitance manometers, ionization gauges, etc. Thus third body stabilization of

$C_5H_5^+$ collision complexes might have been occurring to some extent in the earlier work and not in that reported here. In fact, such collisional stabilization of the association complexes for the reactions of $C_3H_3^+$ and $C_4H_4^+$ with C_2H_2 has been shown to occur in higher pressure SIFT studies (Smith and Adams, 1987; Knight et al., 1987).

The most likely mechanism of the observed isomerization of $C_3H_3^+$ ions by collisions with acetylene is a "reactive" rather than a "non-reactive" one. That is, it results from an intimate encounter of the ion and neutral in the $C_5H_5^+$ collision complex. This hypothesis is confirmed by the fact that deuterated forms of $C_3H_3^+$ were produced when C_2D_2 was the neutral reactant (see Figure 4.4). Kinetic modeling studies (discussed in Chapter 5) indicate that in some cases the $C_5H_5^+$ collision complex dissociates to give the cyclic, unreactive, $C_3H_3^+$ isomer, instead of the reactive, linear form which reacted initially. The possibility of non-reactive collisional isomerization of linear $C_3H_3^+$ to the cyclic isomer has been ruled out because experiments at elevated pressures of xenon (to ca. 1×10^{-5} torr) showed no interconversion. Similar interconversion of $C_4H_4^+$ ions from a linear to cyclic form has also been reported (Jarrold et al., 1984) in the reaction with C_2H_2 and has also been shown to take place via complex formation by using isotopically labeled C_2H_2. To confirm the hypothesis that energetically less stable, reactive, (linear) $C_3H_3^+$ ions interconvert to

more stable, unreactive ones, cyclic $C_3H_3^+$ ions were also reacted with C_2D_2 and no isotope exchange reactions were observed.

Reactivity of l-$C_3H_3^+$ with Diacetylene. Plots of $C_3H_3^+$ ion intensity vs. time for reaction with diacetylene (C_4H_2) (Figure 4.5) indicate a 10-12% increase in the intensity of the unreactive isomer relative to the reaction when the parent precursor only is present. Isomerization of reactive $C_3H_3^+$ was also seen when different precursors were used (compare Tables 4.2 and 4.3). A similar mechanism involving complex formation may be responsible for this isomerization as well, although it was not investigated in any detail.

CHAPTER 5
KINETIC MODELING OF THE REACTIONS OF $C_3H_3^+$

Introduction

As reported in the last chapter, bimolecular reactions of the propargylium form of $C_3H_3^+$ with acetylene most often result in an isomerization to the cyclopropenylium isomer. To help understand this isomerization process, $C_3H_3^+$ reactions with deuterated acetylene were investigated. These studies showed that the isomerization proceeds via the $C_5H_5^+$ ion/molecule reaction complex, which is sufficiently long-lived under the experimental conditions employed that deuterium exchange, as well as isomerization, takes place. Thus with time the reactive propargylium $C_3H_3^+$ isomer is converted to both reactive and unreactive species containing one, two, and three deuterium atoms. There is no evidence, either experimental or theoretical, that the propargylium cation converts into the cyclopropenylium cation in the absence of the $C_5H_5^+$ reaction complex. In order to better understand the isomerization which converts the reactive to the unreactive form of $C_3H_3^+$, kinetic modeling studies of the ion intensity vs. time curves reported in Chapter 4 were

carried out.[1] It was also hoped that fitting procedures would produce improved ion/molecule reaction rate coefficients. Quantum mechanical calculations[2] on $C_3H_3^+$ and $C_5H_5^+$ structures and reactivity were used to guide the modeling effort.

Experimental

A mixture (predominantly propargylium) of the $C_3H_3^+$ isomers was in most cases formed by charge transfer from propargyl iodide to Xe^+, produced by 15 eV electron ionization of Xe (present at pressures > 10x those of other gases). Other conditions such as neutral partial pressures, pulse sequences and reaction times, and the sources of chemicals were kept as close as possible to those reported in Chapter 4 for the duplicate kinetics experiments reported and modeled here. Any significant deviations are given in the text, table headings, or figure captions. All pressures reported in this chapter were determined by a capacitance manometer, and then multiplied by a "system factor" of 0.30 which corrects for the fact that the pressure read by the capacitance manometer is not the same as that in the FTICR

---

[1]The kinetic modeling studies were performed in the Environics Division of Air Force Engineering and Services Center, Tyndall Air Force Base, Florida by F. Wiseman using multiple experimental data sets produced at identical conditions to those reported in Chapter 4.

[2]A. Cameron, J. Leszczynski, M. C. Zerner and B Weiner, submitted. J. Feng, J. Leszczynski and M. C. Zerner, submitted.

cell. Non-linear least-squares fitting routines employing Marquardt's algorithm (Annino and Driver, 1986), implemented on two different computers[3], were used for kinetic modeling. Complete analytical solutions were obtained from the chemical models developed below for the systems $C_3H_3^+ + C_2H_2$ and $C_3H_3^+ + C_4H_2$. A complete analytical solution was not possible when an isotope effect was included in the chemical model for the $C_3H_3^+ + C_2D_2$ system. Numerical integrations used the finite difference method (Annino and Driver, 1986).

Results

Models of $C_3H_3^+ + C_2H_2$ Reaction. As reported in Chapter 4, collision of the propargylium cation, $l\text{-}C_3H_3^+$, with acetylene forms the cyclopropenylium cation, $c\text{-}C_3H_3^+$, which is unreactive on the time scale of the experiments, given the pressures attainable in the FTICR cell. Experiments with C_2D_2 showed that an encounter complex which allows for isotopic scrambling is formed. Hence, whatever the isomeric form of this complex, a structure having the chemical formula $C_5H_5^+$ can be postulated. Since no species of m/z 65 is observed in the mass spectrum, the ($C_5H_5^+$) species must be in steady-state and of low concentration. The simplest scheme which takes into account this information is given in Figure 5.1.

---

[3]Tektronix Model 4054 and Hewlett Packard Model 150.

$$\ell\text{-}C_3H_3^+ + C_2H_2 \xrightarrow{k_f} C_5H_5^+$$

$$\ell\text{-}C_3H_3^+ + C_3H_3I \xrightarrow{k_p} \text{sink}$$

$$C_5H_5^+ \xrightarrow{k_\ell} \ell\text{-}C_3H_3^+ + C_2H_2$$

$$C_5H_5^+ \xrightarrow{k_c} c\text{-}C_3H_3^+ + C_2H_2$$

Figure 5.1. Reaction Scheme Postulated for the Kinetic Modeling of the Reaction of linear $C_3H_3^+$ with Acetylene.

Applying steady-state kinetics to this scheme yields

$$I(t) = I^{o} - k_p' I_1^{o} (1 - e^{-\theta t})/\theta \qquad (5.1)$$

in which I^{o} and $I(t)$ are ion intensities initially and as a function of time, respectively, I_1 refers only to the linear form,

$$k_p' = k_p P_{C_3H_3I} \qquad (5.2)$$

and

$$\theta = [k_f k_c P_{C_2H_2}/(k_1 + k_c)] + k_p' \qquad (5.3)$$

Equation (5.1) was fitted to several kinetic runs reported in Chapter 4. Table 5.1 shows results of these fits. A plot of θ vs. $P_{C_2H_2}$ should be linear, as implied by equation (5.3), and this is demonstrated in Figure 5.2. Results yield $k_f k_c/(k_1 + k_c) = 2.3(.2) \times 10^6$ $torr^{-1}s^{-1}$ and $k_p' = 1.4(0.2)$ s^{-1}.

Models of $C_3H_3^+ + C_2D_2$ Reaction. Reaction of $C_3H_3^+ + C_2D_2$ is complicated by the observation that isotopic scrambling occurs and isotope effects are possible. Several models were tried, including those which allowed for complete isotopic scrambling and those which allowed only partial scrambling. The simplest model allowed for complete scrambling and no isotope effects[4].

---

[4]Lampe and Field (1959) studied the reaction of $CD_4^+ + C_2H_4$, and observed the following yields: $C_3HD_4^+$: 1/10, $C_3H_3D_2^+$: 2/5, $C_3H_2D_3^+$: 2/5, and $C_3HD_4^+$: 1/10. Statistical yields with no isotope effect would have been: $C_3H_4D^+$: 1/14, $C_3H_5D_2^+$: 3/7, $C_3H_2D_3^+$: 3/7, and $C_3HD_4^+$: 1/14, very

TABLE 5.1

Results of fits of equation (5.3) to kinetic data for the $C_3H_3^+ + C_2H_2$ reaction.[a]

$P_{C_2H_2}$/torr	$k_p'I^0$/Arb. units s^{-1}	θ/s^{-1}
0	1.53(.06)	1.58(.08)
4.4×10^{-7}	1.65(.20)	2.40(.31)
1.0×10^{-6}	1.74(.12)	3.60(.24)
1.6×10^{-6}	1.71(.08)	4.82(.23)
2.0×10^{-6}	1.71(.11)	6.33(.38)

[a]The standard error of estimate computed by the fitting program is shown in parentheses.

---

close to the observed values. Hence, since the $C_3L_8^+$ complex exhibited almost complete scrambling, it is reasonable to expect the $C_5L_5^+$ complex modeled here to undergo complete, or nearly complete scrambling.

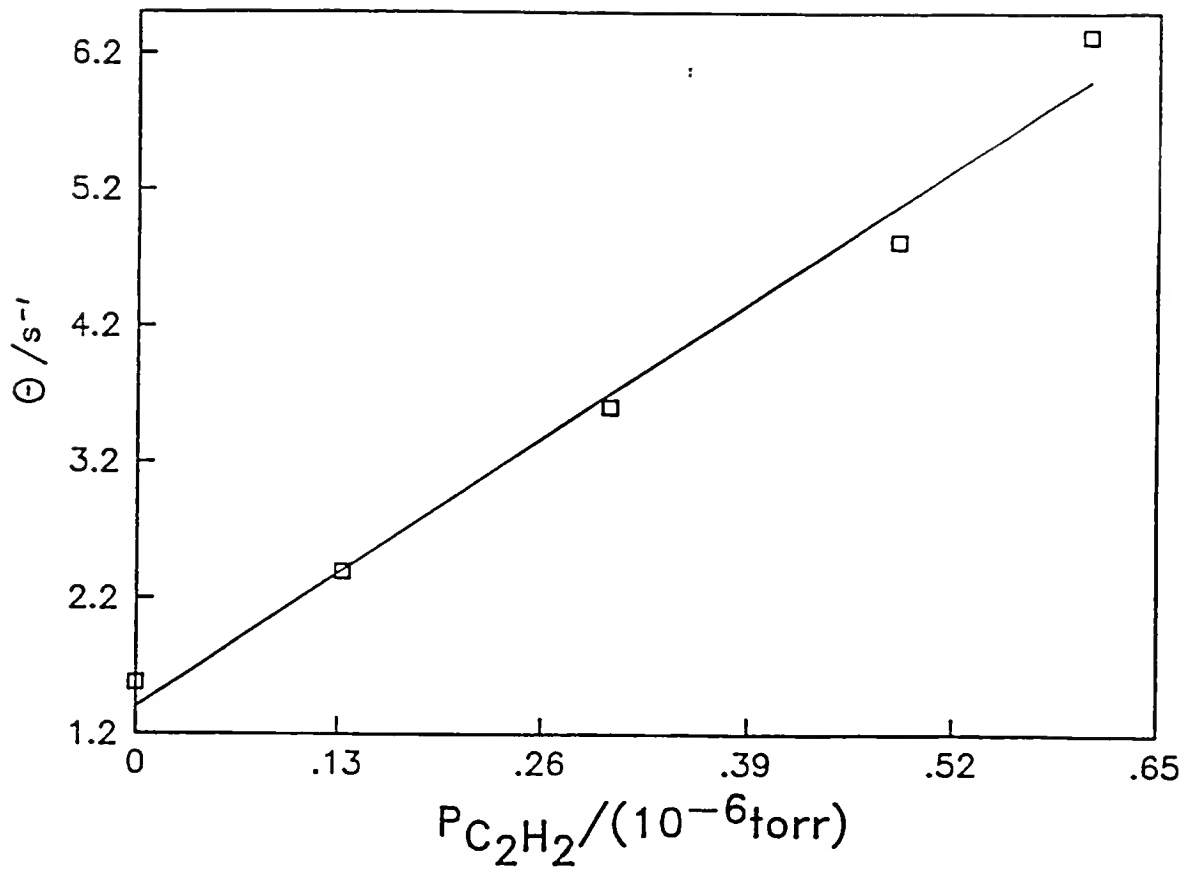

Figure 5.2. The Plot of θ as a Function of Acetylene Pressure (see Equation (5.3)).

Complete scrambling occurs when fragmentation of the complex, $C_5L_5^+$ (L = H, D), yields precursors having a statistical distribution of hydrogen and deuterium atoms. $C_5H_3D_2^+$ will then yield the following ratios of precursors: $C_3H_3^+$ = 1/10, $C_3H_2D^+$ = 3/5, and $C_3HD_2^+$ = 3/10. Using these statistics for obtaining the isotopic distribution in the $C_3L_3^+$ precursors, we obtain the scheme shown in Figure 5.3. With the assumption again that all four $C_5L_5^+$ complexes are in steady-state, a full analytical solution is possible for the set of kinetic differential rate equations. The solutions to the set of equations are given in Appendix II.A. Figure 5.4 shows the best fit curves to a typical data set. Table 5.2 shows the fitted parameters, errors, and residual sum of squares from fits of a typical data set.

An examination of Figure 5.4 shows that the model given by Figure 5.3 does not adequately explain the production of $C_3HD_2^+$. In an attempt to examine this, incomplete, or partial isotopic scrambling was next assumed. To do this correctly requires a detailed knowledge of the chemistry of the system, which is not available. A somewhat crude application of isotope effects applies multiplicative factors to the individual rate constants and this procedure requires but a nominal knowledge of the structure of the

$$\ell\text{-}C_3H_3^+ + C_2D_2 \xrightarrow{k_\ell} C_5H_3D_2^+$$

$$\ell\text{-}C_3H_3^+ + C_3H_3I \xrightarrow{k_p} \text{sink}$$

$$C_5H_3D_2^+ \xrightarrow{k_\ell} \tfrac{1}{10}\,\ell\text{-}C_3H_3^+ + \tfrac{1}{10}\,C_2D_2 + \tfrac{3}{5}\,\ell\text{-}C_3H_2D^+ + \tfrac{3}{5}\,C_2HD + \tfrac{3}{10}\,\ell\text{-}C_3HD_2^+ + \tfrac{3}{10}\,C_2H_2$$

$$C_5H_3D_2^+ \xrightarrow{k_c} \tfrac{1}{10}\,c\text{-}C_3H_3^+ + \tfrac{1}{10}\,C_2D_2 + \tfrac{3}{5}\,c\text{-}C_3H_2D^+ + \tfrac{3}{5}\,C_2HD + \tfrac{3}{10}\,c\text{-}C_3HD_2^+ + \tfrac{3}{10}\,C_2H_2$$

$$\ell\text{-}C_3H_2D^+ + C_2D_2 \xrightarrow{k_\ell} C_5H_2D_3^+$$

$$\ell\text{-}C_3H_2D^+ + C_3H_3I \xrightarrow{k_p} \text{sink}$$

$$C_5H_2D_3^+ \xrightarrow{k_\ell} \tfrac{1}{10}\,\ell\text{-}C_3D_3^+ + \tfrac{1}{10}\,C_2H_2 + \tfrac{3}{5}\,\ell\text{-}C_3HD_2^+ + \tfrac{3}{5}\,C_2HD + \tfrac{3}{10}\,\ell\text{-}C_3H_2D^+ + \tfrac{3}{10}\,C_2D_2$$

$$C_5H_2D_3^+ \xrightarrow{k_c} \tfrac{1}{10}\,c\text{-}C_3D_3^+ + \tfrac{1}{10}\,C_2H_2 + \tfrac{3}{5}\,c\text{-}C_3HD_2^+ + \tfrac{3}{5}\,C_2HD + \tfrac{3}{10}\,c\text{-}C_3H_2D^+ + \tfrac{3}{10}\,C_2D_2$$

$$\ell\text{-}C_3HD_2^+ + C_2D_2 \xrightarrow{k_\ell} C_5HD_4^+$$

$$\ell\text{-}C_3HD_2^+ + C_3H_3I \xrightarrow{k_p} \text{sink}$$

$$C_5HD_4^+ \xrightarrow{k_\ell} \tfrac{3}{5}\,\ell\text{-}C_3HD_2^+ + \tfrac{3}{5}\,C_2D_2 + \tfrac{2}{5}\,\ell\text{-}C_3D_3^+ + \tfrac{2}{5}\,C_2HD$$

$$C_5HD_4^+ \xrightarrow{k_c} \tfrac{3}{5}\,c\text{-}C_3HD_2^+ + \tfrac{3}{5}\,C_2D_2 + \tfrac{2}{5}\,c\text{-}C_3D_3^+ + \tfrac{2}{5}\,C_2HD$$

$$\ell\text{-}C_3D_3^+ + C_2D_2 \xrightarrow{k_\ell} C_5D_5^+$$

$$\ell\text{-}C_3D_3^+ + C_3H_3I \xrightarrow{k_p} \text{sink}$$

$$C_5D_5^+ \xrightarrow{k_\ell} \ell\text{-}C_3D_3^+ + C_2D_2$$

$$C_5D_5^+ \xrightarrow{k_c} c\text{-}C_3D_3^+ + C_2D_2$$

Figure 5.3. Reaction Scheme Postulated for the Kinetic Modeling of the Reaction of linear $C_3H_3^+$ with Deuterated Acetylene Assuming Complete Scrambling and No Isotope Effects.

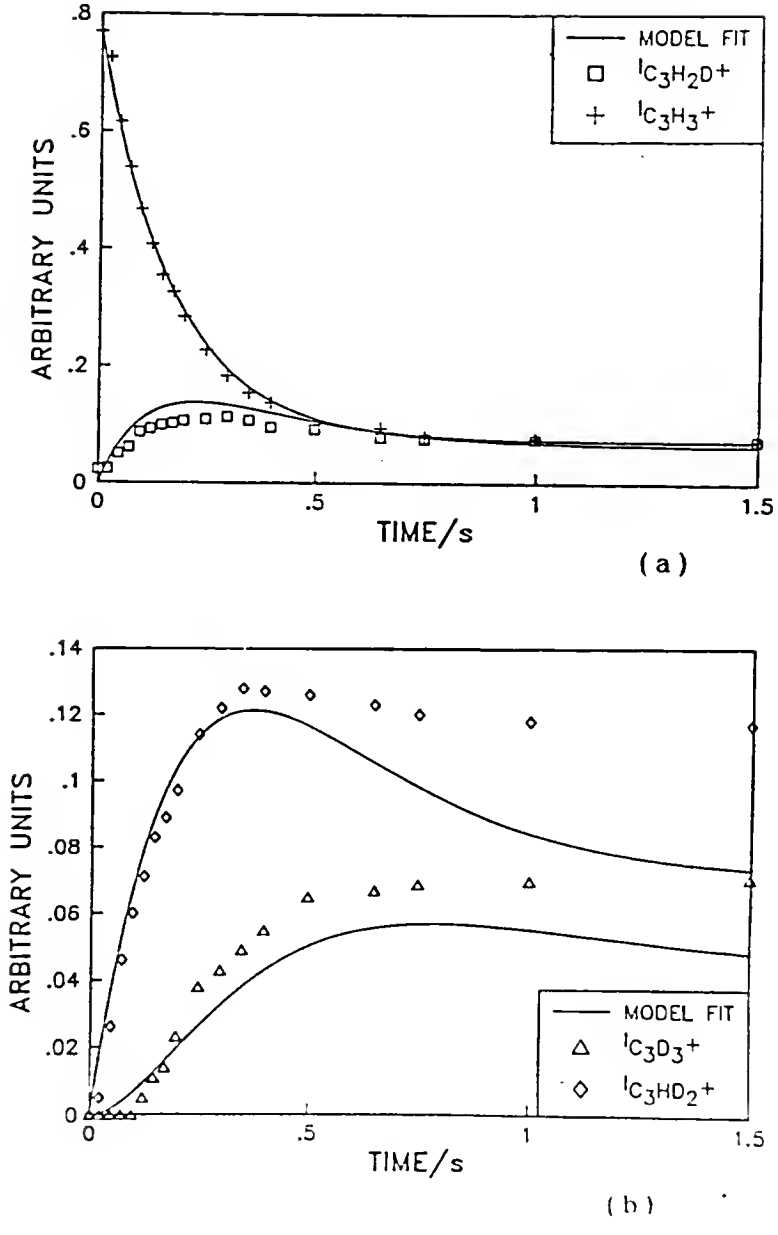

Figure 5.4. Model Fit (using the scheme of Figure 5.3) to a Typical Data Set for $C_3H_3^+ + C_2D_2$ Reactions. Ion Intensity vs. time curves for (a) $C_3H_3^+$ and $C_3H_2D^+$ and (b) $C_3HD_2^+$ and $C_3D_3^+$.

TABLE 5.2

Results of Model Fits (Figures 5.3 and 5.7) for the System $C_3H_3^+$ + C_2D_2 under Various Experimental Conditions.

Pressures (torr)	$k_f P_{C_2D_2}$ (s^{-1})	k_c/k_f	F	$k_p P_{C_3H_3I}$ (s^{-1})	I_f^o (arb units)	I_c^o (arb units)	SOS*
$P_{C_2D_2} = 1.2 \times 10^{-6}$; $P_{C_3H_3I} = 1.1 \times 10^{-7}$	4.17(.15)	.212(.030)	1(fixed)	2.03(.10)	.707(.007)	.063(fixed)	.017
$P_{C_2D_2} = 1.2 \times 10^{-6}$; $P_{C_3H_3I} = 1.1 \times 10^{-7}$	1.11(.14)	.308(.026)	1.86(.11)	2.16(.08)	.703(.005)	.067(fixed)	.0069
$P_{C_2D_2} = 7.8 \times 10^{-7}$; $P_{C_3H_3I} = 1.1 \times 10^{-7}$	.920(.098)	.318(.032)	1.71(.08)	2.20(.09)	.671(.007)	.057(.008)	.0023
$P_{C_2D_2} = 6.2 \times 10^{-7}$; $P_{C_3H_3I} = 1.1 \times 10^{-7}$	1.30(.12)	.389(.026)	1.53(.06)	2.74(.07)	.881(.006)	.100(.006)	.0038
$P_{C_2D_2} = 1.1 \times 10^{-6}$; $P_{C_3H_3I} = 1.3 \times 10^{-7}$	1.86(.34)	.363(.034)	1.58(.13)	2.18(.11)	.856(.007)	.061(fixed)	.024

* Sum of squares.

species involved[5]. This simple scheme was applied as described below.

Quantum mechanical calculations[6] indicate that C_2H_2 does not readily react with the cyclopropenylium cation, but does react with the propargylium cation ($l\text{-}C_3H_3^+$) without barrier with formation of the four possible products shown in Figure 5.5. Thermodynamically, only Structure (5.1) is stable with respect to decomposition to $c\text{-}C_3H_3^+ + C_2H_2$. However, since the $l\text{-}C_3H_3^+ + C_2H_2$ ----> Structure (5.1) reaction is at least 60 kcal/mol exothermic[6] , in the absence of stabilizing collisions this energy then permits many different isomeric forms to be sampled before decomposition back to $C_3H_3^+ + C_2H_2$. If the sampling of all isomers is fast, complete isotopic scrambling is expected. Given the uncertainity in $C_5H_5^+$ structures, total equivalence of carbon atoms in the complex is assumed. For ease of understanding, a cyclic $C_5H_5^+$ complex, in which all C atoms are sp^2 hybridized, might be visualized. With these assumptions, it is a simple matter to determine which carbon atoms undergo hybridization changes during the reaction. For instance, in the attack of C_2H_2 on $l\text{-}C_3H_3^+$, three carbon

---

[5]Although somewhat crude, applying a multiplicative factor to the rate constant for each deuterated site is in keeping with experimental evidence. For instance, in the acetolysis of some identical tosylates, each deuterium atom substitution changed the rate constant by ca. 0.84 (Streitweiser et. al., 1958).

[6]Details of these studies are given in: J. Feng, J. Leszczynski and M. C. Zerner, submitted; and J. Leszczinski, M. C. Zerner and F. Wiseman, submitted.

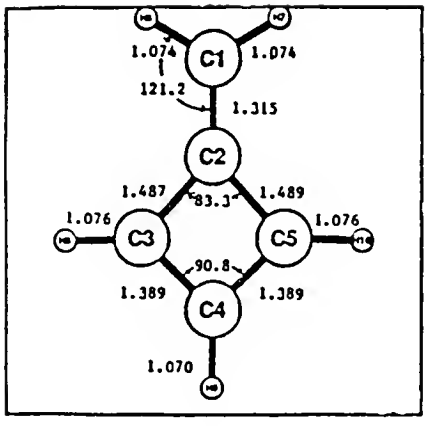

(5.1)

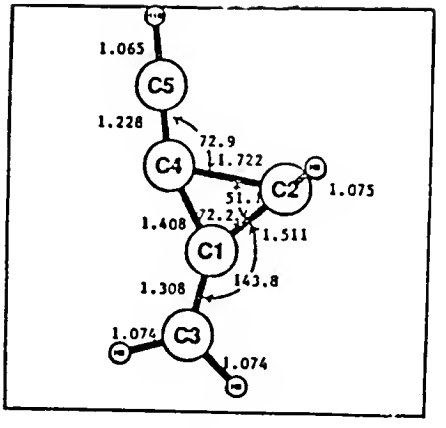

(5.2)

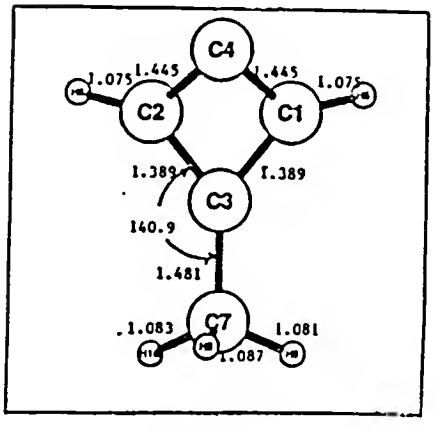

(5.3)

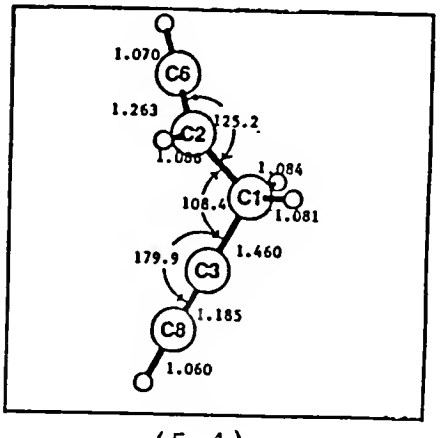

(5.4)

Figure 5.5. $C_5H_5^+$ Structures which are Proposed to Form by the Reaction of Propargylium Ion with Acetylene Without an Energy Barrier.

atoms change from sp to sp^2 hybridized. Upon fragmentation, some carbon atoms remain sp^2 hybridized; others become sp hybridized.

In general, for α-secondary isotope effects, an increase in hybridization in going from the reactant state to the transition state yields an inverse isotope effect ($k_H < k_D$), whereas a decrease in hybridization yields a normal isotope effect ($k_H > k_D$) (Dreuth and Kwart, 1980). In this system the bimolecular addition reaction will have an inverse isotope effect, and the fragmentation reaction should have a normal isotope effect. Figure 5.6 shows how the isotope effects for the reaction of $1\text{-}C_3H_3^+ + C_2L_2$ can arise. For the forward addition reaction, $E_{FH} > E_{FD}$ and for the fragmentation reaction, $E_{RH} < E_{RD}$, in which the subscripts "F" and "R" refer to forward and reverse, respectively, and "H" and "D" refer to protonated and deuterated species, respectively. Since the bimolecular addition is very exothermic for the formation of most $C_5L_5^+$ isomers, it might be expected that the "average" transition state structure might closely resemble the reactants and not any of the $C_5L_5^+$ isomers. This in turn implies that $E_{RD} - E_{RH} > E_{FH} - E_{FD}$ (zero-point effects). However, the excess energy in the reaction will allow longer sampling times for the more energetic $C_5L_5^+$ isomers. The less energetic isomers which are sampled will undoubtedly be in higher rotational and vibrational levels. The overall effect is to

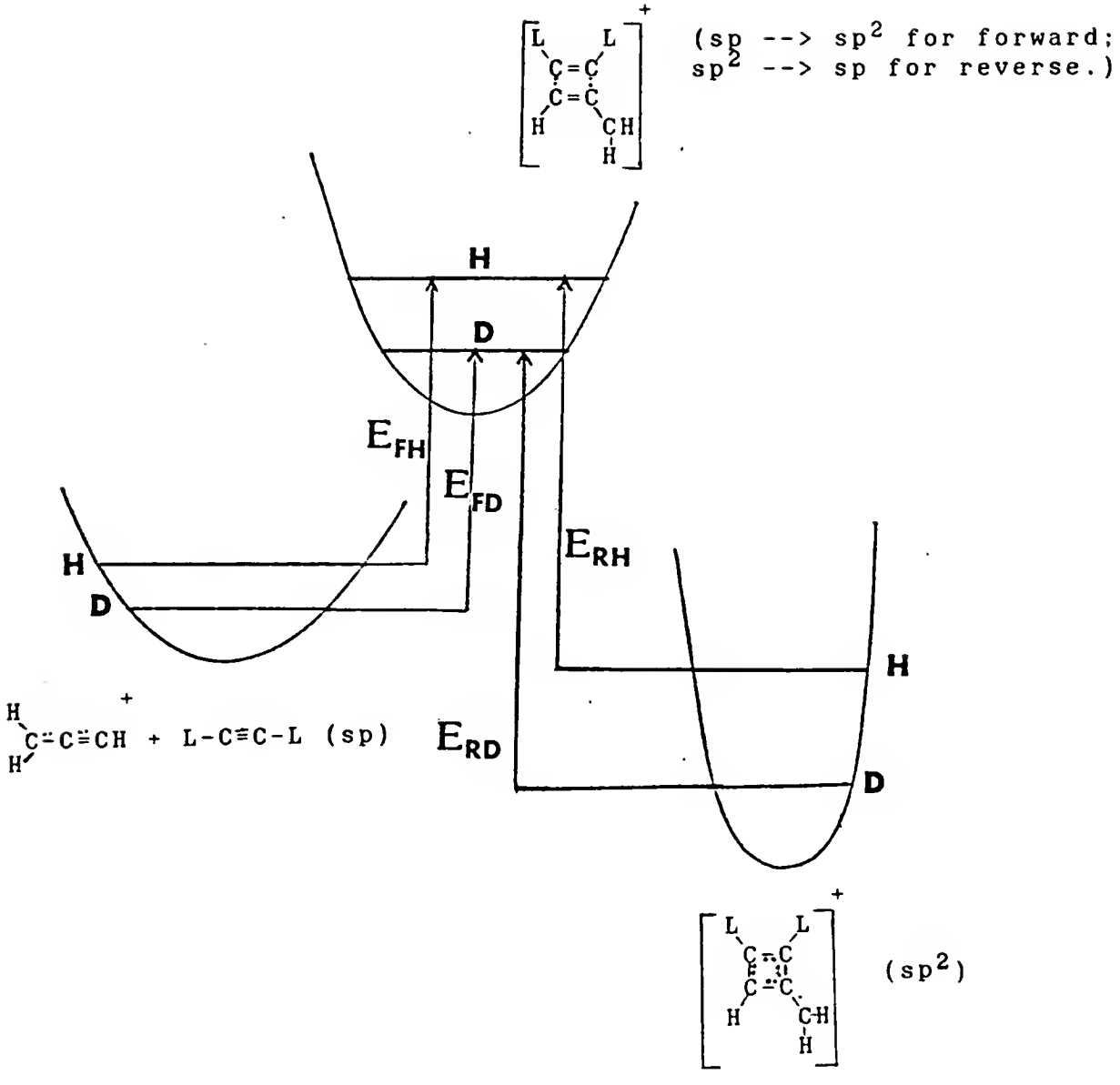

Figure 5.6. A Schematic Representation showing the Qualitative Differences in the Zero-Point Vibration Energy Levels for the Reactants, Transition-State, and a Representative $C_5L_5^+$ Isomer for the Reaction of linear $C_3H_3^+$ with C_2H_2/C_2D_2. (E_{FH}, E_{FD}, E_{RH}, and E_{RD} are explained in the text.)

lessen the normal isotope effects expected in the fragmentation of the $C_5L_5^+$ isomers, unless there are sufficient collisions to stabilize the isomers prior to fragmentation.

In the model development outlined below, only α-secondary isotope effects will be considered important. β-secondary isotope effects, arising predominantly from hyperconjugation, can sometimes be important (Melander, 1960), but will be assumed here to be minor compared to the α-effects. It is also possible that hydride/deuteride shifts may be occurring in the transition- state. However, hydride transfers often exhibit small isotope effects (Melander, and Saunders, 1980) and hydride shifts, if they occur at all, will be assumed here to give negligible contributions to the isotope effects.

Even though the different reactions in Figure 5.3 will have different isotope effects, the introduction of an independent fitting parameter for each type of reaction is not justified. Though crude, only one additional parameter was introduced into the model to account for all potential α-secondary isotope effects. The method for introducing this parameter is outlined as follows.

If a carbon atom bearing a deuterium atom undergoes a hybridization change from sp to sp^2 (force field becoming stronger), the "isotope effect factor", F, is introduced as a multiplicative factor in the rate constant. For two

deuterium atoms, F^2 is the multiplicative factor, etc. If the deuterium atom is attached to an atom changing from sp^2 to sp hybridized, the rate constant is divided by F, for two deuteriums, F^2, etc. Introducing the same factor for both addition and fragmentation reactions implies a constraint which is at best only qualitatively correct. Applied in the numerator the factor corrects for a single deuterium atom (F^2 for two, etc.) attached to a center undergoing hybridization change from sp to sp^2 in the transition-state complex. Applied in the denominator, it corrects for a change from sp^2 to sp hybridization. Since the transition-state complex has a stronger force field than the reactant state ($1\text{-}C_3L_3^+ + C_2L_2$) at these centers, the α-secondary isotope effect will be "inverse" and F should therefore be greater than unity.

Using the structural notation,

$$1\text{-}HDC_3H^+ = [\overset{H}{\underset{D}{\diagdown\diagup}}C\text{-}C\equiv C\text{-}H]^+,\quad 1\text{-}H_2C_3D^+ = [\overset{H}{\underset{H}{\diagdown\diagup}}C\text{-}C\equiv C\text{-}D]^+,$$

$$1\text{-}HDC_3D^+ = [\overset{H}{\underset{D}{\diagdown\diagup}}C\text{-}C\equiv C\text{-}D]^+,\ \text{and}\ 1\text{-}D_2C_3H^+ = [\overset{D}{\underset{D}{\diagdown\diagup}}C\text{-}C\equiv C\text{-}H]^+,$$

the full kinetic scheme is shown in Figure 5.7. The neutral fragmentation products, C_2H_2, C_2HD, and C_2D_2, have not been included for brevity. It is assumed that $1\text{-}C_3L_3^+$ undergoes the same kind of hybridization changes when reacting with C_3H_3I as it does with C_2L_2. As shown in Chapter 4, the

$$\ell\text{-}C_3H_3^+ + C_2D_2 \xrightarrow{F^2k_\ell} C_5H_3D_2^+$$

$$\ell\text{-}C_3H_3^+ + C_3H_3I \xrightarrow{k_p} \text{sink}$$

$$C_5H_3D_2^+ \xrightarrow{k_\ell} \frac{1}{10F^2}\,\ell\text{-}C_3H_3^+ + \frac{2}{5F}\,\ell\text{-}HDC_3H^+ + \frac{1}{5F^2}\,\ell\text{-}H_2C_3D^+ + \frac{1}{5F}\,\ell\text{-}HDC_3D^+ + \frac{1}{10}\,\ell\text{-}D_2C_3H^+$$

$$C_5H_3D_2^+ \xrightarrow{k_c} \frac{1}{10F^2}\,c\text{-}C_3H_3^+ + \frac{3}{5F}\,c\text{-}C_3H_2D^+ + \frac{3}{10}\,c\text{-}C_3HD_2^+$$

$$\ell\text{-}HDC_3H^+ + C_2D_2 \xrightarrow{F^2k_\ell} C_5H_2D_3^+$$

$$\ell\text{-}H_2C_3D^+ + C_2D_2 \xrightarrow{F^3k_\ell} C_5H_2D_3^+$$

$$\ell\text{-}HDC_3H^+ + C_3H_3I \xrightarrow{k_p} \text{sink}$$

$$\ell\text{-}H_2C_3D^+ + C_3H_3I \xrightarrow{Fk_p} \text{sink}$$

$$C_5H_2D_3^+ \xrightarrow{k_\ell} \frac{1}{10F}\,\ell\text{-}C_3D_3^+ + \frac{2}{5F^2}\,\ell\text{-}HDC_3D^+ + \frac{1}{5F}\,\ell\text{-}D_2C_3H^+ + \frac{1}{5F^2}\,\ell\text{-}HDC_3H^+ + \frac{1}{10F^3}\,\ell\text{-}H_2C_3D^+$$

$$C_5H_2D_3^+ \xrightarrow{k_c} \frac{1}{10}\,c\text{-}C_3D_3^+ + \frac{3}{5F}\,c\text{-}C_3HD_2^+ + \frac{3}{10F^2}\,c\text{-}C_3H_2D^+$$

$$\ell\text{-}HDC_3D^+ + C_2D_2 \xrightarrow{F^3k_\ell} C_5HD_4^+$$

$$\ell\text{-}D_2C_3H^+ + C_2D_2 \xrightarrow{F^2k_\ell} C_5HD_4^+$$

$$\ell\text{-}HDC_3D^+ + C_3H_3I \xrightarrow{Fk_p} \text{sink}$$

$$\ell\text{-}D_2C_3H^+ + C_3H_3I \xrightarrow{k_p} \text{sink}$$

$$C_5HD_4^+ \xrightarrow{k_\ell} \frac{2}{5F^2}\,\ell\text{-}C_3D_3^+ + \frac{2}{5F^3}\,\ell\text{-}HDC_3D^+ + \frac{1}{5F^2}\,\ell\text{-}D_2C_3H^+$$

$$C_5HD_4^+ \xrightarrow{k_c} \frac{2}{5F}\,c\text{-}C_3D_3^+ + \frac{3}{5F^2}\,c\text{-}C_3HD_2^+$$

$$\ell\text{-}C_3D_3^+ + C_2D_2 \xrightarrow{F^3k_\ell} C_5D_5^+$$

$$\ell\text{-}C_3D_3^+ + C_3H_3I \xrightarrow{Fk_p} \text{sink}$$

$$C_5D_5^+ \xrightarrow{k_\ell/F^3} \ell\text{-}C_3D_3^+$$

$$C_5D_5^+ \xrightarrow{k_c/F^2} c\text{-}C_3D_3^+$$

Figure 5.7. Reaction Scheme Postulated for the Kinetic Modeling of the Reaction of linear $C_3H_3^+$ with Deuterated Acetylene Assuming Complete Scrambling and α-secondary Isotope Effects.

products of the $1\text{-}C_3L_3^+ + C_3H_3I$ reaction are of higher mass and do not enter further into the kinetic schemes modeled here.

Steady-state conditions are applied for all four $C_5L_5^+$ isotopic species as before (without regard for isomeric differentiation) and the differential rate equations for scheme shown in Figure 5.7 are given in Appendix II.B. Table 5.2 shows fitting results for several data sets using the same kinetic scheme. Figure 5.8 shows plots of the best fit of this model to the same data set as fitted in Figure 5.4.

Some experiments were conducted where certain ions were ejected from the analyzer cell using FTICR double resonance techniques (Comisarow et. al., 1978) as they formed. Among the ions ejected were $C_3H_2D^+$ and $C_3HD_2^+$. Without further fitting, this model was used to predict the behavior of the kinetic system if these ions were ejected. Figure 5.9 shows predicted results and data points.

Models for $C_3H_3^+ + C_4H_2$. The reaction of $C_3H_3^+$ with C_4H_2 (diacetylene) is kinetically more complicated than that of $C_3H_3^+$ with C_2H_2. There are more isomeric possibilities, and ion/molecule reaction products of higher m/z are detected. Several models were tried in attempts to fit the experimental data, and the best of these made the assumptions that $C_7H_5^+$ and the excited forms of $C_9H_5^+$ and

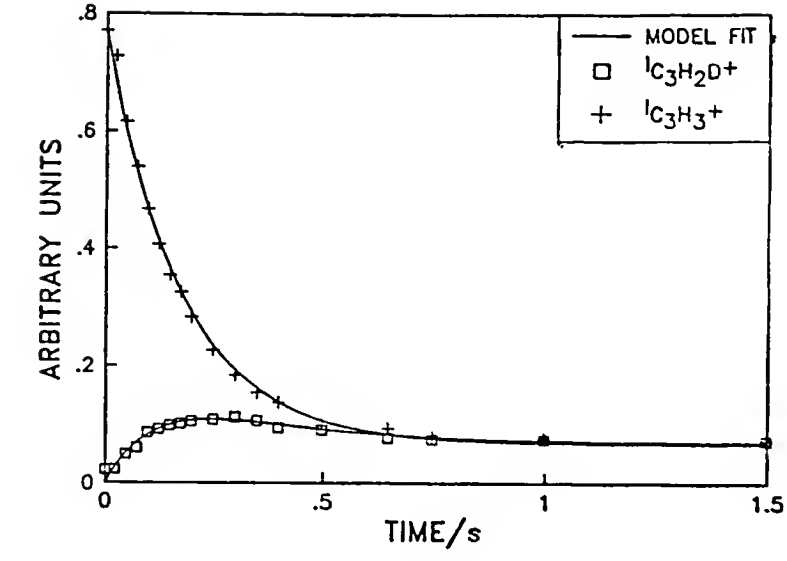

(a)

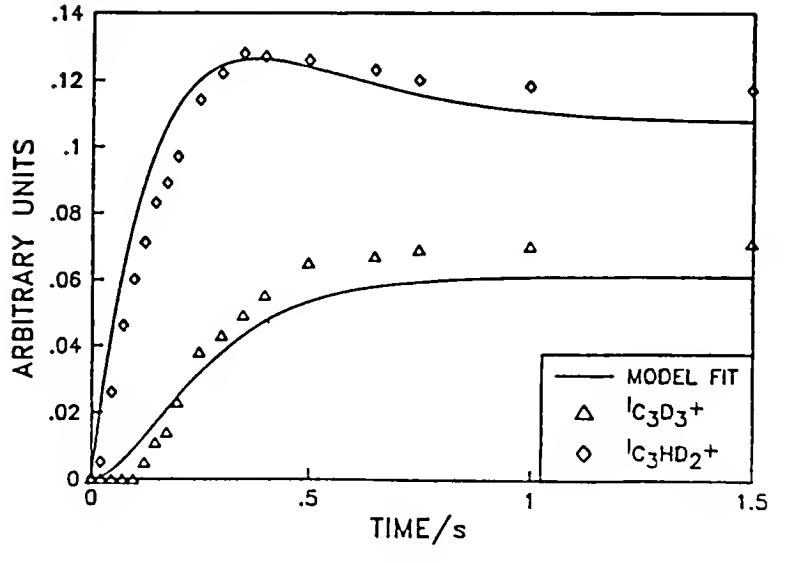

(b)

Figure 5.8. Model Fit (using the scheme of Figure 5.7) to a Typical Data set for linear $C_3H_3^+ + C_2D_2$ Reactions. Ion intensity vs. time curves for (a) $C_3H_3^+$ and $C_3H_2D^+$ and (b) $C_3HD_2^+$ and $C_3D_3^+$.

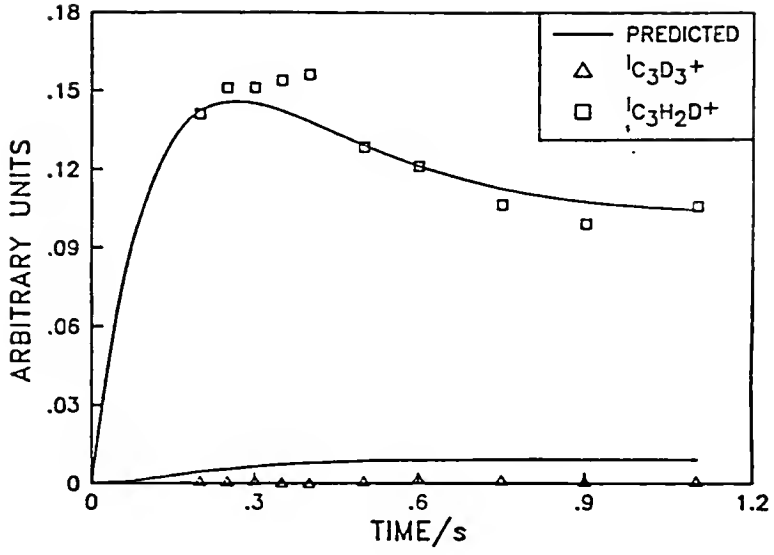

(a)

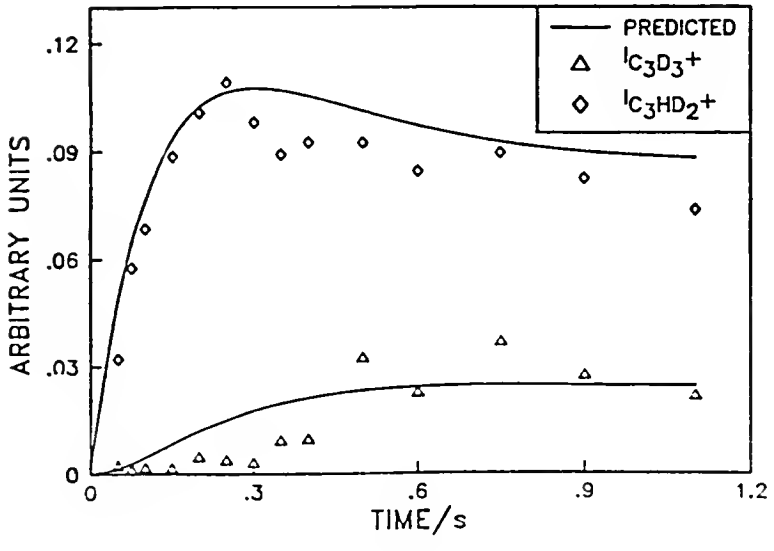

(b)

Figure 5.9. Data from Ejection Studies and Model Prediction. (a) $C_3HD_2^+$ ion is ejected, (b) $C_3H_2D^+$ ion is ejected. (Poor signal/noise raios of experimental data points are due to the effect of the ejection pulse on the neighboring ion.)

$C_{11}H_5^+$ are in steady state, while $C_5H_3^+$ and $C_7H_3^+$ are not. In order to account for the build-up of $C_9H_5^+$ and $C_{11}H_5^+$ ions, it was necessary to include stabilization steps for the excited forms of these ions. A further assumption was made that the stabilized forms of $C_9H_5^+$ and $C_{11}H_5^+$ are not reactive within the time frame (2s) of the experiments. The resulting scheme is shown in Figure 5.10. Reactions involving $C_8H_6I^+$ are included because $C_8H_6^+$ is detected in the ICR experiments. Applying steady-state assumptions to the $C_7H_5^+$, $C_9H_5^+$, $C_{11}H_5^+$, and $C_8H_6^+$ ions yields a model with a full analytical solution (Appendix II.C). Figure 5.11 shows results of the model fit to a typical data set. The kinetic parameters have been grouped as exponential and pre-exponential terms in the equations, yielding 9 fitting parameters. Table 5.3 shows results of model fits of two data sets. The term $k_{p2}P_{C_3H_3I}$, is $-(\theta_2 + k_{-21}\phi_2 + k_{s1}\phi_2)$, and hence can be calculated from the parameters. The results of the first data set fit in Table 5.3 yield $k_{p2}P_{C_3H_3I} = 1.2(0.3)\ s^{-1}$; from the second data set fit, $k_{p2}P_{C_3H_3I} = 1.3\ (0.2)\ s^{-1}$.

Discussion

$\underline{C_3H_3^+ + C_2H_2/C_2D_2}$. Several insights into the mechanism of the $C_3H_3^+ + C_2H_2/C_2D_2$ reactions are obtained from these modeling studies. First, a value of 1.4 (0.2) s^{-1} is obtained for k_p' from the intercept of Figure 5.2 (values

$$\ell\text{-}C_3H_3^+ + C_4H_2 \xrightarrow{k_{f1}} C_7H_5^+$$

$$\ell\text{-}C_3H_3^+ + C_3H_3I \xrightarrow{k_{p1}} C_6H_6I^+$$

$$C_7H_5^+ \xrightarrow{k_{-11}} C_5H_3^+ + C_2H_2$$

$$C_7H_5^+ \xrightarrow{k_{-12}} \ell\text{-}C_3H_3^+ + C_4H_2$$

$$C_7H_5^+ \xrightarrow{k_{-13}} c\text{-}C_3H_3^+ + C_4H_2$$

$$C_5H_3^+ + C_4H_2 \xrightarrow{k_{f2}} C_9H_5^+$$

$$C_5H_3^+ + C_3H_3I \xrightarrow{k_{p2}} C_8H_6I^+$$

$$C_9H_5^+ \xrightarrow{k_{-21}} C_7H_3^+ + C_2H_2$$

$$C_9H_5^+ \xrightarrow{k_{-22}} C_5H_3^+ + C_4H_2$$

$$C_9H_5^+ \xrightarrow{k_{s1}} C_9H_5^+ \text{ (stabilized)}$$

$$C_7H_3^+ + C_4H_2 \xrightarrow{k_{f3}} C_{11}H_5^+$$

$$C_7H_3^+ + C_3H_3I \xrightarrow{k_{p3}} C_{10}H_6I^+$$

$$C_{11}H_5^+ \xrightarrow{k_{-31}} C_9H_3^+ + C_2H_2$$

$$C_{11}H_5^+ \xrightarrow{k_{-32}} C_7H_3^+ + C_4H_2$$

$$C_{11}H_5^+ \xrightarrow{k_{s2}} C_{11}H_5^+ \text{ (stabilized)}$$

$$C_8H_6I^+ \xrightarrow{k_I} C_8H_6^+ + I$$

$$C_8H_6^+ \xrightarrow{k_d} \text{sink}$$

Figure 5.10. Reaction Scheme Postulated for the Kinetic Modeling of the Reaction of linear $C_3H_3^+$ with Diacetylene.

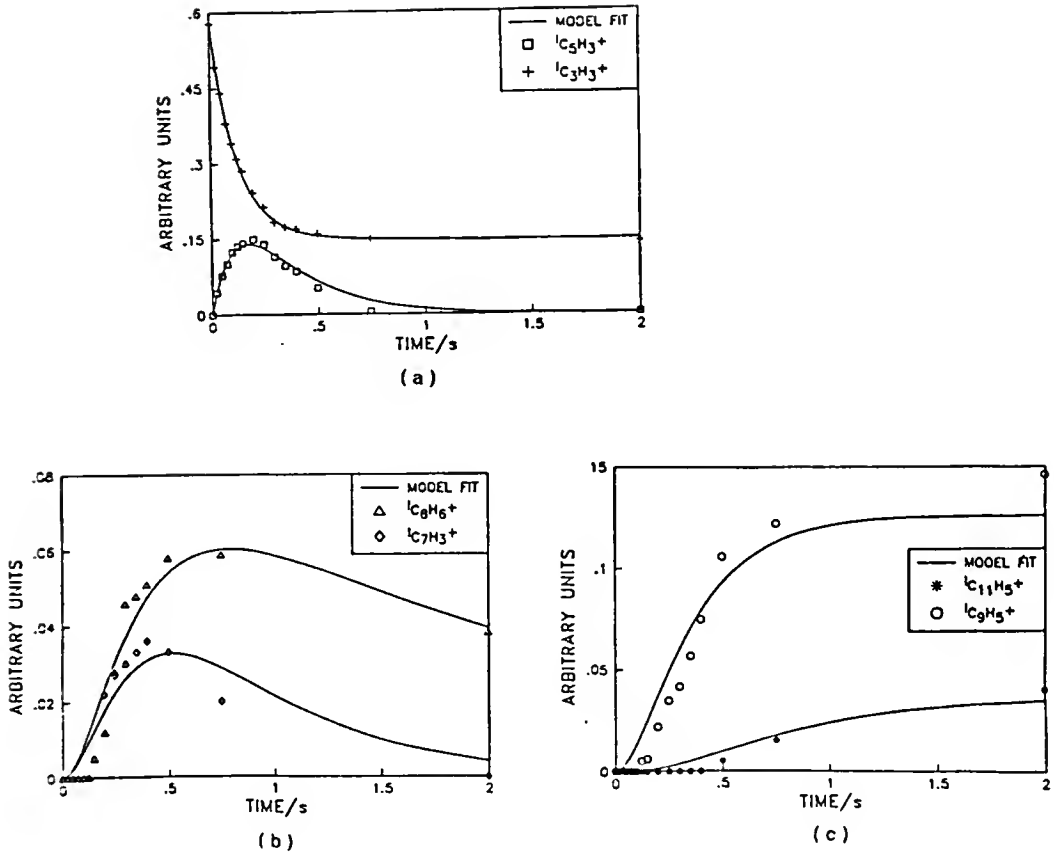

Figure 5.11. Model Fit (using the scheme of Figure 5.10) to a Typical data Set for linear $C_3H_3^+ + C_4H_2$ Reactions. Ion Intensity vs. time curves for (a) $C_3H_3^+$ and $C_5H_3^+$, (b) $C_7H_3^+$ and $C_8H_6^+$, and (c) $C_9H_5^+$ and $C_{11}H_5^+$.

TABLE 5.3

Results of Model Fits (Figure 5.10) for the System $C_3H_3^+ + C_4H_2$ under Various Experimental Conditions.*

Pressures (torr)	$\theta_1(s^{-1})^{\ddagger}$	$\theta_2(s^{-1})^{\ddagger}$	$\theta_3(s^{-1})^{\ddagger}$	$(1-k_{-31}\phi_1/\theta_1)I_{\ell}^{o\ddagger}$ (Arb units)	$k_{-11}\phi_1 I_{\ell}^{o}/\theta_{12}^{\ddagger}$ (Arb units)
$P_{C_3H_3I} = 1.1 \times 10^{-7}$; $P_{C_4H_2} = 4.8 \times 10^{-7}$; $P_{X_e} \cong 6.2 \times 10^{-6}$;	-8.1(.2)	-3.9(.2)	-1.9(.7)	.743(.007)	-.93(.07)
$P_{C_3H_3I} = 1.4 \times 10^{-7}$; $P_{C_4H_2} = 5.7 \times 10^{-7}$; $P_{X_e} \cong 5.3 \times 10^{-6}$;	-8.4(.2)	-3.9(.1)	-3.4(.7)	.829(.007)	-1.23(.08)

	$k_{-21}\phi_2(s^{-1})^{\ddagger}$	$k_{s1}\phi_2(s^{-1})^{\ddagger}$	$k_{s2}\phi_3(s^{-1})^{\ddagger}$	$k_d(s^{-1})$	SOS
	1.0(.1)	1.79(.07)	1.0(.3)	.5(.1)	.0051
	1.2(.1)	1.45(.05)	.7(.2)	.2(.2)	.015

* Initial readings were scaled to one arbitrary unit for comparison.

‡ $\theta_1 = -(k_{-11} + k_{-13})k_{f1} P_{C_4H_2}/(k_{-11} + k_{-12} + k_{-13}) - k_{p1} P_{C_3H_3I}$; $\theta_2 = -(k_{-21} + k_{s1})k_{f2} P_{C_4H_2}/(k_{-21} + k_{-22} + k_{s1}) - k_{p2} P_{C_3H_3I}$; $\theta_3 = -(k_{-31} + k_{s2})k_{f3} P_{C_4H_2}/(k_{-31} + k_{-32} + k_{s2}) - k_{p3} P_{C_3H_3I}$; $\phi_1 = k_{f1} P_{C_4H_2}/(k_{-11} + k_{-12} + k_{13})$; $\theta_{12} = \theta_1 - \theta_2$; $\phi_2 = k_{f2} P_{C_4H_2}/(k_{-21} + k_{-22} + k_{s1})$; $\phi_3 = k_{f3} P_{C_4H_2}/(k_{-31} + k_{-32} + k_{s2})$.

for k_p' are a little higher from model fits shown in Table 5.2). Assuming a cell temperature of 363K and given that $P_{C_3H_3I} = 3.3 \times 10^{-8}$ torr (after system factor correction), $k_p = 1.6\ (0.2) \times 10^{-9}$ cm^3 s^{-1}, in good agreement with an experimentally determined value[7]. Second, the model gives branching ratios for the complex $C_5L_5^+$. The ratio, k_c/k_l, is ca. 0.34 (.03) (Table 5.2), implying that $C_5L_5^+$ fragments to l-$C_3H_3^+$ at a rate three times that of fragmentation to c-$C_3H_3^+$. Since c-$C_3H_3^+$ is thermodynamically more stable than l-$C_3H_3^+$ by ca. 25 kcal mol^{-1} (Lossing, 1972), any factor affecting the internal energy of $C_5L_5^+$, such as a collisional stabilization, will undoubtedly affect the ratio k_c/k_l. Hence, k_c/k_l is probably very sensitive to experimental conditions (method of ionization, total pressure, and temperature). Finally the "direction" and magnitude of F (1.67 (.10)) suggest not only that the model is reasonable, but that the isotope effect plays an important part in the overall kinetics.

It should be remembered that F is not an overall isotope effect; isotope effects are ratios of rate constants. The magnitude of F does, however, indicate the kinetic contribution of replacing one hydrogen atom with a deuterium atom on a hydrogenic site undergoing a hybridization change in the transition-state structure. F is

---

[7] $k_p = (3.0 \pm 1.2) \times 10^{-9}$ cm^3 mol^{-1} s^{-1} was determined experimentally using a typical reaction conditions given in Chapter 4.

the α-secondary kinetic isotope effect for the elementary bimolecular addition reactions per hydrogenic site (only those sites giving rise to α-secondary effects included). 1/F is the isotope effect for the elementary fragmentation reactions (to l-$C_3H_3^+$ and c-$C_3H_3^+$) per hydrogenic site (again only those sites giving rise to α-secondary effects included). Because of the complexity of the scheme in Figure 5.7, overall isotope effects cannot be obtained by determining product ratios, as is often done in isotopic studies of more elementary ion/molecule reactions. However, F can be compared to isotope effects found in elementary ion/molecule reactions.

α-secondary kinetic isotope effects can be quite large (Mead, et.al., 1980; Tumas, et. al., 1987). The larger effects found in ion/molecule reactions are due to a narrow (non- Boltzmann) energy distribution centered close to the threshold energy (Derrick, 1983). The magnitude of the isotope effect factor, F, indicates a fair amount of bond rearrangement in the transition state structures. Due to the number of assumptions and the indirect method for obtaining F, it is not attempted to calculate isotope effects from molecular models and calculated vibrational frequencies.

$\underline{C_3H_3^+ + C_4H_2}$. Kinetic data and modeling of this system reveal some insight into the mechanism for the reaction of $C_3H_3^+$ and C_4H_2. Although the scheme shown in Figure 5.10

does not account for specific isomeric reactivities, the scheme does account reasonably well for the data. The signal-to-noise ratios of the available data do not warrant further refinements of the model. Several crude models were attempted, and the model reported here may not be the best or only model which can adequately explain the results. However, of the variations of the scheme in Figure 5.10 which were tried, the one reported gave the best fitting results. In particular, a scheme was tried in which stable forms of $C_9H_5^+$ and $C_{11}H_5^+$ were formed from the corresponding bimolecular additions reactions rather than requiring stabilization steps of "hot" $C_9H_5^+$ and $C_{11}H_5^+$ ions. This scheme did not fit the data. Apparently, only in the ions larger than $C_7H_5^+$ are there enough internal vibrational modes to give rise to an ion/molecule collision complex of sufficient lifetime to allow collisional stabilization at these pressures.

Interestingly, the value for k_{p2} in the scheme of Figure 5.10 is the same, within error, as the value for k_p in the scheme of Figure 5.7. The ratio of the reduced masses of the two reacting systems $(C_3H_3^+ + C_3H_3I)/(C_5H_3^+ + C_3H_3I)$ is 0.83, which is well within the error for the value of k_{p2}/k_p. Hence, it cannot be determined from this comparison whether the reactions with C_3H_3I are collision-controlled or not. However, if the reactions of $C_3L_3^+$ with C_3H_3I and C_2L_2 are collision-controlled, there

would only be a small kinetic isotopes effect arising from the rotational partition functions. If the scheme in Figure 5.7 is correct, there is a transition-state structure for the reaction of $C_3H_3^+$ and C_2H_2, and undoubtedly with $C_3H_3^+$ and C_4H_2 as well, which does have bond changes. This implies that the rate is predicted to be lower than collision-controlled.

Figure 5.10 does not show $C_5H_5^+$ and $C_7H_3^+$ fragmenting to any products. Undoubtedly any isomers of $C_5H_3^+$ and $C_7H_3^+$ which form are all resonance-stabilized. Any fragmentation product would be highly energetic and unlikely to form, even at the energy levels available in these reacting systems. Hence, once $C_5H_3^+$ and $C_7H_3^+$ are formed, they will react only in bimolecular addition reactions, which are orders of magnitude slower than the unimolecular fragmentation reactions of $C_7H_5^+$, $C_9H_5^+$, and $C_{11}H_5^+$. Hence, there is a non-steady-state build up of $C_5H_3^+$ and $C_7H_3^+$ ions at the first part of the reaction.

CHAPTER 6

REACTIONS OF $C_5H_3^+$ AND $C_5H_5^+$ IONS WITH ACETYLENE AND DIACETYLENE

Introduction

According to the proposed ion/molecule mechanism of soot formation (Calcote, 1981; Olson and Calcote, 1981a), $C_3H_3^+$ forms $C_5H_3^+$ and $C_5H_5^+$ in reactions with acetylene, and $C_7H_5^+$ when reacting with diacetylene. However, as seen in Chapter 4, investigation of the reactions of $C_3H_3^+$ with acetylene and diacetylene did not reveal facile formation of $C_5H_3^+$ or $C_5H_5^+$ by reaction of this ion with acetylene, although $C_3H_3^+$ did react readily with diacetylene, yielding $C_5H_3^+$ and $C_7H_3^+$. All three of the postulated products of $C_3H_3^+$ reactions with acetylene and diacetylene ($C_5H_3^+$, $C_5H_5^+$, $C_7H_5^+$) have been identified by mass spectrometry (Michaud et al., 1981; Olson and Calcote, 1981b) in flames, but it remains to be determined which, if any, of them may be important in soot formation mechanisms.

Heats of formation of the $C_5H_3^+$ ion from different precursors have been reported in three experimental studies (Franklin and Carroll, 1969; Dannacher et al., 1979; Baer et al., 1979). Dannacher, et al (1979) suggested the presence of two different linear structures, $CH_3-C\equiv C-C\equiv C^+$ and $HC\equiv C-C\equiv C-CH_2^+$ for the $C_5H_3^+$ ions produced by $.CH_3$ and H.

loss from 2,4-hexadiyne and 1,3-pentadiyne parent ions, respectively.

There are many possible structures for the $C_5H_5^+$ ion, and despite a number of theoretical and experimental studies involving it, few definitive results exist regarding the specific relative energies of various isomeric forms. Experimental studies concentrated on determining the appearance potential and heats of formation of $C_5H_5^+$ ions from different sources by mass spectrometric methods (Pottie and Lossing 1963; Dorman, 1965; Harrison et al., 1965; Occolowitz and White, 1968; Franklin and Carroll, 1969; Lossing and Traeger, 1975; McCreary and Freiser, 1978). These resulted in heat of formation values ranging from 239 to 309 kcal/mole depending on the source and technique of $C_5H_5^+$ production. Probably the best estimate of heat of formation is for the cyclopentadienyl ion (ΔH_f = 255 kcal/mole), obtained by Lossing and Traeger (1975) from measurement of the ionization potential of the cyclopentadienyl radical with an electron monochromator-mass spectrometer. Other than this, all the ΔH_f's measured from different sources using electron impact techniques fall into two categories: 270-290 kcal/mole and 300-309 kcal/mole. Evaluating these differences in terms of different isomeric structures cannot be justified considering the large uncertainty in the internal energies of ions which may be present following electron impact ionization. Early ICR

experiments were carried out to identify structures of $C_5H_5^+$ according to their reactivity with different neutrals (Brill and Eyler, 1981; Buckley, 1982; Brill, 1983, Eyler, 1984). Several precursors were used in the formation of $C_5H_5^+$ ions and the results of the reactivity studies indicated the possibility of four different isomers of $C_5H_5^+$ (Brill, 1983). Acetylene reacted quite slowly with the $C_5H_5^+$ ions (Buckley, 1982; Brill, 1983) while diacetylene and aromatics with side chains reacted at an appreciable rate (Buckley, 1982). As a result, it has been suggested that soot nucleation may proceed by adding a few large molecules rather than through addition of many smaller ones (Buckley, 1982; Baykut et al., 1986). No definitive assignment of $C_5H_5^+$ isomeric structure was possible in the earlier studies (Buckley, 1982; Brill, 1983). Proton-transfer reactions involving one relatively unreactive $C_5H_5^+$ isomer gave (Buckley, 1982) a proton affinity of 227.9 $\pm$ 0.3 kcal/mole for the C_5H_4 neutral which remained after proton transfer. When combined with estimates of the heats of formation of possible C_5H_4 species, the results were consistent with (but did not conclusively prove) a vinylcyclopropenylium form for the $C_5H_5^+$ isomer.

A number of theoretical studies have examined $C_5H_5^+$ structures (Stohrer and Hoffman, 1972; Hehre and Schleyer, 1973; Dewar and Haddon, 1973; Kollmar et al, 1973; Borden and Haddon, 1979). Schleyer and co-workers located two

minimum energy forms on the $C_5H_5^+$ potential surface, the more stable one corresponding to planar cyclopentadienyl, the other one to a square-based pyramid structure (Kollmar et al, 1973; Hehre and Schleyer, 1973). Similar results were reported by Stohrer and Hoffman (1972) although they proposed the pyramidal structure as the more stable form compared to the planar cyclopentadienyl. Recent calculations[8] have shown that the vinylcyclopropenylium ion has the lowest energy (ΔH_f = 256.7 kcal/mole) among a number of other possible structures as shown in Figure 6.1. All of these structures were found to be no more than 30 kcal/mole higher in energy than the lowest energy structure[7].

In this work, the kinetics and reaction mechanisms of $C_5H_3^+$ and $C_5H_5^+$ ions produced from different precursors and reacting with acetylene and diacetylene have been studied in order to identify isomeric structures and to obtain rate coefficients. Also, the energetics of $C_5H_5^+$ formation from norbornadiene and cycloheptatriene were followed to investigate two possible competing pathways of $C_5H_5^+$ formation which could lead to different isomeric structures.

Experimental

Reaction rate coefficients were determined by monitoring the intensity of the $C_5H_3^+$ or $C_5H_5^+$ ions, respectively, as a function of time after ejection of all

---

[8] J. Feng, J. Leszczynski and M. C. Zerner, submitted.

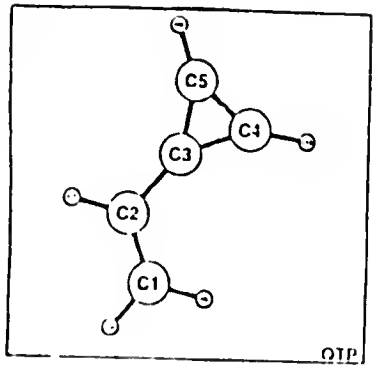

(6.1)
ΔH_f = 256.7kcal/mol

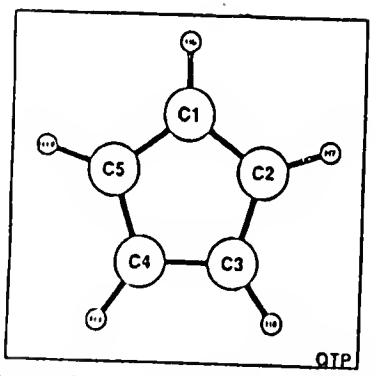

(6.2) is triplet, and
(6.3) is singlet[a]

ΔH_f = 265.9kcal/mol

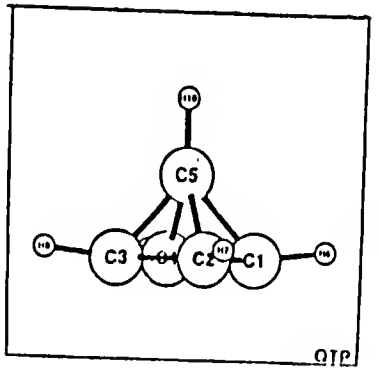

(6.4)
ΔH_f = 269.6kcal/mol

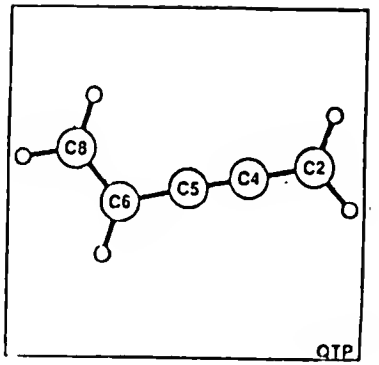

(6.6)
ΔH_f = 274.7kcal/mol

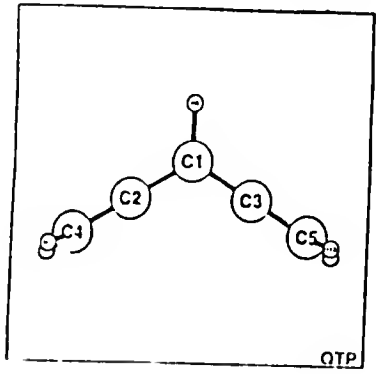

(6.7)
ΔH_f = 277.7kcal/mol

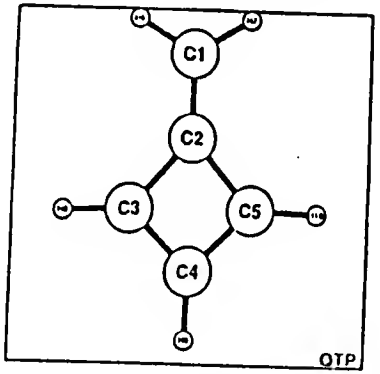

(6.8)
ΔH_f = 278.3kcal/mol

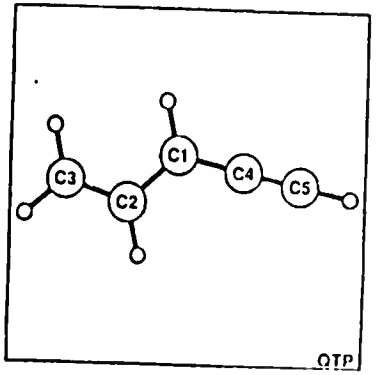

(6.9)
ΔH_f = 283.0kcal/mol

Figure 6.1. $C_5H_5^+$ Structures and Theoretical Heats of Formation. [a](6.5) is also a singlet cyclopentadienyl structure with ΔH_f = 273.1 kcal/mol.

other ions from the analyzer cell. Excitation amplitude and total pressure were kept constant at optimized values for all the kinetic runs in order to minimize the unwanted effects of such factors on ion intensities, which have been discussed in detail elsewhere.[9]

$C_5H_3^+$ ions were produced by 50 eV electron ionization of 2,4-hexadiyne and by the reaction of $C_3H_3^+$ with diacetylene. $C_3H_3^+$ ions used to produce $C_5H_3^+$ were formed by Xe^+ charge transfer reactions with propargyl iodide at an ionizing energy of 15 eV. After 30 ms reaction time with C_4H_2, all the other ions except $C_5H_3^+$ were ejected from the cell to follow the reactions of this ion with diacetylene as a function of time. $C_5H_5^+$ ions were produced by charge transfer reactions of various precursors (dicyclopentadiene, cyclopentadiene, norbornadiene, 1-penten-3-yne, cycloheptatriene) with different charge transfer agents (Xe^+, N_2^+, Ar^+) formed with an electron beam pulse of 5 ms duration at an ionizing energy of 13, 16.5, and 20 eV, respectively.

Cyclopentadiene was prepared by cracking dicyclopentadiene and was kept in dry ice when not used to prevent the dimerization process. All the other compounds used were obtained commercially and their purity was checked

---

[9]M. Moini and J. R. Eyler, to be published.

by obtaining wide mass range spectra. All the samples were used after multiple freeze-pump-thaw cycles.

All reactions were followed at a cell temperature of 363 K. Some $C_5H_3^+$ and all $C_5H_5^+$ ions used in rate constant determination studies were produced by chemical reactions in order to minimize the internal energy imparted to the ions. Also, since the total pressure in the reaction cell was almost 1×10^{-5} torr and the reactant ion formation time was $\geq$30 ms, substantial collisional relaxation of the ions took place before kinetic data were collected.

Results

Reactions of $C_5H_3^+$. A very low number of $C_5H_3^+$ ions were produced from 2,4-hexadiyne at electron energies above 30 eV. Reactivity of these ions was monitored at an electron energy of 50 eV although the ion intensity was still very low. Although almost all of the $C_5H_3^+$ ions produced reacted with the 2,4-hexadiyne precursor, no reaction was observed with either C_2H_2 or C_4H_2. Reactions of $C_5H_3^+$ with 2,4-hexadiyne were:

$$C_5H_3^+ + C_6H_6 \longrightarrow C_6H_6^+ + [C_5H_3] \quad (6.1)$$

$$C_5H_3^+ + C_6H_6 \longrightarrow C_9H_7^+ + [C_2H_2] \quad (6.2)$$

$$C_5H_3^+ + C_6H_6 \longrightarrow C_6H_5^+ + [C_5H_4] \quad (6.3)$$

$$C_5H_3^+ + C_6H_6 \longrightarrow C_7H_7^+ + [C_4H_2] \quad (6.4)$$

$$C_5H_3^+ + C_6H_6 \longrightarrow C_{11}H_9^+ \quad (6.5)$$

$$C_9H_7^+ + C_6H_6 \text{ ----> } C_{15}H_{13}^+ \quad (6.6)$$

$C_5H_3^+$ ions produced as products of the reaction of $C_3H_3^+ + C_4H_2$ were 100% reactive with both propargyl iodide and with diacetylene (the neutrals present in the reaction medium).

$C_5H_3^+$ reactions with C_4H_2 were:

$$C_5H_3^+ + C_4H_2 \text{ ----> } C_7H_3^+ + [C_2H_2] \quad (6.7)$$

$$C_5H_3^+ + C_4H_2 \text{ ----> } C_9H_5^+ \quad (6.8)$$

$$C_7H_3^+ + C_4H_2 \text{ ----> } C_{11}H_5^+ \quad (6.9)$$

$$C_9H_5^+ + C_4H_2 \text{ ----> } C_{13}H_7^+ \quad (6.10)$$

Some of the product ions were observed to react further with propargyl iodide by displacing atomic iodine:

$$C_7H_3^+ + C_3H_3I \text{ ----> } C_{10}H_6^+ + I \quad (6.11)$$

$$C_9H_5^+ + C_3H_3I \text{ ----> } C_{12}H_8^+ + I \quad (6.12)$$

$C_5H_3^+$ reactions with propargyl iodide were:

$$C_5H_3^+ + C_3H_3I \text{ ----> } C_8H_6^+ + I \quad (6.13)$$

$$C_8H_6^+ + C_3H_3I \text{ ----> } C_{11}H_9^+ + I \quad (6.14)$$

The $C_8H_6^+$ ion reacted further with C_4H_2:

$$C_8H_6^+ + C_4H_2 \text{ ----->} C_{12}H_8^+ \qquad (6.15)$$

Ion intensity vs. time curves for the $C_5H_3^+/(C_4H_2 + C_3H_3I)$ system are shown in Figure 6.2. The decay of $C_5H_3^+$ ions involved reaction with both C_4H_2 and propargyl iodide.

The procedure for rate coefficient determination used in previous studies of $C_3H_3^+$ and $C_5H_5^+$ ion/molecule reactions required subtraction of the observed rate constant for the reaction of the ion with the precursor neutral from the observed rate constant for the sum of the reactions with precursor and reactant neutrals. In this case, however, the reactant neutral (C_4H_2) was also the precursor of the ion of interest ($C_5H_3^+$), and thus the subtraction procedure could not be used. An alternative method for rate constant determination was thus required. Following ejection of all other ions from the FTICR cell, the decay of $C_5H_3^+$ as a function of time is given by:

$$[C_5H_3^+]_t = [C_5H_3^+]_0 e^{-(n_p k_p + n_d k_d)t} \qquad (6.16)$$

where $n_p k_p$ and $n_d k_d$ refer to the products of the number densities and ion/molecule rate coefficients for propargyl iodide and diacetylene, respectively (Reactions (6.7), (6.8) and (6.13)). The quantity $n_d k_d + n_p k_p$ can thus be determined from the slope of a semilog plot of $C_5H_3^+$ decay as a function of time. At short reaction times, the following expressions hold true:

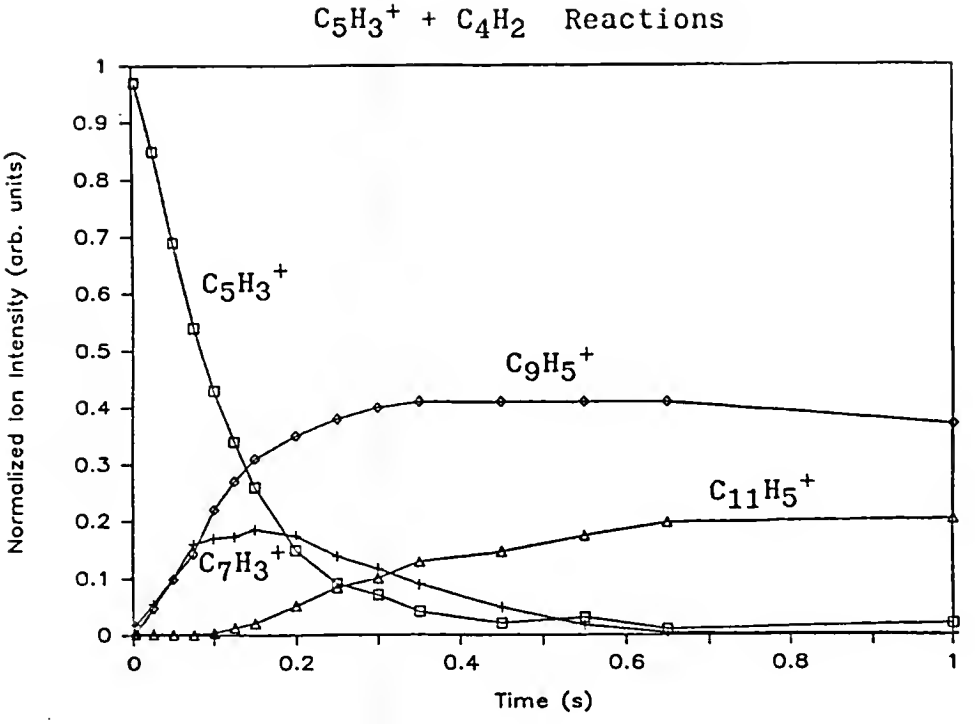

Figure 6.2. Reactions of $C_5H_3^+$ with C_4H_2. Disappearance of $C_5H_3^+$ and product ions includes reactions with propargyl iodide. $C_5H_3^+$ ions were produced from the reaction of $C_3H_3^+$ with diacetylene within 30 ms reaction time. $C_3H_3^+$ ions were produced from propargyl iodide by charge transfer reactions with Xe^+. $p(C_3H_3I) = 1.9 \times 10^{-7}$ torr, $p(C_4H_2) = 1.3 \times 10^{-6}$ torr, $p(Xe) = 5.4 \times 10^{-6}$ torr.

$$dD/dt = n_d k_d [C_5H_3^+]_0 e^{-(n_p k_p + n_d k_d)t} \quad (6.17)$$

and

$$dP/dt = n_p k_p [C_5H_3^+]_0 e^{-(n_p k_p + n_d k_d)t} \quad (6.18)$$

where D and P refer to product ions of the reaction with diacetylene ($C_7H_3^+$ and $C_9H_5^+$, Reactions (6.7) and (6.8)) and with propargyl iodide ($C_8H_6^+$, Reaction 6.13) respectively. Thus, the ratio $n_d k_d / n_p k_p$ was calculated from the ratio of slopes of product formation as a function of time. Next $n_d k_d$ was obtained using the calculated sum and ratio of the two rate constants. Finally the absolute rate constant was determined following the usual procedure. It was found that $C_5H_3^+$ ions reacted with C_4H_2 with a rate constant of $(5.6 \pm 1.7) \times 10^{-10}$ cm^3/s.

Kinetic Modeling of $C_5H_3^+$ reactions with diacetylene.

In order to better understand the reaction mechanisms involved in the $C_5H_3^+ + C_4H_2$ system, kinetic modeling studies of the ion intensity vs. time curves shown in Figure 6.2 were carried out.[10] Details of the modeling methodology are given in Chapter 5. A kinetic model involving the

---

[10]The kinetic modeling studies were performed in the Environics Division of Air Force Engineering and Services Center, Tyndall Air Force Base, Florida by F. Wiseman using multiple experimental data sets produced at identical conditions to those reported for Figure 6.2.

reactions above was fitted to the experimental data assuming steady-state concentrations for the excited forms of $(C_9H_5^+)^*$ and $(C_{11}H_5^+)^*$ intermediate complexes. The complete reaction scheme used for modeling is shown in Figure 6.3.

Comparison of the model fit with the experimental data is shown in Figures 6.4a and 6.4b.

$C_5H_5^+$

Effect of Precursor Neutrals. $C_5H_5^+$ ions produced from different precursors exhibited behavior indicative of both reactive and unreactive populations toward both the precursors and the reactant neutrals. Figures 6.5a and 6.5b show $C_5H_5^+$ normalized ion intensity vs. time curves for two (cycloheptatriene and 1-penten-3-yne) of the five precursors used to form ions before reaction with diacetylene and acetylene. Following an exponential decay indicative of pseudo-first order kinetics, a substantial fraction of unreactive ions remains at long reaction times, particularly in Figure 6.5b. Table 6.1 shows the method of preparation of $C_5H_5^+$ ions from different precursors and the percent of unreactive ions remaining at long reaction times.

Two (norbornadiene and cycloheptatriene) of the five precursors mentioned above produce $C_7H_8^+$ rather than $C_5H_6^+$ parent ions. The $C_7H_8^+$ ions produced from norbornadiene were reported (Davidson and Skell, 1973; Ausloos, 1982)

$$C_5H_3^+ + C_4H_2 \xrightarrow{k_{f2}} (C_9H_5^+)^*$$

$$C_5H_3^+ + C_3H_3I \xrightarrow{k_{p2}} C_8H_6I^+$$

$$(C_9H_5^+)^* \xrightarrow{k_{-22}} C_5H_3^+ + C_4H_2$$

$$(C_9H_5^+)^* \xrightarrow{k_{-21}} C_7H_3^+ + C_2H_2$$

$$(C_9H_5^+)^* \xrightarrow{k_{s1}} C_9H_5^+ \text{ (stabilized)}$$

$$C_9H_5^+ + C_4H_2 \xrightarrow{k_{94}} C_{13}H_7^+$$

$$C_7H_3^+ + C_4H_2 \xrightarrow{k_{f3}} C_{11}H_5^+$$

$$C_7H_3^+ + C_3H_3I \xrightarrow{k_{p3}} C_{10}H_6I^+$$

$$(C_{11}H_5^+)^* \xrightarrow{k_{-32}} C_7H_3^+ + C_4H_2$$

$$(C_{11}H_5^+)^* \xrightarrow{k_{-31}} C_9H_3^+ + C_2H_2$$

$$(C_{11}H_5^+)^* \xrightarrow{k_{s2}} C_{11}H_5^+ \text{ (stabilized)}$$

Figure 6.3. Reaction Scheme Postulated for the Kinetic Modeling of the Reaction of $C_5H_3^+$ with Diacetylene.

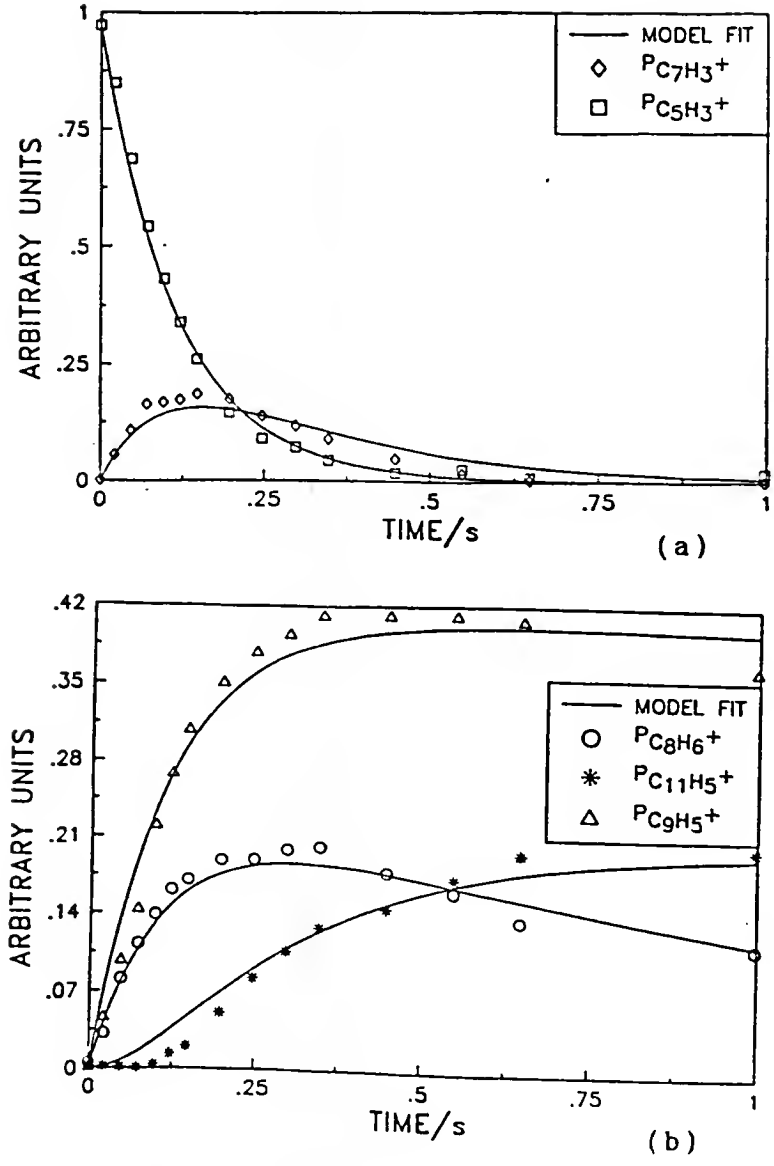

Figure 6.4. Model Fit to Typical Data Set for $C_5H_3^+ + C_4H_2$ Reactions.[a] (a) Ion intensity vs time curves for $C_5H_3^+$ and $C_7H_3^+$. (b) Ion intensity vs time curves for $C_8H_6^+$, $C_9H_5^+$, and $C_{11}H_5^+$.

[a]The best fit values for the fitting parameters were: $\theta_2 = -8.7(.2)/s$, $\theta_3 = -4.6(.4)/s$, $k_{-21}\phi_1 = 2.8(.1)/s$, $k_{s1}\phi_1 = 3.7(.1)/s$, $k_{s2}\phi_2 = 2.9(.2)/s$, $k_{94} = .04(.06)/s$, and $k_d = .8(.2)/s$ where

$$\theta_2 = -(k_{-21} + k_{s1})k_{f2}P_{C_4H_2}/(k_{-21} + k_{-22} + k_{s1}) - k_{p2}P_{C_3H_3I},$$

$$\phi_1 = k_{f2}P_{C_4H_2}/(k_{-21} + k_{-22} + k_{s1}) \text{ and}$$

$$\phi_2 = k_{f3}P_{C_4H_2}/(k_{-31} + k_{-32} + k_{s2}).$$

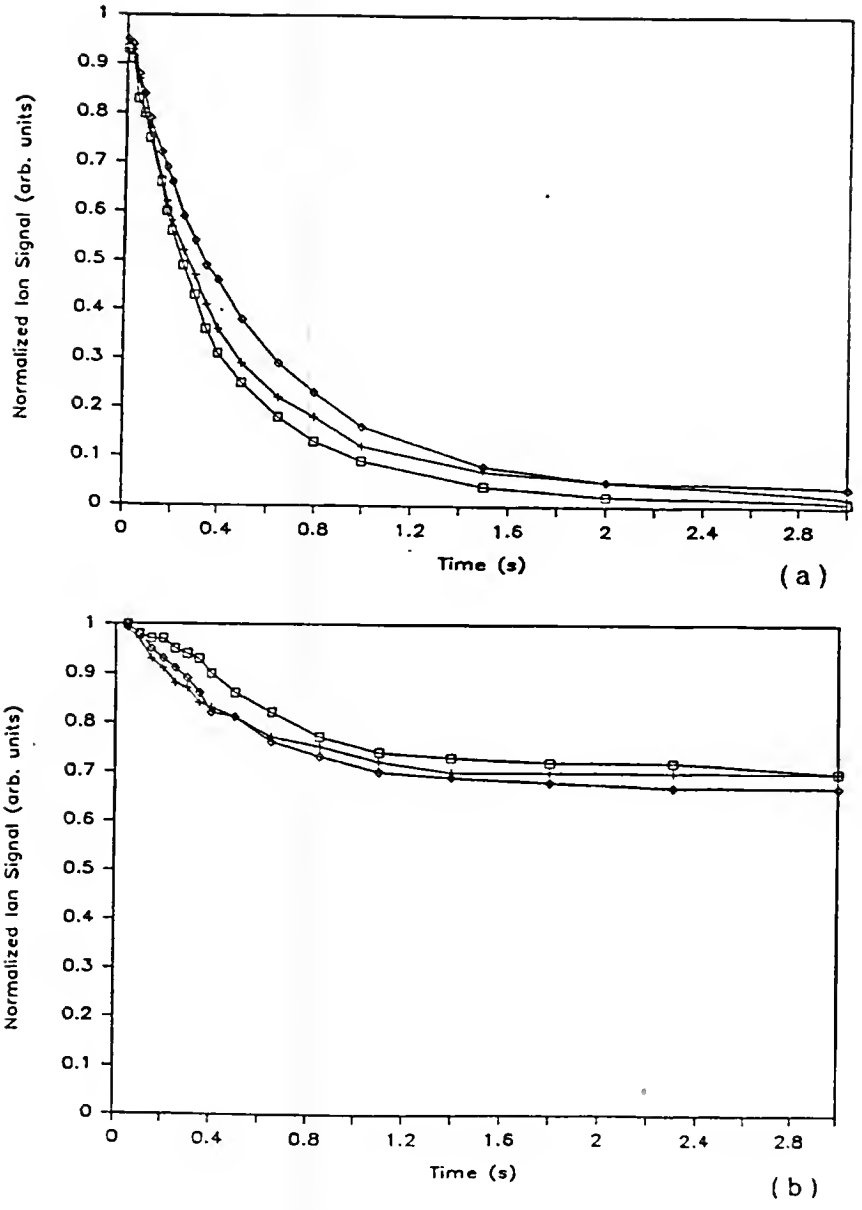

Figure 6.5. $C_5H_5^+$ Ion Decay Curves for Various Reactions. (a) $C_5H_5^+$ with cycloheptatriene(◇), with cycloheptatriene and acetylene(+), and with cycloheptatriene and diacetylene(□). $C_5H_5^+$ ions were produced from cycloheptatriene by charge transfer reactions with Ar^+. $p(C_7H_8) = 1.3 \times 10^{-7}$ torr, $p(C_2H_2) = 1.1 \times 10^{-6}$ torr, $p(C_4H_2) = 6.6 \times 10^{-7}$ torr, $p(Ar) = 10.4 \times 10^{-6}$ torr.
(b) $C_5H_5^+$ with 1-penten-3-yne(◇), with 1- penten-3-yne and acetylene(+), and with 1-penten-3-yne and diacetylene(□). $C_5H_5^+$ ions were produced from 1-penten-3-yne by charge transfer reactions with Xe^+. $p(C_5H_6) = 4.2 \times 10^{-7}$ torr, $p(C_2H_2) = 1.4 \times 10^{-6}$ torr, $p(C_4H_2) = 8.4 \times 10^{-7}$ torr, $p(Xe) = 5.4 \times 10^{-6}$ torr.

TABLE 6.1

Percentages[a] of unreactive $C_5H_5^+$ found from various precursors by charge transfer chemical ionization monitored by observing reaction with the precursor neutral.

Precursor Neutral	Charge Transfer Agent	% unreactive $C_5H_5^+$
dicyclopentadiene	N_2^+/Ar^+	20
cyclopentadiene	Xe^+	17
1-penten-3-yne	Xe^+	65-70
cycloheptatriene	Ar^+	0-5
norbornadiene	N_2^+/Ar^+ Kr^+	18-20 5-10

[a]Estimated error is 5%.

earlier to lead to two different channels (Reactions (6.19) and (6.20)) for $C_5H_5^+$ ion formation.

$$C_7H_8^+ \text{ ----> } C_7H_7^+ + H^{\cdot} \qquad (6.19a)$$

$$C_7H_7^+ \text{ ----> } C_5H_5^+ + C_2H_2 \qquad (6.19b)$$

or

$$C_7H_8^+ \text{ ----> } C_5H_6^+ + C_2H_2 \qquad (6.20a)$$

$$C_5H_6^+ \text{ ----> } C_5H_5^+ + H \qquad (6.20b)$$

Thus, $C_5H_5^+$ ion formation pathways were studied in more detail for norbornadiene and cycloheptatriene. When different charge transfer gases were used for ionization of norbornadiene, different percentages of reactive $C_5H_5^+$ were observed, as is noted in Table 6.1. Also the abundances of $C_7H_7^+$, $C_5H_6^+$ and $C_5H_5^+$ ions were measured following charge transfer ionization, and different behavior was observed for compounds with ionization potentials in the range of 14 to 16 eV. Table 6.2 shows this effect for two reagent gases (Kr^+ and N_2^+) which have ionization energies of 14.0 and 15.7 eV respectively.

In order to further investigate this behavior, the relative ion abundances vs. electron energy for cycloheptatriene and norbornadiene were obtained (see Figures 6.6 and 6.7).[11]

---

[11]Electron impact ionization was used for this study and therefore the energy scale in Figures 6.6 and 6.7 should be considered as approximate with at least ± 1 eV uncertainty.

TABLE 6.2

Changes in ion abundances at two different ionization energies for norbornadiene.

Ionizing energy/eV (charge transfer agent)	Abundances as a fraction of total ion signal[a]			
	$C_7H_8^+$	$C_7H_7^+$	$C_5H_6^+$	$C_5H_5^+$
14.0 (Kr^+)	0.07	0.45	0.32	0.16
15.7 (N_2^+)	0.09	0.28	0.16	0.47

[a]Estimated error is $\pm$0.02.

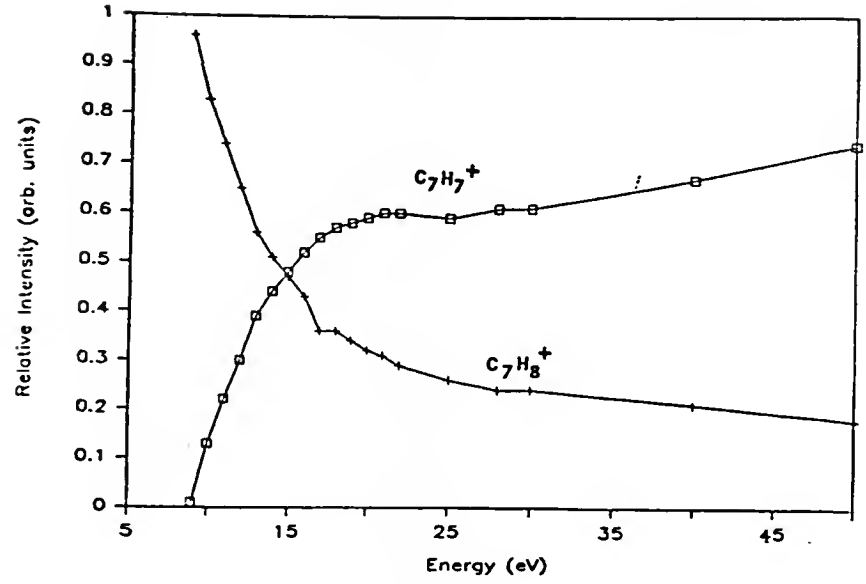

(a)

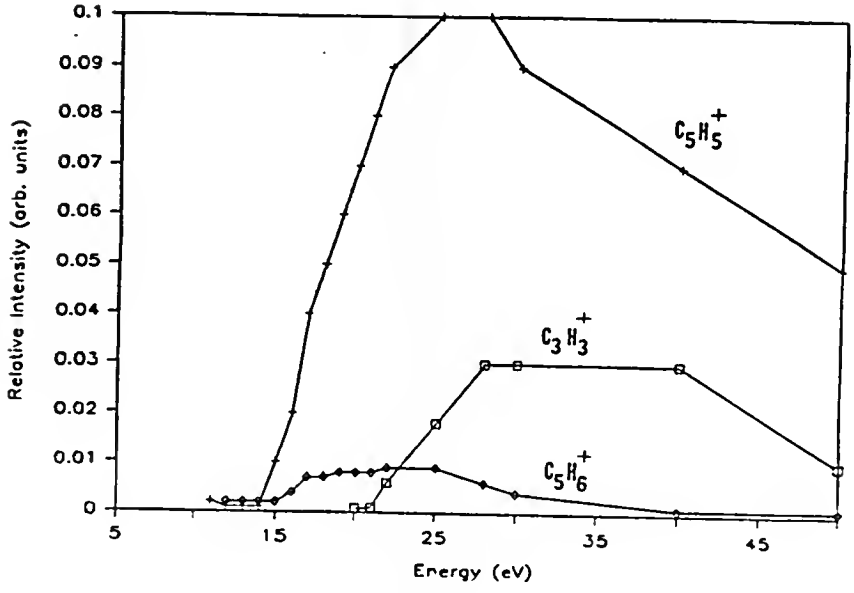

(b)

Figure 6.6. Relative Ion Intensities Produced from Cycloheptatriene as a Function of Electron Impact Energy. (a) $C_7H_8^+$ and $C_7H_7^+$ and (b) $C_5H_6^+$, $C_5H_5^+$, and $C_3H_3^+$.

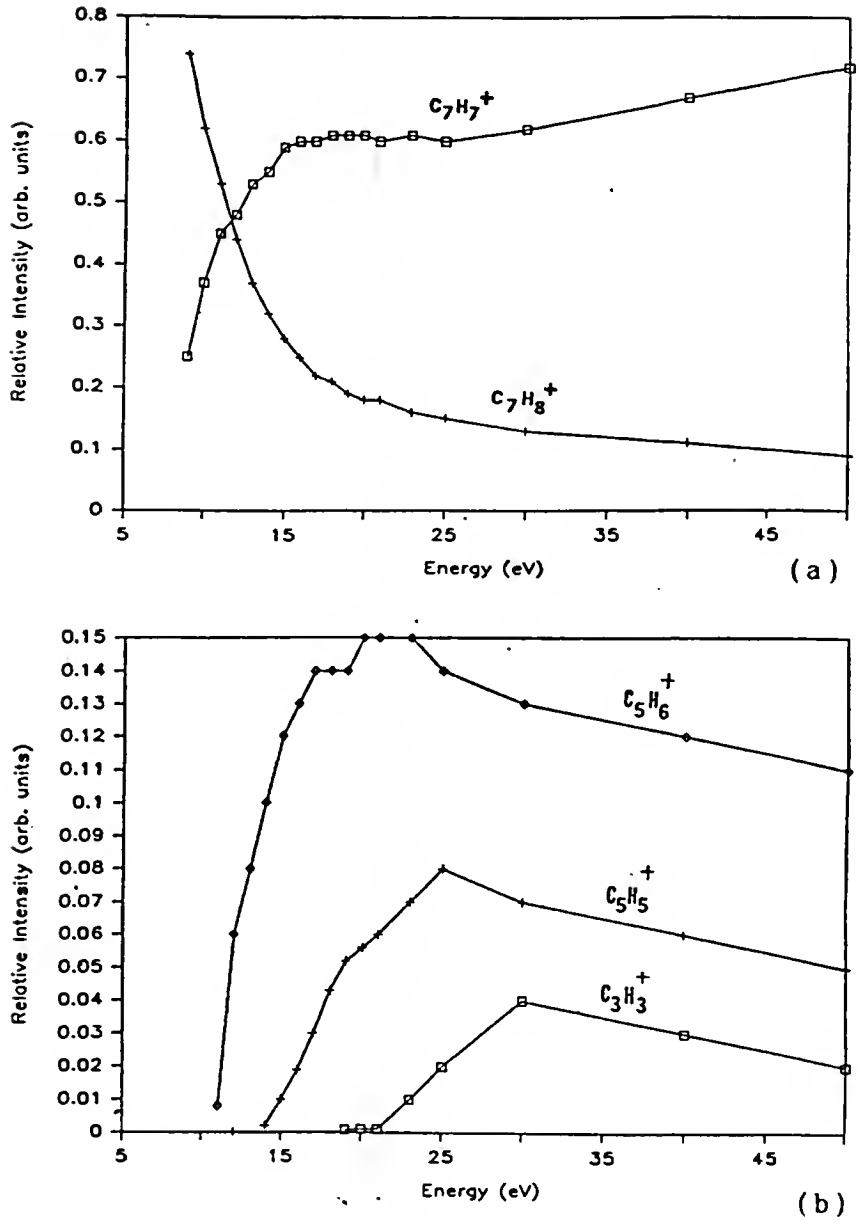

Figure 6.7. Relative Ion Intensities Produced from Norbornadiene as a Function of Electron Impact Energy. (a) $C_7H_8^+$ and $C_7H_7^+$ and (b) $C_5H_6^+$, $C_5H_5^+$, and $C_3H_3^+$.

$\underline{C_5H_5^+ \text{ reactions with diacetylene.}}$ After ejection of all ions except $C_5H_5^+$ following charge transfer chemical ionization of a mixture of diacetylene and a precursor compound, the ion/molecule reactions as a function of time were monitored. Independent of the precursor used, the main reaction was the addition of C_4H_2 to $C_5H_5^+$ to produce the $C_9H_7^+$ ion.

$$C_5H_5^+ + C_4H_2 \text{ ----> } C_9H_7^+ \qquad (6.21)$$

Other minor reactions observed were:

$$C_5H_5^+ + C_4H_2 \text{ ----> } C_7H_5^+ + [C_2H_2] \qquad (6.22)$$

$$C_5H_5^+ + C_4H_2 \text{ ----> } C_7H_7^+ + [C_2] \qquad (6.23)$$

$$C_7H_7^+ + C_4H_2 \text{ ----> } C_{11}H_9^+ \qquad (6.24)$$

$$C_9H_7^+ + C_4H_2 \text{ ----> } C_{13}H_9^+ \qquad (6.25)$$

For $C_5H_5^+$ ions produced from cyclopentadiene, the C_2 addition reaction (6.22) was not observed with C_4H_2.

The rate coefficient for the disappearance of $C_5H_5^+$ was calculated as described earlier in Chapter 3 and the values found for $C_5H_5^+$ ions produced from different precursors are given in Table 6.3.

$\underline{C_5H_5^+ \text{ reactions with acetylene.}}$ $C_5H_5^+$ ions formed from four of the five precursors (cyclopentadiene,

TABLE 6.3

Rate coefficients for the reaction of $C_5H_5^+$ ions from different precursors[a] with diacetylene and acetylene.

Precursor	Absolute rate coefficient with $C_4H_2/(10^{-10}$ cm^3/s)	$C_2H_2/(10^{-11}$ cm^3/s)
cyclopentadiene	(1.0 ± 0.5)	(4.8 ± 1.9)
1-penten-3-yne	(2.0 ± 1.0)	(2.7 ± 1.0)
norbornadiene	(2.9 ± 1.4)	(3.1 ± 1.3)
cycloheptatriene	(3.3 ± 1.9)	(1.8 ± 0.7)
dicyclopentadiene[b]	(1.6 ± 0.8)	

[a] $C_5H_5^+$ ions were produced by charge transfer chemical ionization using different gases as shown in Table 6.1.
[b] Ion signal for dicyclopentadiene was too small to produce reproducible results for the rate coefficient of the reaction with acetylene.

1-penten-3-yne, norbornadiene, cycloheptatriene) reacted very slowly with C_2H_2, producing very small amounts of $C_7H_7^+$ and $C_9H_9^+$.

$$C_5H_5^+ + C_2H_2 \text{ ----> } C_7H_7^+ \quad (6.26)$$

$$C_7H_7^+ + C_2H_2 \text{ ----> } C_9H_9^+ \quad (6.27)$$

Rate constants for the $C_5H_5^+ + C_2H_2$ reaction were about one order of magnitude less than those for reactions with C_4H_2 (see Table 6.3).

Discussion

$\underline{C_5H_3^+}$. Two different $C_5H_3^+$ structures were postulated (Dannacher et al., 1979) based on PIPECO measurements of appearance energies of $C_5H_3^+$ ions from 1,3-pentadiyne and 2,4-hexadiyne. In the work reported here, $C_5H_3^+$ ions were produced from 2,4-hexadiyne and by reaction of $C_3H_3^+$ with diacetylene. Although $C_5H_3^+$ ions produced either way were reactive toward their precursor neutrals, $C_5H_3^+$ ions from 2,4-hexadiyne were unreactive with both C_4H_2 and C_2H_2, while those formed as ion/molecule reaction products reacted with C_4H_2 with the relatively high rate constant of $(5.6 \pm 1.7) \times 10^{-10}$ cm^3/s. Dannacher et al. (1979) suggested the structures $CH_3-C\equiv C-C\equiv C^+$ and $HC\equiv C-C\equiv C-CH_2^+$ for the $C_5H_3^+$ ions produced from 2,4-hexadiyne and 1,3-pentadiyne respectively. Experimental appearance potentials for these ions suggested

that the former probably had a higher heat of formation, <1431 kJ/mole (Baer et al., 1979), compared to the latter, 1317 kJ/mole (Dannacher et al., 1979). In this study, enhanced reactivity of $C_5H_3^+$ ions produced by the $C_3H_3^+$ + C_4H_2 reaction compared to those produced by electron ionization of 2,4-hexadiyne suggests that the former have a higher heat of formation with a stable structure different from those reported earlier for $C_5H_3^+$ ions from both 2,4-hexadiyne and 1,3-pentadiyne. Enhanced reactivity does not always correlate with a higher heat of formation, but this has often been found true for isomers of other small hydrocarbon ions. Our observation that $C_5H_3^+$ is formed in an exothermic reaction of linear $C_3H_3^+$ with diacetylene leads to an upper limit of 1375.9 kJ/mole for ΔH_f of the $C_5H_3^+$ ion formed in this manner.[12] This value is not inconsistent with either of those reported earlier.

Although no structural assignment can be made for the $C_5H_3^+$ ion produced by reacting $C_3H_3^+$ with diacetylene based on the results of this study, several structures can be considered possible on the basis of initial charge distribution on $C_3H_3^+$ leading to the formation of three product ion structures by reaction mechanisms shown in Figure 6.8. The three possible $C_5H_3^+$ product ions shown in

---

[12]This calculation assumes no significant internal energy in the $C_3H_3^+$ ions prior to reaction and heats of formation of 281 kcal mol^{-1} (Lossing, 1972), for 1-$C_3H_3^+$, 54.2 kcal mol^{-1} (Wagman et al., 1968), and 102 kcal mol^{-1} for C_4H_2 (Coats and Anderson, 1957).

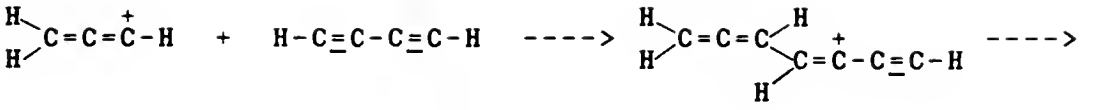

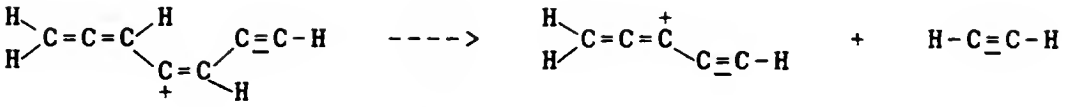

(6.10)

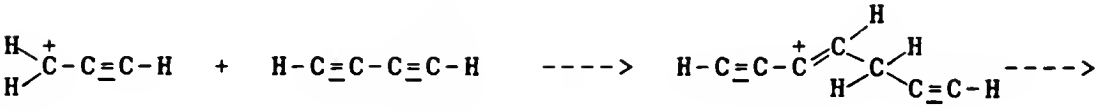

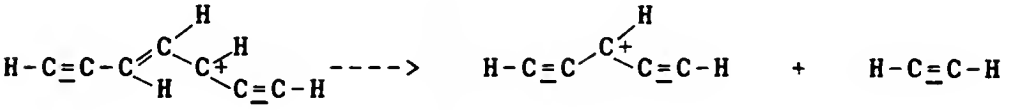

(6.11)

and/or

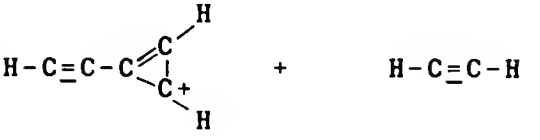

(6.12)

Figure 6.8. Proposed Reaction Mechanisms for the Reaction of the Propargylium Cation with Diacetylene, Leading to Three Different $C_5H_3^+$ Product Ions with Resultant Loss of Acetylene.

Figure 6.8 have structures which differ from those postulated (Dannacher et al., 1979) earlier. While no definitive theoretical or experimental evidence as to the relative stability of these (or other) $C_5H_3^+$ isomers is available, Structure (6.12) is most similar to the vinylcyclopropenylium ion found most stable among the $C_5H_5^+$ isomers. Thus Structure (6.10) or (6.11) might be the unstable, reactive structure formed in these experiments. When deuterated diacetylene was reacted with $C_3H_3^+$ ion, the deuterated product ratios, $C_5H_2D^+$:$C_5HD_2^+$:$C_5H_3^+$ were found to be 6:3:1. This result is also consistent with the reaction mechanisms of formation of the three $C_5H_3^+$ structures shown in Figure 6.8 assuming complete scrambling of hydrogens in the intermediate $C_7H_5^+$ complex.

$C_5H_5^+$ ion structures produced from different precursors. $C_5H_5^+$ ions produced from different precursors all exhibited at least two populations, one reactive, other unreactive. This behavior for numerous other ionic reactants has been used previously (Ausloos and Lias, 1981; Smyth et al., 1982; Wagner-Redeker et al., 1983; Smith and Adams, 1987) to argue for the existence of at least two different structural isomers; one reactive and one non-reactive. These results are in agreement with the earlier reactivity study of $C_5H_5^+$ ions from different precursors (Brill, 1983). To distinguish the reactive $C_5H_5^+$

structures, their reaction mechanisms and reaction rates with acetylene and diacetylene were studied. Although they reacted with their precursor neutrals with different rates, they all reacted with acetylene and diacetylene at similar rates within the experimental error limits, as shown in Table 6.3. Thus no isomeric differentiation based on reactivity can be made. Rate coefficients for the reaction with acetylene were similar to those determined earlier (Buckley, 1982; Brill, 1983), i.e. in the range of 10^{-11} cm^3/s. Reaction mechanisms were similar for all $C_5H_5^+$ ions with the exception of cyclopentadiene, which didn't give C_2 addition reactions with C_4H_2.

Although no definitive structure assignment can be made for the $C_5H_5^+$ ions produced, several suggestions are possible from the results of this study. Similar reaction rates within experimental error suggest the formation of the same reactive $C_5H_5^+$ structure from all precursors. Assuming that the latest theoretical information[13] on the energies of different $C_5H_5^+$ structures is fairly accurate, we can identify the possible structures which are energetically accessible by the initial internal energy transferred to neutral parents by chemical ionization. As shown in Table 6.4 , simple calculation using the thermochemical data[14]

---

[13]J. Feng, J. Leszczynski and M. C. Zerner, submitted.

[14]This calculation assumed heats of formation of 31.8 kcal mol^{-1} for cyclopentadiene (Harrison et al., 1960), 43.5 kcal mol^{-1} for cycloheptatriene (Finke et al., 1956), and

TABLE 6.4

Comparison of the energy transferred to neutral precursors by chemical ionization with theoretical appearance energies (assuming no reverse activation energy) of different $C_5H_5^+$ structures from the corresponding precursors.

Neutral precursor	charge transfer agent and (IP/eV)	structure[a]	theoretical AP/eV
Cyclopentadiene	Xe^+ (12.1)	6.1	12.0
		6.2&6.3	12.4
		6.4	12.6
		6.5	12.7
		6.6	12.8
		6.7	12.9
		6.8	13.0
		6.9	13.2
Norbornadiene	Kr^+ (14.0) Ar^+ (15.8)	6.1	13.1
		6.2&6.3	13.5
		6.4	13.6
		6.5	13.8
		6.6	13.8
		6.7	14.0
		6.8	14.0
		6.9	14.2
Cycloheptatriene	N_2^+ (15.6)	6.1	13.9
		6.2&6.3	14.2
		6.4	14.4
		6.5	14.6
		6.6	14.6
		6.7	14.8
		6.8	14.8
		6.9	15.0

[a]Numbers refer to the structures shown in Figure 6.1.

62.3 kcal mol^{-1} for norbornadiene (Lifshitz and Bauer, 1963).

available for cyclopentadiene, norbornadiene and cycloheptatriene indicates that $C_5H_5^+$ formed from cyclopentadiene by Xe^+ charge transfer chemical ionization can only have the lowest energy structure (Structure 6.1). On the other hand, $C_5H_5^+$ ions produced from norbornadiene and cycloheptatriene by N_2^+/Ar^+ charge transfer chemical ionization have enough excess energy to sample almost all the isomeric structures shown in Figure 6.1. Since the energy barriers between these structures are not yet known, nothing can be said concerning the possibility of isomerization between these structures. Experimental data indicates that at least two stable (reactive and unreactive) structures are formed in all the cases studied. More definitive identification of $C_5H_5^+$ structures may be forthcoming when better theoretical calculations are reported, although identification of the vinylcyclopropenylium ion as (one of) the unreactive structure(s) seems reasonable in the light of the recent calculations and earlier ICR studies.

To compare the behavior of ions produced from cycloheptatriene and norbornadiene precursors (both having the formula C_7H_8), relative abundances as a function of electron energy shown in Figures 6.6 and 6.7 were obtained. As shown, the curves for $C_7H_7^+$ (Figures 6.6a and 6.7a) and $C_5H_5^+$ and $C_3H_3^+$ (Figures 6.6b and 6.7b) are very similar both in terms of energetics and of general shape.

Differences in $C_5H_5^+$ relative intensities are probably due to the normalization procedure used in each case. An increase in the relative intensity of $C_5H_5^+$ ions in both cases in the energy range of 15-25 eV along with the fact that the $C_7H_7^+$ curves no longer increase in this energy range implies that most of the $C_5H_5^+$ ions are produced from $C_7H_7^+$. Similar behavior is seen for $C_3H_3^+$ ions, i.e., the intensity of these ions increases at about 22 eV (on the energy scale shown on Figures 6.6b and 6.7b) where the rate of increase in the intensity of $C_5H_5^+$ is decreased. This similar behavior implies that $C_7H_7^+$ ions formed from cycloheptatriene and norbornadiene follow the same fragmentation pathways in the same energy range. Similar behavior for $C_7H_7^+$ ions from these two compounds has also been reported earlier in collisional activation studies (Winkler and McLafferty, 1973).

As seen in Figures 6.6b and 6.7b, formation of $C_5H_6^+$, both in terms of energetics and relative intensity, is different for cycloheptatriene and norbornadiene, indicating that $C_7H_8^+$ ions formed from these compounds by electron impact have different structures (according to Reaction (6.20a). Based on the significantly higher relative intensity of $C_5H_6^+$ for norbornadiene along with the results shown in Tables 6.1 and 6.2, there exists the possibility of formation of $C_5H_5^+$ ions from the $C_5H_6^+$ channel by Reaction (6.20b) for norbornadiene. As shown in Table 6.1, the

percent of unreactive $C_5H_5^+$ increases from (5-10)% to (18-20)% with changing ionizing charge transfer energy for norbornadiene while no such change in $C_5H_5^+$ reactivity was observed for cycloheptatriene under the same conditions. Relative ion intensities at two different energies of charge transfer chemical ionization are shown in Table 6.2 for norbornadiene. The results indicate that when Ar^+/N_2^+ replaces Kr^+ as the charge donor, the relative intensity of the observed $C_5H_5^+$ increases while there is a corresponding decrease in the yield of the $C_5H_6^+$ ion. Thus, evaluation of the results on $C_5H_5^+$ reactivity (Table 6.1) together with the results on relative ion intensity (Table 6.2) implies that $C_5H_5^+$ formed from $C_5H_6^+$ channel has a higher percent of unreactive isomer compared to that formed from $C_7H_7^+$ channel.

CHAPTER 7
REACTIONS OF GASEOUS $C_7H_7^+$ IONS

Introduction

The $C_7H_7^+$ ion has been proposed as one species involved in an ion/molecule mechanism of soot formation (Olson and Calcote, 1981a; Calcote, 1981). Mass spectrometric measurements have shown that as premixed flames approach a sooting condition, the predominant $C_3H_3^+$ ion is replaced by larger ions (Olson and Calcote, 1981b) including $C_7H_7^+$. These ions in turn have been postulated to react with neutrals such as acetylene and diacetylene, forming still larger ions (Olson and Calcote, 1981a). According to the proposed ion/molecule mechanism, $C_5H_5^+$ forms $C_7H_7^+$ in reactions with acetylene. However, the reactions of $C_5H_5^+$ with acetylene did not reveal significant formation of $C_7H_7^+$ (see Chapter 6). Much higher concentrations of $C_7H_7^+$ than observed experimentally were predicted (Olson and Calcote, 1981a) by a simple model which assumed a benzyl structure for the ion. To account for this difference between experiment and theory, it was suggested that the actual ion in the flame, presumably formed by ion/molecule reactions of $C_3H_x^+$ and $C_5H_x^+$ ions, is some

other $C_7H_7^+$ isomer less stable than benzyl (Olson and Calcote, 1981a).

There have been a significant number of both theoretical and experimental studies on structural characterization of $C_7H_7^+$ ions. Theoretical studies (Abbaund et al., 1976; Cone et al.,1977) on the determination of heats of formation for $C_7H_7^+$ ions indicated that tropylium, with ΔH_f=207.9 kcal/mol (Abbaund et al., 1976), and 195.6 kcal/mol (Cone et al.,1977) and benzyl, with ΔH_f=217.1 kcal/mol (Abbaund et al., 1976), and 220.4 kcal/mol (Cone et al.,1977) are the most stable structures with an activation energy of 32.7 kcal/mol (Cone et al., 1977) for benzyl ---> tropylium isomerization. Experimental measurements of ionization potentials for tropylium and benzyl radicals by monoenergetic electron impact gave calculated values of ΔH_f=209 and 211 kcal/mol (Thrush and Zwolenik, 1963; Elder and Parr, 1969; Lossing, 1971) respectively. Studies of metastable ions (Cooks et al., 1973; Mclafferty and Winkler, 1974; Grotemeyer and Grueitzmacher, 1981) collisional activation (Winkler and McLafferty, 1973; Koeppel et al., 1978McLafferty and Bockhoff, 1979), gas phase radiolysis (Yamamoto et al., 1969; Takamuku et al., 1972; Takamuku et al., 1973; Sagi et al., 1974), photoionization/photodissociation (Dunbar, 1975; Traeger and McLoughlin, 1977; McCreary and Freiser, 1978; Traeger and McLoughlin, 1978; McLoughlin et al., 1979;

Yaroslavtsev et al., 1984), PEPICO (Bombach et al., 1983a, and b), and ion/molecule reactions (Shen et al., 1974; Jackson, 1977; Jackson et al., 1977; Ausloos et al., 1980; Sharma and Kebarle, 1981) of $C_7H_7^+$ ions from different precursors were used to characterize the different structures. General experimental evidence including the determination of appearance potentials and heats of formation (Traeger and McLoughlin, 1977; Traeger and McLoughlin, 1978; McLoughlin et al., 1979; Bombach et al., 1983a,and b) supported that these ions exist in the gas phase with at least two structures; tropylium, and benzyl. Unreactive and reactive $C_7H_7^+$ observed in ion/molecule reactions have been attributed to the tropylium and benzyl structures, respectively (Shen et al., 1974; Jackson, 1977; Jackson et al., 1977; Ausloos et al., 1980; Sharma and Kebarle, 1981). Furthermore, it was proposed that there is an equilibrium between these two structures (McLafferty and Bockhoff, 1979; Andrews and Keelan, 1981) similar to that proposed between the parent ions toluene and cycloheptatriene (Mclafferty and Bockhoff, 1979; Ausloos, 1982) (see Figure 7.1). Several groups studied the effect of the energy above $C_7H_7^+$ formation threshold on the dominance of one structure over the other (McLafferty and Winkler, 1974; Shen and Dunbar, 1974; Dunbar, 1975; Ausloos, 1982). Their results in general were supportive of the equilibria between different structures mentioned above.

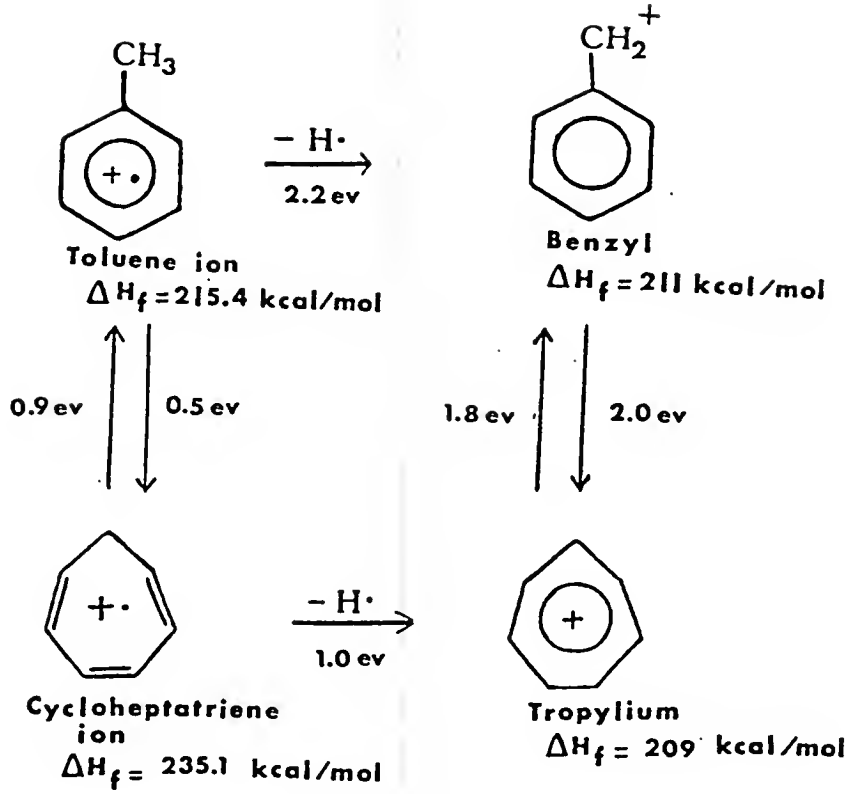

Figure 7.1. Proposed (Mclafferty and Bockhoff, 1979; Ausloos, 1982) Equlibriums between Different $C_7H_8^+$ and $C_7H_7^+$ Structures.

Although McLafferty et al (Winkler and McLafferty, 1973; McLafferty and Winkler, 1974) reported evidence for stable tolyl and norbornadienyl structures in their earlier collisional activation studies no definitive indication for stable structures other than benzyl and tropylium was provided by later studies using different precursors (Jackson et al.; 1977; Koeppel et al., 1978; McLafferty and Bockhoff, 1979; Ausloos, 1982). In the work reported here $C_7H_7^+$ ions have been produced from three different precursors using different charge transfer gases. Reaction pathways and the rate coefficients for the reaction of $C_7H_7^+$ ions with precursor neutrals, acetylene and diacetylene near room temperature were investigated.

Experimental

$C_7H_7^+$ ions were produced from toluene, cycloheptatriene and norbornadiene by dissociative charge transfer . Percentages of reactive/unreactive isomers were determined when the three neutrals above reacted with different charge transfer agents ($C_4H_2^+$, Xe^+, Kr^+ and Ar^+) formed with an electron beam pulse of 5ms duration at an ionizing energy of 11.5, 13, 15, and 20eV, respectively. To do this, all ions except $C_7H_7^+$ were ejected from the cell and enough reaction time (typically 3s) at the pressures used (typically 10^{-6}-10^{-5} torr) was allowed so that the reactive structures could

be lost via ion/molecule reactions, thus leaving an unreactive population.

However, in the case of cycloheptatriene, as reported earlier (Jackson et al., 1977; Ausloos, 1982), because of the growth of unreactive $C_7H_7^+$ by time as a result of the ion/molecule reactions (7.1a) and (7.1b), this approach required some adjustments in the experimental sequence in order to obtain accurate percentages of $C_7H_7^+$ populations.

$$C_7H_7^+ + C_7H_8 \text{ -----> } C_7H_8^+ + C_7H_7 \qquad (7.1a)$$

$$C_7H_8^+ + C_7H_8 \text{ -----> } C_7H_7^+ \text{ (unreactive)} + C_7H_9 \qquad (7.1b)$$

Thus, at long reaction times $C_7H_8^+$ was ejected continously during reaction time in order to avoid reaction (7.1b).

All reactions were followed at a cell temperature of 363K. In order to avoid any possible effect of differences in initial internal energy distribution of $C_7H_7^+$ ions on rate coefficient determination, charge transfer agents which produce $C_7H_7^+$ ions with similar internal energies from different precursors were used for kinetic runs. Also, since the total pressure in the reaction cell was almost 1×10^{-5} torr and the charge transfer time was 100ms, substantial collisional relaxation of the ions took place before kinetic data were collected.

Results

Effect of Precursor Neutrals: $C_7H_7^+$ ions produced from different precursors exhibited behavior indicative of both reactive and unreactive populations toward the precursors. Figures 7.2a, 7.2b, and 7.2c show normalized ion intensities of $C_7H_7^+$ and product ions vs time for reactions with precursor neutrals; toluene, norbornadiene and cycloheptatriene respectively. Following an exponential decay indicative of first order kinetics, a substantial fraction of unreactive ions remains at long reaction times. Table 7.1 shows the charge transfer agents used to produce $C_7H_7^+$ ions from different precursors, the initial internal energy imparted to the ions, and the percent of unreactive ions remaining at long reaction times.

The major reaction of $C_7H_7^+$ produced by charge transfer from toluene with the toluene neutral gives $C_8H_9^+$ (reaction (7.2)); when norbornadiene is used as a precursor and neutral reactant, reaction (7.3) is observed.

$$C_7H_7^+ + C_7H_8 \text{ -----> } C_8H_9^+ + C_6H_6 \qquad (7.2)$$

$$C_7H_7^+ + C_7H_8 \text{ -----> } C_9H_9^+ + C_5H_6 \qquad (7.3)$$

$C_7H_7^+$ from norbornadiene also reacted to give small amounts of higher molecular weight products. On the other hand, $C_7H_7^+$ produced from cycloheptatriene reacted with its precursor neutral to give significant amounts of higher

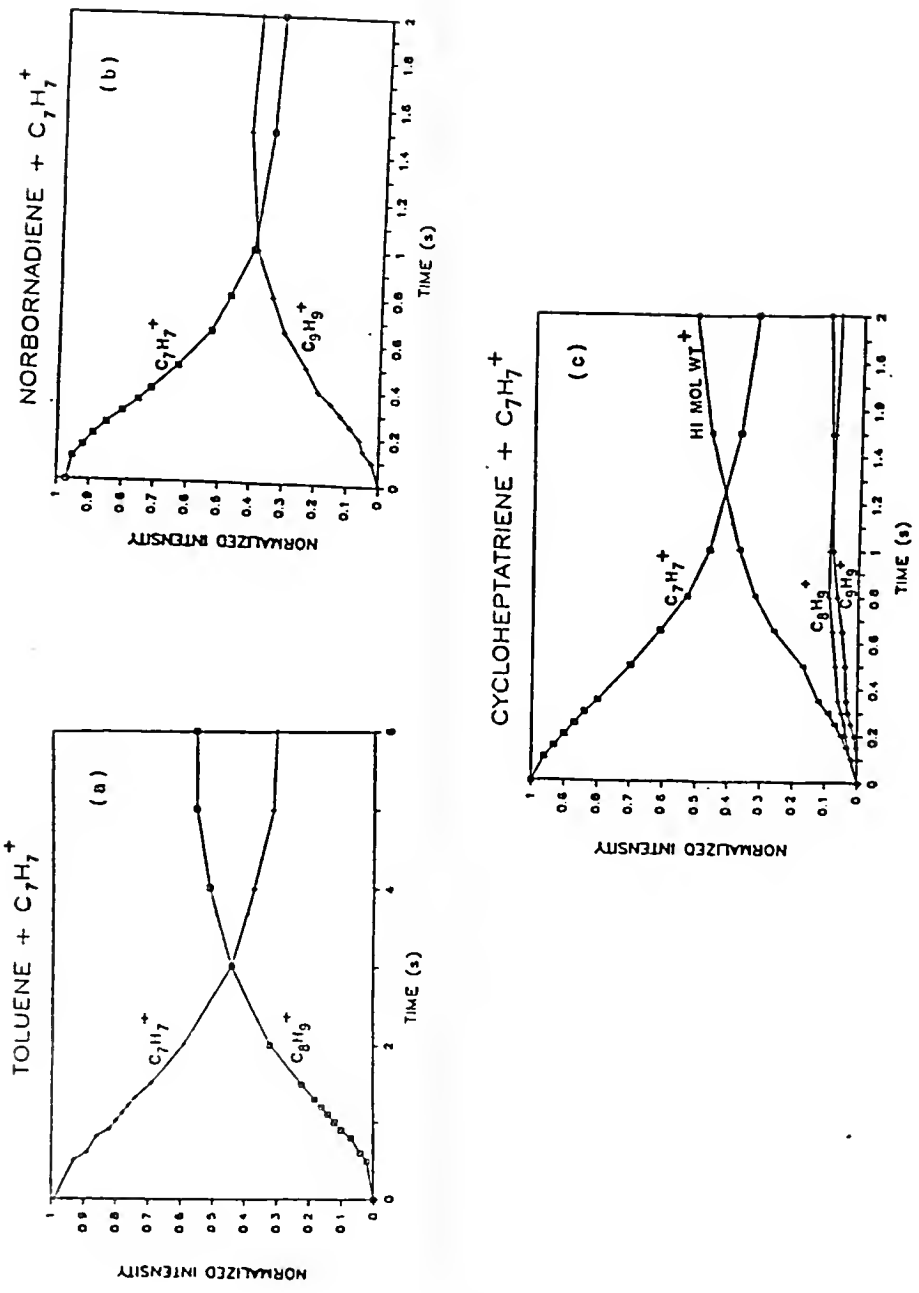

Figure 7.2. Reactions of $C_7H_7^+$ Ions with Their Precursor Neutrals. (a) $C_7H_7^+$ + toluene, (b) $C_7H_7^+$ + norbornadiene and (c) $C_7H_7^+$ + cycloheptatriene.

TABLE 7.1

Percentages of unreactive $C_7H_7^+$ found from various precursors by different ionization methods monitored by observing reaction with the precursor neutral.[a]

Precursor Neutral	Ionizing charge transfer agents	Maximum Internal Energy (eV)[b]	Percent Unreactive
Toluene	Xe^+	1.4	45-50
	Kr^+	3.3	25-30
	Ar^+	5.0	25-30
Norbornadiene	$C_4H_2^+$	0.9	70-75
	Xe^+	2.5	30-35
	Kr^+	4.4	25-30
Cycloheptatriene	$C_4H_2^+$	1.1	70-75
	Xe^+	2.8	35-40
	Kr^+	4.6	35-40

[a]For those ions produced by $C_4H_2^+$ charge transfer, reactions with both precursor neutral and diacetylene were monitored. [b]Based on $C_7H_7^+$ appearance energies given Traeger and McLoughlin, (1978).

molecular weight product ions along with smaller amounts of $C_8H_9^+$ and $C_9H_9^+$ product ions:

$$C_7H_7^+ + C_7H_8 \text{ -----> } C_8H_9^+ + C_6H_6 \quad (7.4)$$

$$C_7H_7^+ + C_7H_8 \text{ -----> } C_9H_9^+ + C_5H_6 \quad (7.5)$$

$$C_7H_7^+ + C_7H_8 \text{ -----> } C_{10}H_9^+ + C_4H_6 \quad (7.6)$$

$$C_7H_7^+ + C_7H_8 \text{ -----> } C_{11}H_9^+ + C_3H_6 \quad (7.7)$$

$$C_7H_7^+ + C_7H_8 \text{ -----> } C_{12}H_{11}^+ + C_2H_4 \quad (7.8)$$

$$C_7H_7^+ + C_7H_8 \text{ -----> } C_{13}H_{11}^+ + CH_4 \quad (7.9)$$

$$C_7H_7^+ + C_7H_8 \text{ -----> } C_{14}H_{11}^+ + 2H_2 \quad (7.10)$$

$$C_7H_7^+ + C_7H_8 \text{ -----> } C_{14}H_{13}^+ + H_2 \quad (7.11)$$

Deuteration Studies: In order to further investigate the mechanisms of some of the reactions shown above, deuterated toluene was used both to produce $C_7D_7^+$ for reactions with neutral precursors and as a neutral reactant for reactions of $C_7H_7^+$ produced from different precursors. Reactions of $C_7D_7^+$ with toluene and norbornadiene were respectively:

$$C_7D_7^+ + C_7H_8 \text{ (toluene) -----> } C_8H_7D_2^+ + C_6HD_5 \quad (7.12)$$

$$C_7D_7^+ + C_7H_8 \text{ (NBD) -----> } C_9D_7H_2^+ + C_5H_6 \quad (7.13)$$

When $C_7D_7^+$ reacted with cycloheptatriene, the major product

observed was unreactive $C_7H_7^+$ due to reactions (7.14) and (7.15).

$$C_7D_7^+ + C_7H_8 \text{ -----> } C_7H_8^+ + C_7D_7 \qquad (7.14)$$

$$C_7H_8^+ + C_7H_8 \text{ -----> } C_7H_7^+ \text{ (unreactive)} + C_7H_9 \qquad (7.15)$$

Other reactions observed were:

$$C_7D_7^+ + C_7H_8 \text{ -----> } C_9D_6H_3^+ + C_5H_5D \qquad (7.16)$$

$$C_7D_7^+ + C_7H_8 \text{ -----> } C_{10}D_6H_3^+ + C_4H_5D \qquad (7.17)$$

$$C_7D_7^+ + C_7H_8 \text{ -----> } C_{11}D_6H_3^+ + C_3H_5D \qquad (7.18)$$

$$C_7D_7^+ + C_7H_8 \text{ -----> } C_{12}D_7H_4^+ + C_2H_4 \qquad (7.19)$$

$C_7H_7^+$ ions produced from toluene reacted with deuterated toluene as shown by equation (7.20):

$$C_7H_7^+ + C_7D_8 \text{ -----> } C_8D_7H_2^+ + C_6H_5D \qquad (7.20)$$

Very low intensities of this product ion were also observed in the mass spectra of $C_7H_7^+$ ions produced from cycloheptatriene and norbornadiene. The rate coefficients for the disappearance of $C_7H_7^+/C_7D_7^+$ by reactions with precursor neutrals were calculated as described earlier and the values are shown in Table 7.2.

TABLE 7.2

Rate coefficients for different $C_7H_7^+/C_7H_8$ reaction systems.

Precursor	k /10^{-10} cm^3s^{-1}		
Ion / Neutral	Toluene-d_8	NBD	CHT
Toluene-d_8	(3.5 ± 1.0)[a]	(0.8 ± 0.3)	(1.7 ± 0.5)
NBD	(3.2 ± 1.0)	(5.4 ± 1.7)	
CHT	(4.6 ± 1.5)		(8.2 ± 2.6)

[a]Previously reported as 4.0 x 10^{-10} cm^3/s for the reaction of benzyl ions with toluene (Dunbar, 1975).

$C_7H_7^+$ Reactions with Acetylene: $C_7H_7^+$ ions produced by Xe^+ dissociative charge transfer of norbornadiene and cycloheptatriene reacted slowly with acetylene to produce very small amounts of $C_9H_9^+$.

$$C_7H_7^+ + C_2H_2 \text{ -----> } C_9H_9^+ \qquad (7.21)$$

The following reaction was also observed with the ions produced from cycloheptatriene:

$$C_7H_7^+ + C_2H_2 \text{ -----> } C_7H_9^+ + C_2 \qquad (7.22)$$

The rate coefficients for the disappearance of $C_7H_7^+$ ions produced from norbornadiene and cycloheptatriene were found to be $(1.0 \pm 1.0) * 10^{-11}$ and $(3.6 \pm 1.3) \times 10^{-11}$ cm^3/s respectively. However, when toluene was used as a precursor for $C_7H_7^+$ production by Kr^+ dissociative charge transfer, no reaction with acetylene was observed.

$C_7H_7^+$ Reactions with Diacetylene: $C_7H_7^+$ ions from different precursors were reacted with both diacetylene and deuterated diacetylene in order to identify the reaction products from those with the precursor neutral (for instance the reactions with both diacetylene and cycloheptatriene give $C_{11}H_9^+$). The following reactions of $C_7H_7^+$ with diacetylene were observed.

$$C_7H_7^+ + C_4H_2 \text{ -----> } C_9H_7^+ + C_2H_2 \qquad (7.23a)$$

$$C_7H_7^+ + C_4D_2 \text{ -----> } C_9H_5D_2^+ + C_2H_2 \qquad (7.23b)$$

$$C_7H_7^+ + C_4H_2 \text{ -----> } C_{11}H_9^+ \qquad (7.24a)$$

$$C_7H_7^+ + C_4D_2 \text{ -----> } C_{11}H_7D_2^+ \qquad (7.24b)$$

$$C_9H_7^+ + C_4H_2 \text{ -----> } C_{13}H_9^+ \qquad (7.25a)$$

$$C_9H_5D_2^+ + C_4D_2 \text{ -----> } C_{13}H_5D_4^+ \qquad (7.25b)$$

In the toluene case, the following reaction was also observed:

$$C_8H_9^+ + C_4H_2 \text{ -----> } C_{12}H_9^+ + H_2 \qquad (7.26a)$$

$$C_8H_9^+ + C_4D_2 \text{ -----> } C_{12}H_7D_2^+ + H_2 \qquad (7.26b)$$

Ion intensity vs time curves of $C_7H_7^+$ (produced by Kr^+ charge transfer from toluene) and product ions for the reaction with diacetylene are shown in Figure 7.3. The rate coefficients for the disappearance of $C_7H_7^+$ by the sum of reactions (7.23) and (7.24) for different precursors are given in Table 7.3.

When $C_7H_7^+$ ions were produced in a 100ms reaction time by Xe^+ dissociative charge transfer from norbornadiene and cycloheptatriene in the presence of C_4H_2, production of unreactive $C_7H_7^+$ was observed by the following reactions.

$$Xe^+ + C_4H_2 \text{ -----> } C_4H_2^+ + Xe \qquad (7.27)$$

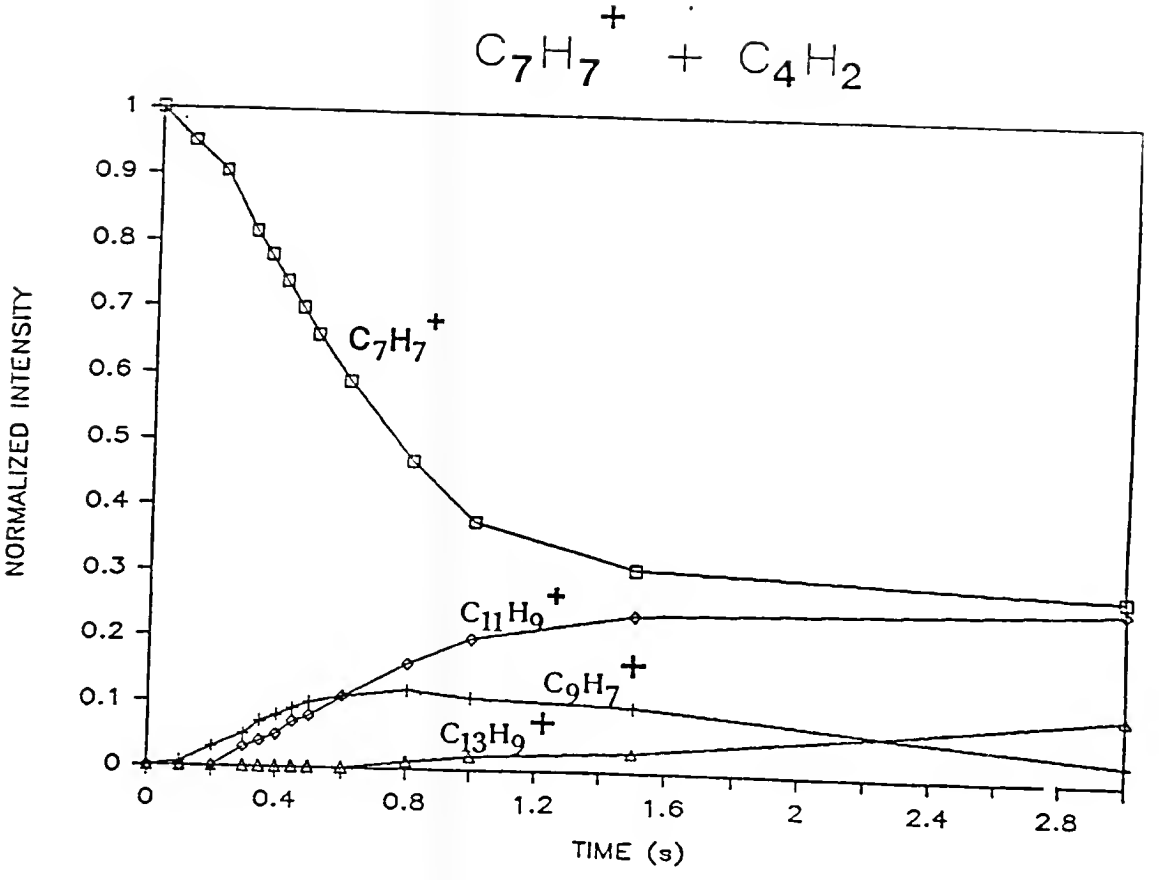

Figure 7.3. Reactions of $C_7H_7^+$ Ions Formed from Toluene by Kr^+ Chemical Ionization with Diacetylene.

TABLE 7.3

Reaction rate coefficients for $C_7H_7^+ + C_4H_2$ reaction.

Precursor	$k/10^{-10}$ cm^3s^{-1}
Toluene	(1.50 ± 0.50)
Norbornadiene	(0.25 ± 0.19)
Cycloheptatriene	(0.75 ± 0.25)

$$C_4H_2^+ + C_7H_8 \text{ -----> } C_7H_7^+(\text{unreactive}) + C_4H_2 + H \quad (7.28)$$

Thus in order to obtain accurate information on reaction kinetics of the $C_7H_7^+ + C_4H_2$ reaction, the $C_4H_2^+$ ion was continuously ejected during $C_7H_7^+$ ion formation by dissociative charge transfer using Xe^+.

Also in this study, the relative abundances of the ions produced from toluene as a function of electron impact energy were determined for the purpose of comparison with results obtained for norbornadiene and cycloheptatriene (see Chapter 6). Relative abundances of $C_5H_5^+$ and $C_3H_3^+$ as a function of energy for toluene are shown in Figure 7.4. Results of the earlier study given in Chapter 6 for norbornadiene and cycloheptatriene are also included in the figure for comparison.

Discussion

Since numerous earlier investigations (Dunbar, 1975; Jackson et al., 1977; Traeger and McLoughlin, 1978; McLafferty and Bockhoff, 1979; Sharma and Kebarle, 1981) have demonstrated that $C_7H_7^+$ ions have at least two stable structures, one reactive and the other unreactive, the results of this study are interpreted in terms of the possibility of other stable structure(s).

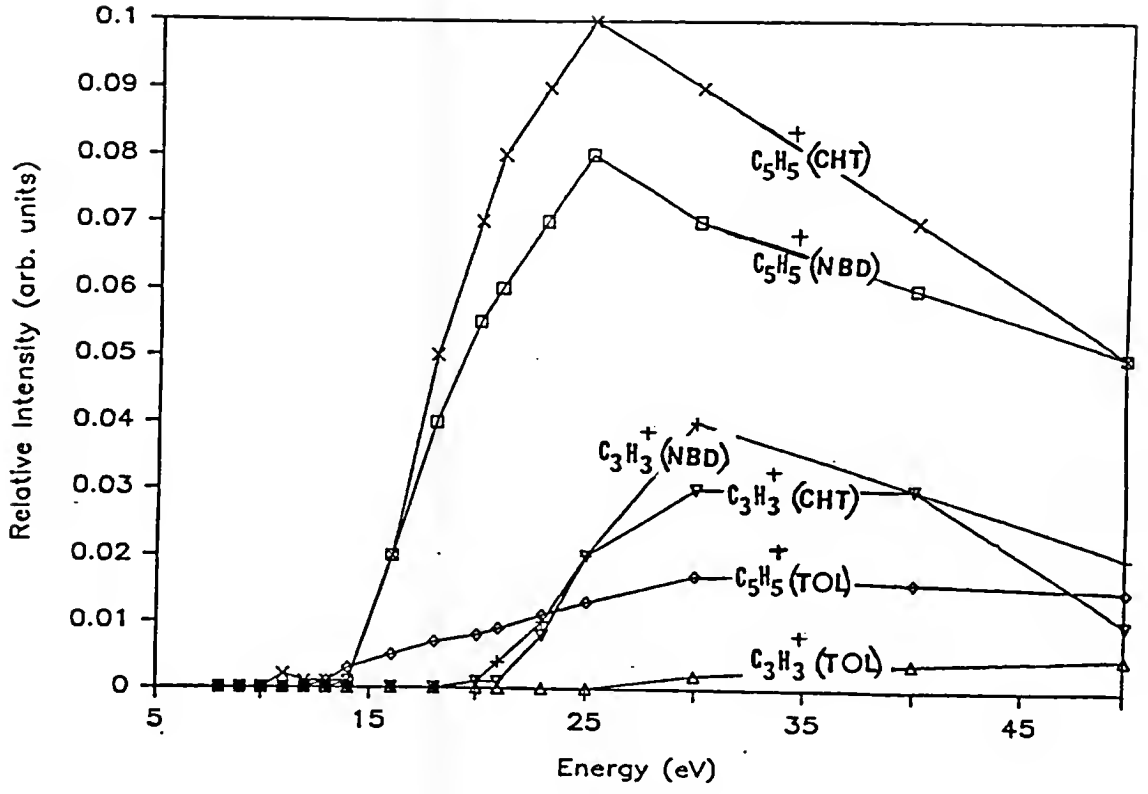

Figure 7.4. Relative Intensities of Fragment Ions from Different $C_7H_7^+$ Precursors as a Function of Electron Energy. Toluene, norbornadiene and cycloheptatriene are abbreviated as (TOL), (NBD) and (CHT) respectively.

The nature of the reaction products observed for the reactions of $C_7H_7^+$ ions with their precursor neutrals, toluene, norbornadiene and cycloheptatriene, were significantly different, as shown in Figures 7.1a, 7.1b and 7.1c respectively. In order to determine whether these differences were due to the neutral or ion structures deuterated toluene was used to monitor the reaction mechanisms with different neutral precursors. As seen in equations (7.12)-(7.19), $C_7D_7^+$ ions reacted with the precursor neutrals, producing deuterated analogues of the same product ions observed for each non-deuterated ion/precursor reaction system. This result showed that the differences in reaction products are the result of the different structures of neutral precursors, and not necessarily of different ion structures. Then deuterated toluene was used as a reactant neutral for $C_7H_7^+$ ions produced from different precursors. As seen from equation (7.20), $C_7H_7^+$ ions produced from all three precursors reacted with C_7D_8 to produce $C_8D_7H_2^+$, although very low ion intensities were produced with cycloheptatriene and norbornadiene precursorsors. The reaction mechanism which gives this product ion is also operative in reaction (7.12) and is believed (Shen and Dunbar, 1974; Dunbar, 1975; Jackson et al., 1977; McCreary and Freiser, 1978) to be indicative of the benzyl structure for $C_7H_7^+$ ions (see Figure 7.5). This mechanism has also been studied earlier

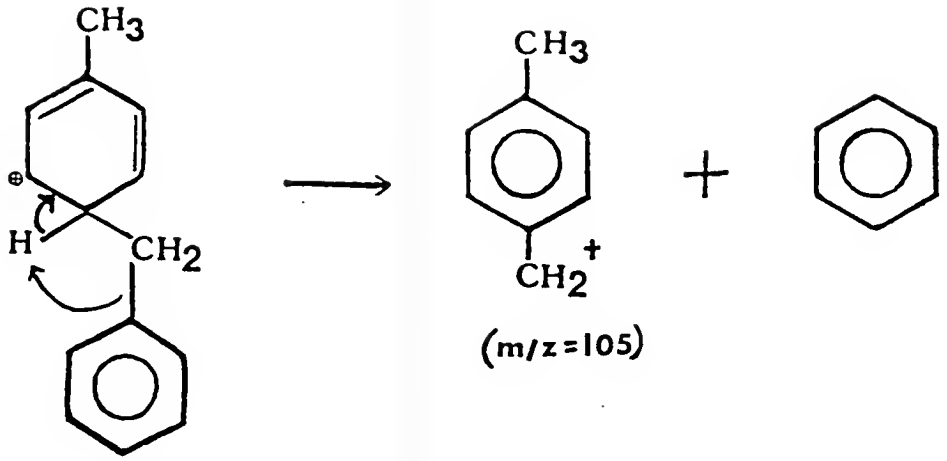

Figure 7.5. Proposed (Shen and Dunbar, 1974; Dunbar, 1975; Jackson et al., 1977; McCreary and Freiser, 1978) Mechanism of $C_8H_9^+$ Formation from the Reaction of Benzyl Ion with Toluene.

by similar isotopic labeling experiments (Jackson et al., 1977; Ausloos et al., 1980). The only important difference in the behavior of reactive $C_7H_7^+$ ions produced from different precursors was their reaction rates with precursor neutrals. $C_7H_7^+/C_7D_7^+$ ions produced from toluene/deuterated toluene reacted at similar rates with toluene, norbornadiene and cycloheptatriene whereas $C_7H_7^+$ ions produced either from norbornadiene and cycloheptatriene reacted at much slower rates with toluene than with their own precursor neutrals (see Table 7.2).

Reactions of $C_7H_7^+$ and product ions with diacetylene are represented by equations (7.23)-(7.25) independent of the precursor used. An interesting mechanism is observed for C_2 and C_4 addition reactions shown by equations (7.23b) and (7.26b) which is indicative of an ion/molecule complex from which C_2H_2 and H_2, respectively, rather than C_2D_2 and D_2 are the apparent neutral products. Since complete scrambling of product ions is not observed, preferential retention of C_2D_2 and D_2 is probably due to a specific structure of the intermediate complex which does not rearrange fast enough to give complete scrambling before falling apart to give the products. Reaction rates with diacetylene followed a different trend than those with precursor neutrals for $C_7H_7^+$ ions from different precursors. In this case, $C_7H_7^+$ ions from toluene reacted

faster than those from norbornadiene and cycloheptatriene (see Table 7.3).

Different behavior was observed when C_2H_2 was used as a reactant neutral. $C_7H_7^+$ from norbornadiene and cycloheptatriene reacted slowly with acetylene as shown by equations (7.21) and (7.22). On the other hand, no reaction products were observed with $C_7H_7^+$ from toluene.

Table 7.1 shows the percent of unreactive $C_7H_7^+$ as a function of the internal energy of the ion formed from different precursors. At the lowest internal energies above the $C_7H_7^+$ formation threshold, $C_7H_7^+$ from toluene had a much smaller percentage of unreactive isomer than $C_7H_7^+$ from norbornadiene and cycloheptatriene. Formation of unreactive $C_7H_7^+$ from all three precursors decreased with increasing internal energy and stayed constant at high enough energy. This behavior is different from that observed previously for toluene and norbornadiene (Dunbar, 1975; Ausloos, 1982) in which the unreactive percent first decreased and then increased with internal energy. The previous results were interpreted in terms of the interplay between the two equilibria involving different $C_7H_8^+$ and $C_7H_7^+$ structures (Sagi et al., 1974; McLafferty and Bockhoff, 1979; Andrews and Keelan, 1981; Ausloos, 1982). The different behavior observed in an earlier ICR study (Jackson et al., 1977), which is similar to that observed in this work, was suggested (McLafferty and Bockhoff, 1974;

Ausloos, 1980) to be the result of the displacement of the equilibrium between two $C_7H_7^+$ structures by the removal of the reactive $C_7H_7^+$ ions through chemical reaction.

In Chapter 6, the relative abundances of ions produced from norbornadiene and cycloheptatriene as a function of ionizing electron energy were reported. Similarities of $C_7H_7^+$, $C_5H_5^+$ and $C_3H_3^+$ appareance curves were interpreted to imply that $C_7H_7^+$ formed from these two compounds behaves similarly, i.e., follows the same fragmentation pathways in the same energy range. Differences in the appareance curve of $C_5H_6^+$ for norbornadiene and cycloheptatriene were interpreted as suggesting that $C_7H_8^+$ formed from these compounds by electron impact may have different structures. Extensive fragmentation of $C_7H_8^+$ to give $C_5H_6^+$ was also reported earlier for norbornadiene (Ausloos, 1982). In this study, the relative abundances of the ions produced from toluene as a function of energy were determined for the purpose of comparison with earlier results obtained for norbornadiene and cycloheptatriene. In contrast to the observed similarity mentioned above between norbornadiene and cycloheptatriene fragment ion appareance curves, those of toluene were significantly different both in terms of energetics and of general shape. For example, the onsets of formation for both $C_5H_5^+$ and $C_3H_3^+$ were different than those values observed for the other two precursors. Furthermore,

the relative intensities for $C_5H_5^+$ and $C_3H_3^+$ increased much more slowly with energy relative to those from norbornadiene and cycloheptatriene. The maximum relative intensities for $C_5H_5^+$ and $C_3H_3^+$ ions were respectively 0.017 and 0.005 for toluene and 0.10 and 0.035 for norbornadiene and cycloheptatriene (see Figure 7.4). This different behavior in the fragmentation of $C_7H_7^+$ produced from toluene suggests the involvement of a different structure (benzyl$^+$) for $C_7H_7^+$ in the case of toluene.

A possible potential energy surface for $C_7H_7^+/C_7H_8^+$ system is shown in Figure 7.6. Based on the differences in behavior observed in this study for $C_7H_7^+$ ions produced from three precursors, the possibility of stable structure(s) other than benzyl and tropylium must be considered. The unreactive structure which was observed in all three cases has been shown to be cyclic tropylium by a number of previous experimental (see for example, Jackson et al., 1977) and theoretical (Abbaund and Hehre, 1976; Cone et al., 1977) studies. Similarly, the reactive isomer produced from toluene was identified as the benzyl structure numerous times previously (see for example, Ausloos et al., 1980; Bombach et al., 1983). However, the results of this study have shown that it behaves somewhat differently from the reactive $C_7H_7^+$ isomers produced from norbornadiene and cycloheptatriene. Although no definitive assignment for reactive $C_7H_7^+$ ion structure(s) produced from norbornadiene

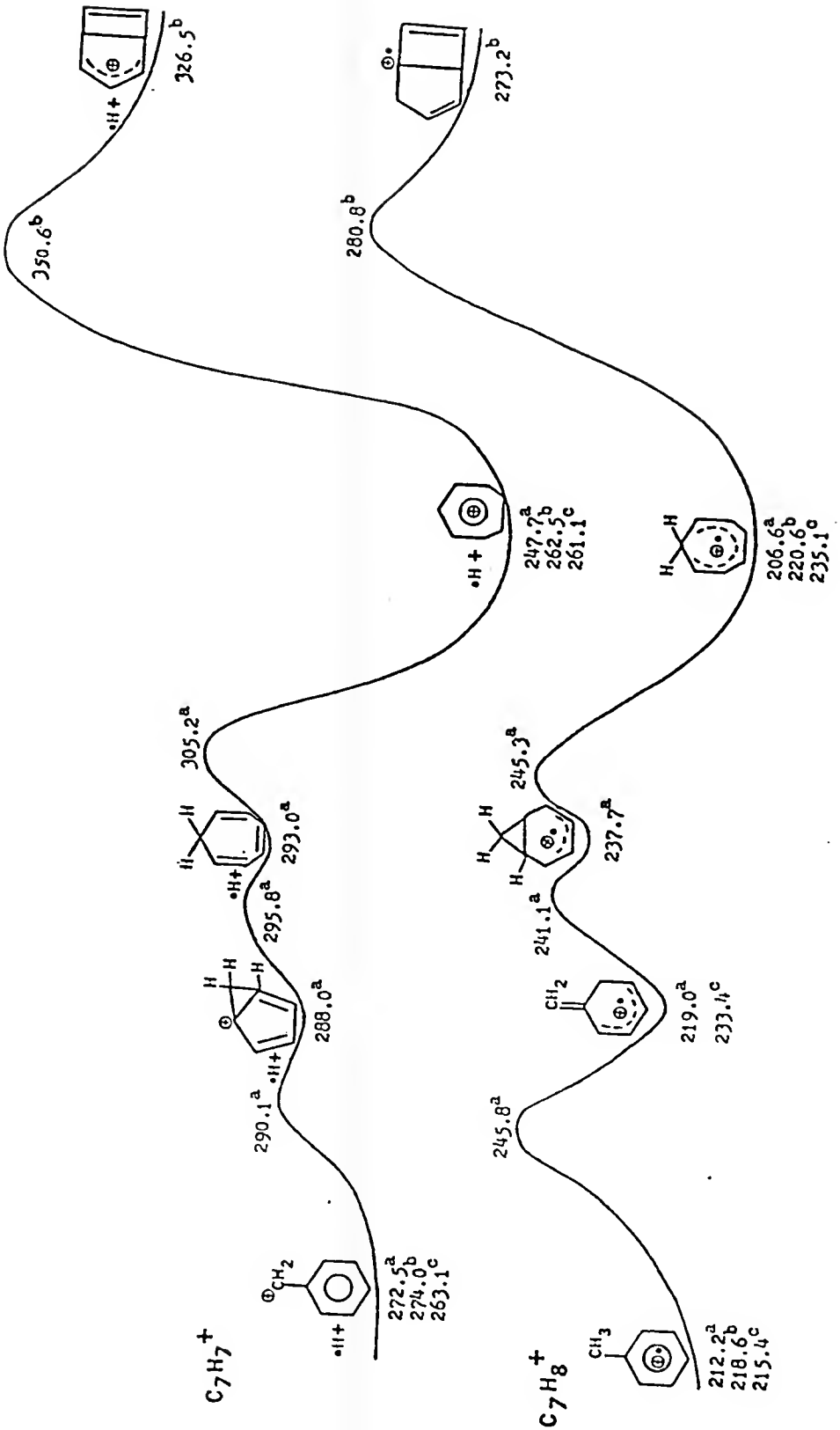

Figure 7.6. Potential Energy Surface for $C_7H_7^+/C_7H_8^+$ System. Numbers refer to heats of formation values in units of kcal/mol. [a]MINDO. [b]AM1 and [c]experimental.

and cycloheptatriene can be made at this point, the most probable structures will be discussed considering the energetics of $C_7H_7^+$ ions.

Cycloheptatriene. AM1 calculations for the $C_7H_8^+/C_7H_7^+$ surface[15] suggest the structure produced by hydrogen loss from the bicyclo[3.2.0]heptadiene radical cation (BCH^+), is a possible stable $C_7H_7^+$ isomer, accessible at about 2.8 eV above the appearance potential of tropylium from cycloheptatriene (see Figure 7.6). This structure is in a sufficiently deep potential well that it might reasonably be expected to live for an extended time. It was also suggested[14] that this structure is most probably formed from cycloheptatriene by isomerization on the radical cation surface followed by hydrogen loss from (BCH^+). Isomerization of $(BCH-H)^+$, (ΔH_f=274.4kcal/mol)[14] to tropylium is considered unlikely due to the high energy barrier between two structures as seen in Figure 7.6. Although the barrier to form the toluene ion is lower than that for (BCH^+), it was suggested[14] that the simplicity of the rearrangement to the latter, compared to the convoluted surface leading to benzyl or toluene radical ion may make formation of BCH^+, a faster rearrangement at high enough energy. Consistent with these calculations, our experimental results show that the percent of unreactive

[15] J. E. Bartmess, private communication.

$C_7H_7^+$ from cycloheptatriene decreases very rapidly with increasing internal energy. This can be interpreted as a result of increased isomerization of the cycloheptatriene cation to (BCH^+). At high energy, when the equilibrium between these two parent ions is established, the percent of unreactive isomer stays constant due to the absence of isomerization between two $C_7H_7^+$ structures with an energy barrier of 14.1 kcal/mol[16]. Other experimental evidence for the involvement of different structures for $C_7H_8^+$ ions formed from toluene and cycloheptatriene comes from the strikingly different photodissociation curves of these ions (Dunbar and Fu, 1973).

Norbornadiene. In spite of the general similarity of the behavior of $C_7H_7^+$ ions from cycloheptatriene and norbornadiene, differences in reactivity (see Tables 7.2 and 7.3) suggest the formation of a $C_7H_7^+$ structure different from that discussed above for cycloheptatriene. A simple bond breakage in norbornadiene can directly form an ipso-protonated benzyl radical, $C_6H_5(H^+)CH_2$ ion, in which a 1,2-hydrogen shift leads to the intermediate, 5-methylene-1,3-cyclohexadiene ion, (MCH^+) with a theoretical ΔH_f = 219 kcal/mol (Dewar and Landman, 1977) (see Figure 7.6). This ion was proposed to account for the ring expansion of the toluene ion in the $toluene^+$ ---> $cycloheptatriene^+$

---

[16]J. E. Bartmess, private communication.

isomerization process (Dewar and Landman, 1977). The formation of (MCH^+) from other precursor cations at least with a transitory existence has been indicated by previous experimental evidence (Leusen et al., 1973). After the availability (Gajewski and Gortva, 1982) of 5-methylene-1,3-cyclohexadiene, experimental determination of its ionization potential indicated a heat of formation value 18 kcal/mol higher than that of the toluene ion (Bartmess, 1982).

Once this intermediate ion is formed, it can rearrange to another structure or decompose directly to the $C_7H_7^+$ ion. In fact, it was suggested that direct decomposition of this ion is in competition with rearrangement to other structures, cycloheptatriene cation being the most probable rearrangement product (Bursey et al., 1973). The competition between these two processes is believed to depend on the internal energy with rearrangement being favored at lower energies (Dunbar and Klein, 1977). Thus at low energies, fragmentation to $C_7H_7^+$ after rearrangement to cycloheptatriene but not to toluene ion is expected due to the lower activation barrier for fragmentation of cycloheptatriene ion relative to toluene parent ion (Dunbar, 1975). This is consistent with our results which indicate a high percent of unreactive $C_7H_7^+$ (tropylium$^+$) formed from norbornadiene at low energy (see Table 7.1). Furthermore, as a result of the photodissociation study of $C_7H_8^+$ structures (Dunbar and Fu, 1973), possibility for conversion of about

half the norbornadiene cations to the cycloheptatriene structure was not inconsistent with the data. On the other hand, it has been reported that there is no rearrangement of this ion to toluene ion on a time scale of 10^{-2} s (Bursey et al., 1971).

Photodissociation spectra of n-butylbenzene and 2-phenylethanol ions which are believed to form (MCH^+) were studied in order to identify any possible rearrangement products (Dunbar and Klein, 1977). The results were consistent with the retention of the (MCH^+) structure, with less than 20 percent rearrangement to cycloheptatriene ion. Although there was not any evidence for ready interconversion among $C_7H_8^+$ structures for nondecomposing methylenecyclohexadiene ions, it was suggested the that more energetic, decomposing ions may interconvert to other structures. In this study, the decrease in the percent of tropylium structure with the increase in energy is interpreted as a result of decomposition of (MCH^+) becoming competitive with rearrangement to the cycloheptatriene ion. Thus, the $C_7H_7^+$ structure formed by hydrogen loss from (MCH^+) can be suggested as the reactive isomer observed for norbornadiene. The overall results of this study in terms of the proposed structures for $C_7H_7^+$ ions formed from different precursors are given in Table 7.4.

TABLE 7.4

Proposed $C_7H_7^+$ structures from different precursors.

Precursor	Unreactive structure	Reactive structure	ΔH_f (kcal/mol)
Toluene	Tropylium$^+$	Benzyl$^+$	211
NBD	Tropylium$^+$	(BCH-H)$^+$[a]	271
CHT	Tropylium$^+$	(MCH-H)$^+$[b]	?(236)

[a]Structure produced by hydrogen loss from bicyclo[3.2.0]heptadiene.
[b]Structure produced by hydrogen loss from 5-methylene-1,3-cyclohexadiene ion.

An ICR study (Bartmess, 1982) involving the formation of $(MCH)^+$ from its precursor neutral at 30eV electron energy indicated ion/molecule chemistry different from that of toluene. $C_7H_7^+$ produced from (MCH^+) was reported to have a different rate coefficient and reaction efficiency for the formation of $C_8H_9^+$. It is interesting to note that the rate coefficient reported (0.6×10^{-10} cm^3/s) (Bartmess, 1982) for this reaction agrees very closely with the value, (0.8 ± 0.3) $\times 10^{-10}$ cm^3/s found in this work for the reaction of $C_7H_7^+$ formed from norbornadiene with toluene (see Table 7.2). Although a definitive structure can not be assigned to $C_7H_7^+$ formed from (MCH^+) yet, one possible structure is the norcaradienyl ion, which was calculated to be stable with ΔH_f = 235.9 kcal/mol (Cone et al., 1977) (see Figure 7.6).

Supporting experimental evidence for the existence of stable $C_7H_7^+$ structures other than benzyl and tropylium comes from a UV absorption study of $C_7H_7^+$ ions in solid argon (Andrews and Keelan, 1981). In relation to rate coefficient data for reactions with precursor neutrals, acetylene, and diacetylene the same trend was observed for norbornadiene and cycloheptatriene. In all three cases, the reactive structure formed from norbornadiene reacted more slowly than that formed from cycloheptatriene. This is consistent with the general observation that less reactive structures of small hydrocarbon ions have lower heats of

formation since the $C_7H_7^+$ structure formed from (MCH^+) has a lower heat of formation than that formed from (BCH^+).

Finally, in relation to the ionic soot formation mechanism, the existence of a different $C_7H_7^+$ ion less stable than benzyl in flames would account for the disagreement between experiment and theory in relation to $C_7H_7^+$ concentration in flames (Olson and Calcote, 1981a).

CHAPTER 8
CONCLUSIONS AND RECOMMENDATIONS

The experimental work reported here contributes significantly to an understanding of the reactivity, energetics, and structures of small hydrocarbon ions. However, it does not prove or disprove an ionic mechanism of soot formation. It does lead to several clarifications of the ionic mechanism, which will be discussed below.

The extensive ion/molecule condensation reactions at rates approaching the Langevin limit observed when $C_3H_3^+$, $C_5H_5^+$ and $C_7H_7^+$ react with C_4H_2 suggest that this aspect of the proposed (Calcote, 1981; Olson and Calcote, 1981a) ionic path to soot formation is quite credible. The general reaction

$$C_xH_y^+ + C_4H_2 \text{ ---> } C_{x+2}H_y^+ + C_2H_2 \qquad (8.1)$$

appeares to occur in a facile manner and could be quite important in soot nucleation. Some of the product ions formed (e.g. $C_5H_3^+$ and $C_7H_5^+$) have been seen to be abundant in both nonsooting and sooting flames (Olson and Calcote, 1981b). Furthermore, product ions with increased C:H ratios having as many as 13 carbon atoms have been observed in the

reaction of $C_7H_7^+$ with diacetylene. On the other hand, the observation of $C_3H_3^+$ isomerization and not condensation with acetylene as well as low bimolecular reactivity of acetylene with $C_5H_5^+$ and $C_7H_7^+$ suggests that the proposed sequential acetylene addition reactions to $C_3H_3^+$ in the ionic soot formation mechanism be reconsidered. Other channels such as direct reaction of neutral aromatics with $C_3H_3^+$ (Michaud et al., 1981; Baykut et al., 1986) may be as important in the formation of small polycyclic ions.

These experiments were carried out at significantly lower temperatures (363K) and pressures ($p \leq 5 \times 10^{-5}$ torr) than those found in most combustion environments. It is thus quite possible that third-body collisions in atmospheric pressure flames can stabilize a fraction of the reaction complexes leading to significant <u>termolecular</u> reactivity of the ions studied with acetylene. In fact, such collisional stabilization of the association complexes for the reactions of $C_3H_3^+$ and $C_4H_4^+$ with C_2H_2 has been shown to occur in higher pressure SIFT studies (Smith and Adams, 1987; Knight et al., 1987).

Continuation of this work in several directions could have a major impact on assessing the importance of an ionic mechanism of soot formation. First, experiments should be carried out at higher pressures, using a high pressure source for the FTICR mass spectrometer, to assess the importance of third-body stabilization of ion/molecule

collision complexes. Actual sampling of ions from flames into the FTICR mass spectrometer, in order to probe their structures and reactivity, would extend the isolated studies done here to an actual combustion environment.

A crucial argument in favor of an ion/molecule soot nucleation route is the ease with which cyclic ions, which could lead to polycyclic aromatic hydrocarbons, are formed. Yet the work reported here did not identify definitively when the first cyclic ions were formed. Predicted spectra from theoretical calculations on $C_5H_5^+$, $C_5H_3^+$ and $C_7H_x^+$ ions should be combined with laser spectroscopic studies on these ions to determine which, if any, have cyclic structures. Also, theoretical studies which probe the geometries of the ion/molecule collision complexes, such as those reported in Chapter 5 for $C_3H_3^+$ + acetylene, should be extended to other important reactions, e.g. with diacetylene, and the nature of the proposed chemi-ionization reaction which forms the $C_3H_3^+$ ion (see Chapter 1) should be investigated.

APPENDIX I

PROGRAM TO CALCULATE ABSOLUTE RATE CONSTANTS AND THEIR 95% CONFIDENCE LIMITS FROM RAW OR NORMALIZED INTEGRATED PEAK AREAS OF THE REACTING ION AS A FUNCTION OF TIME IN FOURIER TRANSFORM ION CYCLOTRON RESONANCE MASS SPECTROSCOPY.

WRITTEN JULY AND AUGUST 1986 BY FEZA OZTURK AND BRYAN HEARN
Adapted for use with the IBM pc on 9-17-87 by CLIFF WATSON.
UNDER THE DIRECTION OF DR. JOHN EYLER
DEPARTMENT OF CHEMISTRY
UNIVERSITY OF FLORIDA
GAINESVILLE, FLORIDA 32611

TYPICAL ORDER OF EXECUTION:

A. Calculation of the system factor using the literature value of a well-known rate constant for a reference reaction (this involves calculating the observed rate constant for the reference reaction, #3, the actual pressure, #1, then the system factor, #4, which uses the literature value for the absolute rate constant along with your experimental observed rate constant and actual pressure just calculated using #3 and #1). The system factor will be used later in the absolute rate constant calculation, so it should be noted. If this calculation is not desired, a value of 1 may be input for the system factor.

B. Running the program a second time, calculate the observed rate constant for the reaction of the ion with its precursor neutral, #3.

Step 3 should be followed by step 9 here if the no baseline correction option is chosen in the calculation of k.

C. Calculation of the observed rate constant for the reaction of the ion with reactant neutral (gives the sum and individual rate constants with precursor and reactant neutrals, # 5). This should be followed by step 10 if the no baseline correction option is chosen in the calculation of k_2.

D. Determination of the actual pressure for the reactant neutral by entering the ionization gauge and capacitance manometer readings manually (Baratron factor is determined from the slope by linear least squares, # 1).

E. Calculation of the absolute rate constant using the actual pressure and system factor (# 6).

For steps B and C, raw or normalized integrated peak areas of the reacting ion as a function of time should be entered manually.

System factor is a correction factor for pressure calibration due to the fact that ionization gauge and capacitance manometer are located at different points of the instrument.

Options 2, 8, 11 and 12 can be used to input the appropriate values once they are calculated. This allows one to calculate absolute rate constants without going through the entire process by entering the precalculated values.

Baseline correction is needed to correct for the unreactive population of the reacting ion when both reactive and unreactive isomers exist (#'s 9 and 10 are used when there is no unreactive isomer).

```
      DIMENSION
RDATA(50,50),TIMES(100),TIC(50),TMPDAT(50),TMP2DT(50)
      DIMENSION
YP(100),XP(100),TEMP(50),ETEMP(50),CMA(100),TXGRAF(52),
     &TYGRAF(52)
      REAL K,IG,LITK,K2
      INTEGER FLAG
      CHARACTER*1 YESNO
 10   WRITE(*,*)' '
      WRITE(*,*)' '
      WRITE(*,*)' 1 PRESSURE CALC (MANUAL) 2 ENTER BF '
      WRITE(*,*)' 3 K AND 95% CONFIDENCE   4 SYSTEM FACTOR '
      WRITE(*,*)' 5 K2 AND 95% CONFIDENCE  6 ABSOLUTE RATE
CONSTANT   '
      WRITE(*,*)' 7 STOP              8 INPUT SYSTEM FACTOR  '
      WRITE(*,*)' 9 NO BASELINE CORR(FOR K) 10 NO BASELINE
CORR(K2) '
      WRITE(*,*)' 11 ENTER K AND 95% CL     12 ENTER K2 AND
95% CL  '
      WRITE(*,*)' '
      WRITE(*,*)'     INPUT CHOICE     '
      READ(*,*)I
      GOTO(100,200,300,400,500,600,700,800,900,1000,1300,
     &1400)I
      GOTO 10
 100  WRITE(*,*)' NUMBER OF POINTS TO ENTER MANUALLY FOR
PRESSURE '
      READ(*,*)NPRESS
      DO 123 I=1,NPRESS
      WRITE(*,120)I
 120  FORMAT(' INPUT IG READING # ',I5)
      READ(*,*)XP(I)
```

```
      WRITE(*,129)I
  129 FORMAT(' INPUT BARATRON READING # ',I5)
  123 READ(*,*)YP(I)
      CALL GRAF2D(XP,YP,NPRESS)
      WRITE(*,*)' INPUT THE NUMBER OF POINTS FOR LLSQ '
      READ(*,*)NPRESS
      FLAG=3
      CALL LLSQ(XP,YP,EYP,NPRESS,BF,EBF,FLAG,INT)
      DO 196 I=1,NPRESS
      TYGRAF(I)=YP(I)
  196 TXGRAF(I)=XP(I)
      TXGRAF(NPRESS+1)=XP(NPRESS)
      TYGRAF(NPRESS+1)=BF*XP(NPRESS)
      TXGRAF(NPRESS+2)=XP(1)
      TYGRAF(NPRESS+2)=BF*XP(1)
      CALL GRAF2D(TXGRAF,TYGRAF,(NPRESS+2))
      WRITE(*,*)' THE BARATRON FACTOR IS'
      WRITE(*,*)BF
      WRITE(*,*)' THE 95% CONFIDENCE LIMIT FOR BARATRON
FACTOR IS '
      WRITE(*,*)EBF
  150 WRITE(*,*)' INPUT THE IONIZATION GAUGE READING '
      READ(*,*)IG
      P=IG*BF
      WRITE(*,*)' THE PRESSURE IS '
      WRITE(*,*)P
      WRITE(*,*)' DEFAULT 95% CON.LIMIT FOR IG IS 0.1*GAUGE:
CHANGE=Y '
      READ(*,88)YESNO
      IF(YESNO.EQ.'Y')THEN
      WRITE(*,*)' INPUT THE % MULTIPLIER DESIRED 95% CON.
LIMIT FOR IG '
           READ(*,*)EI
           EI=EI*IG
           GOTO 152
      ENDIF
      EI=0.1*IG
C DEFAULT 95% CONF.LIMIT FOR ION. GAUGE READING IS EST'ED AS
0.1*ION.GAUGE
  152 EP=SQRT(BF*BF*EI*EI+IG*IG*EBF*EBF)
      WRITE(*,*)' THE 95% CONFIDENCE LIMIT FOR PRESSURE IS'
      WRITE(*,*)EP
      GOTO 10
  200 WRITE(*,*)' ENTER THE BARATRON FACTOR '
      READ(*,*)BF
      WRITE(*,*)' ENTER THE 95% CONF. LIMIT OF BF '
      READ(*,*)EBF
      GOTO 150
300   WRITE(*,*)'  NUMBER OF POINTS TO ENTER MANUALLY ='
      READ(*,*)NTIM
      DO 366 I=1,NTIM
      WRITE(*,364)I
```

```
 364  FORMAT(' ENTER TIME #',I5)
      READ(*,*)TIMES(I)
      WRITE(*,*)' ENTER THE CIN OR CIN NORMALIZED TO TOTAL
ION CIN '
      READ(*,*)TEMP(I)
 366  CONTINUE
 345  WRITE(*,*)' DO YOU WISH BASELINE CORRECTION? YES=1 '
      READ(*,*)NANS
      IF(NANS.NE.1) GOTO 10
      CALL CNIC(NTIM,TEMP,ETEMP,XMAX,EXMAX)
 390  YLSTPT=TEMP(1)
      KOUNT =1
      DO 391 I=2,(NTIM-1)
      IF(TEMP(I).GT.YLSTPT)GOTO 392
      YLSTPT=TEMP(I)
 391  KOUNT=KOUNT + 1
 392  CALL GRAF2D(TIMES,TEMP,KOUNT)
      WRITE(*,*)' INPUT THE NUMBER OF POINTS TO USE '
      READ(*,*)NPOINT
 395  CALL LLSQ(TIMES,TEMP,ETEMP,NPOINT,K,ERRK,FLAG,YINT)
      DO 396 I=1,NPOINT
      TYGRAF(I)=TEMP(I)
 396  TXGRAF(I)=TIMES(I)
      TXGRAF(NPOINT+1)=TIMES(NPOINT)
      TYGRAF(NPOINT+1)=K*TIMES(NPOINT)+YINT
      TXGRAF(NPOINT+2)=TIMES(1)
      TYGRAF(NPOINT+2)=K*TIMES(1)+YINT
      CALL GRAF2D(TXGRAF,TYGRAF,(NPOINT+2))
      K=-K
      WRITE(*,*)'  K AND 95% CONFIDENCE LIMIT IN K='
      WRITE(*,*)K,ERRK
      GOTO 10
 400  WRITE(*,*)' HAVE YOU CALCULATED THE PRESSURE? YES=1'
      READ(*,*)NANS
      IF (NANS.NE.1)GOTO 10
      WRITE(*,*)' INPUT THE LITERATURE VALUE K '
      READ(*,*)LITK
      WRITE(*,*)' INPUT THE LITERATURE ERROR VALUE  '
      READ(*,*)ELIT
      WRITE(*,*)' INPUT THE TEMPERATURE '
      READ(*,*)T
      WRITE(*,*)' THE DEFAULT ERROR IN TEMP IS 2 DEGREES.
CHANGE=Y '
      READ(*,88)YESNO
      IF(YESNO.EQ.'Y')THEN
           WRITE(*,*)' INPUT THE DESIRED ERROR IN TEMP. '
           READ(*,*)ET
           GOTO 415
      ENDIF
      ET=2
C DEFAULT ERROR IN TEMPERATURE IS ESTIMATED AS 2 DEGREES
 415  K=1.036E-19*T*K/P
```

```
      EK=SQRT(ET*ET/(T*T)+EK*EK/(K*K)+EP*EP/(P*P))*K
      SF=K/LITK
      ESF=SQRT(EK*EK/(K*K)+ELIT*ELIT/(LITK*LITK))*SF
      WRITE(*,*)' THE SYSTEM FACTOR AND ITS 95% CONFID.
LIMIT IS '
      WRITE(*,*)SF,ESF
      GOTO 10
500   WRITE(*,*)'  NUMBER OF POINTS TO ENTER MANUALLY ='
      READ(*,*)NTIM
      DO 566 I=1,NTIM
      WRITE(*,564)I
 564  FORMAT(' ENTER TIME #',I5)
      READ(*,*)TIMES(I)
      WRITE(*,*)' ENTER THE CIN OR CIN NORMALIZED TO TOTAL
CIN '
      READ(*,*)TEMP(I)
 566  CONTINUE
 545  WRITE(*,*)' DO YOU WANT BASELINE CORRECTION? YES=1 '
      READ(*,*)NANS
      IF(NANS.NE.1)GOTO 10
      CALL CNIC(NTIM,TEMP,ETEMP,XMAX,EXMAX)
 590  YLSTPT=TEMP(1)
      KOUNT =1
      DO 591 I=2,(NTIM-1)
      IF(TEMP(I).GT.YLSTPT)GOTO 592
      YLSTPT=TEMP(I)
 591  KOUNT=KOUNT + 1
 592  CALL GRAF2D(TIMES,TEMP,KOUNT)
      WRITE(*,*)' INPUT THE NUMBER OF POINTS TO USE '
      READ(*,*)NPOINT
      CALL LLSQ(TIMES,TEMP,ETEMP,NPOINT,K2,ERRK2,FLAG,YINT)
      DO 596 I=1,NPOINT
      TYGRAF(I)=TEMP(I)
 596  TXGRAF(I)=TIMES(I)
      TXGRAF(NPOINT+1)=TIMES(NPOINT)
      TYGRAF(NPOINT+1)=K2*TIMES(NPOINT)+YINT
      TXGRAF(NPOINT+2)=TIMES(1)
      TYGRAF(NPOINT+2)=K2*TIMES(1)+YINT
      CALL GRAF2D(TXGRAF,TYGRAF,(NPOINT+2))
      K2=-K2
      WRITE(*,*)' THE OBSERVED SLOPES (K1 AND K2) ARE '
      WRITE(*,*)K,K2
      WRITE(*,*)' THE ERRORS IN K1 AND K2 ARE '
      WRITE(*,*)ERRK,ERRK2
 598  K=K2-K
      EK=SQRT(ERRK*ERRK+ERRK2*ERRK2)
      WRITE(*,*)' THE NET RATE CONSTANT IS'
      WRITE(*,*)K
      WRITE(*,*)' THE 95% CON. LIMIT IN THE OBSERVED RATE
CONSTANT IS'
      WRITE(*,*)EK
      GOTO 10
```

```
 600  WRITE(*,*)'CALCULATED THE SYSTEM FACTOR AND PRESSURE?
Y=1 '
      READ(*,*)NANS
      IF(NANS.NE.1)GOTO 10
      WRITE(*,*)' INPUT THE TEMPERATURE'
      READ(*,*)T
      TRUEK=1.036E-19*K*T/(SF*P)
      WRITE(*,*)' THE TRUE K IS '
      WRITE(*,*)TRUEK
      WRITE(*,*)' THE DEFAULT ERROR IN TEMP IS 2 DEGREES.
CHANGE=Y '
      READ(*,88)YESNO
      IF(YESNO.EQ.'Y')THEN
           WRITE(*,*)' INPUT THE DESIRED ERROR IN TEMP. '
           READ(*,*)ET
           GOTO 615
      ENDIF
      ET=2
C DEFAULT ERROR IN TEMPERATURE IS ESTIMATED AS 2 DEGREES
 615
ETRUEK=SQRT(EK*EK/(K*K)+ET*ET/(T*T)+ESF*ESF/(SF*SF)+EP*EP/
     &(P*P))*TRUEK
      WRITE(*,*)' THE 95% CONFIDENCE LIMIT FOR TRUE K IS '
      WRITE(*,*)ETRUEK
      GOTO 10
 800  WRITE(*,*)' INPUT SYSTEM FACTOR'
      READ(*,*)SF
      WRITE(*,*)' INPUT THE ERROR IN THE SYSTEM FACTOR '
      READ(*,*)ESF
      GOTO 10
 900  WRITE(*,*)'****NO BASELINE CORRECTION****'
      WRITE(*,*)'DEFAULT ERROR MULTIPLIER IN CIN IS 0.1
CHANGE=Y'
      READ(*,88)YESNO
      IF(YESNO.EQ.'Y')THEN
          WRITE(*,*)' INPUT THE DESIRED MULTIPLIER OF ERROR
IN CIN '
          READ(*,*)ECIN
           GOTO 915
      ENDIF
      ECIN=0.1
 915  DO 910 I=1,NTIM
      ETEMP(I)=ECIN*TEMP(I)
      ETEMP(I)=ETEMP(I)/TEMP(I)
 910  CONTINUE
      DO 920 I=1,NTIM
 920  TEMP(I)=LOG(TEMP(I))
 990  YLSTPT=TEMP(1)
      KOUNT =1
      DO 991 I=2,NTIM
      IF(TEMP(I).GT.YLSTPT)GOTO 992
      YLSTPT=TEMP(I)
```

```
 991  KOUNT=KOUNT + 1
 992  CALL GRAF2D(TIMES,TEMP,KOUNT)
      WRITE(*,*)' INPUT THE NUMBER OF POINTS TO USE IN LLSQ
CALC. '
      READ(*,*)NPOINT
      FLAG=2
      CALL LLSQ(TIMES,TEMP,ETEMP,NPOINT,K,ERRK,FLAG,YINT)
      DO 996 I=1,NPOINT
      TYGRAF(I)=TEMP(I)
 996  TXGRAF(I)=TIMES(I)
      TXGRAF(NPOINT+1)=TIMES(NPOINT)
      TYGRAF(NPOINT+1)=K*TIMES(NPOINT)+YINT
      TXGRAF(NPOINT+2)=TIMES(1)
      TYGRAF(NPOINT+2)=K*TIMES(1)+YINT
      CALL GRAF2D(TXGRAF,TYGRAF,(NPOINT+2))
      K=-K
      WRITE(*,*)' OBSERVED RATE CONSTANT AND 95% CONFIDENCE
LIMIT IS '
      WRITE(*,*)K,ERRK
      GOTO 10
 1000 WRITE(*,*)'****NO BASELINE CORRECTION****'
      WRITE(*,*)'DEFAULT ERROR MULTIPLIER IN CIN IS 0.1
CHANGE=Y'
      READ(*,88)YESNO
 88   format(a)
      IF(YESNO.EQ.'Y')THEN
           WRITE(*,*)' INPUT THE DESIRED MULTIPLIER OF ERROR
IN CIN '
         READ(*,*)ECIN
           GOTO 1015
      ENDIF
      ECIN=0.1
 1015 DO 1060 I=1,NTIM
      ETEMP(I)=ECIN*ETEMP(I)
      ETEMP(I)=ETEMP(I)/TEMP(I)
 1060 CONTINUE
      DO 1070 I=1,NTIM
 1070 TEMP(I)=LOG(TEMP(I))
 1090 YLSTPT=TEMP(1)
      KOUNT =1
      DO 1091 I=2,NTIM
      IF(TEMP(I).GT.YLSTPT)GOTO 1092
      YLSTPT=TEMP(I)
 1091  KOUNT=KOUNT + 1
 1092 CALL GRAF2D(TIMES,TEMP,KOUNT)
      WRITE(*,*)' INPUT THE NUMBER OF POINTS TO USE IN LLSQ
CALC. '
      READ(*,*)NPOINT
      FLAG=2
      CALL LLSQ(TIMES,TEMP,ETEMP,NPOINT,K2,ERRK2,FLAG,YINT)
      DO 1096 I=1,NPOINT
      TYGRAF(I)=TEMP(I)
```

```
 1096  TXGRAF(I)=TIMES(I)
       TXGRAF(NPOINT+1)=TIMES(NPOINT)
       TYGRAF(NPOINT+1)=K2*TIMES(NPOINT)+YINT
       TXGRAF(NPOINT+2)=TIMES(1)
       TYGRAF(NPOINT+2)=K2*TIMES(1)+YINT
       CALL GRAF2D(TXGRAF,TYGRAF,(NPOINT+2))
       K2=-K2
       WRITE(*,*)'OBSERVED RATE CONSTANT AND 95% CONFIDENCE
LIMITS ARE '
       WRITE(*,*)K2,ERRK2
       GOTO 10
 1300  WRITE(*,*)' ENTER OBSERVED RATE CONSTANT '
       READ(*,*)K
       WRITE(*,*)' ENTER 95% CONF. LIMIT OF K '
       READ(*,*)ERRK
       GOTO 10
 1400  WRITE(*,*)' ENTER K2 '
       READ(*,*)K2
       WRITE(*,*)' ENTER 95% CONF. LIMIT IN K2 '
       READ(*,*)ERRK2
       GOTO 598
 700   STOP
       END
       SUBROUTINE LLSQ(T,D,ERRD,NPOINT,SLOPE,ERRS,FLAG,YINT)
C THIS SUBROUTINE CALCULATES THE SLOPE AND ITS 95%
CONFIDENCE LIMITS.
C EITHER ESTIMATED OR "T TEST" GENERATED ERR Y IS USED.
       DIMENSION D(100),T(100),ERRD(100)
       INTEGER FLAG
       CHARACTER*1 YESNO
       DIMENSION CT(31)
       DOUBLE PRECISION
SUMX,SUMY,SUMXY,SUMYS,SUMXS,BOTTOM,SIGMAY,SUMRS
       DATA
CT(1),CT(2),CT(3),CT(4),CT(5)/12.706,4.303,3.182,2.776,
       &2.571/
       DATA
CT(6),CT(7),CT(8),CT(9),CT(10)/2.447,2.365,2.306,2.262,
      &2.228/
       DATA
CT(11),CT(12),CT(13),CT(14),CT(15)/2.201,2.179,2.160,2.145,
      &2.131/
       DATA
CT(16),CT(17),CT(18),CT(19),CT(20)/2.120,2.110,2.101,2.093,
      &2.086/
       DATA
CT(21),CT(22),CT(23),CT(24),CT(25)/2.080,2.074,2.069,2.064,
      &2.060/
       DATA
CT(26),CT(27),CT(28),CT(29),CT(30)/2.056,2.052,2.048,2.045,
      &2.042/
       IF(FLAG.EQ.2)GOTO 600
```

```
      IF(FLAG.EQ.3)GOTO 100
      WRITE(*,*)' 0=ZERO INTERCEPT      1=NON-ZERO INTERCEPT
'
      READ(*,*)N
      IF(N.EQ.0)GOTO 100
C  ************NON ZERO INTERCEPT LEAST SQUARES**********
 600  SUMX=0
      SUMY=0
      SUMXY=0
      SUMXS=0
      SUMYS=0
      SUMRS=0
      DO 870 I=1,NPOINT
            SUMX=SUMX+T(I)
            SUMY=SUMY+D(I)
            SUMXS=SUMXS+T(I)*T(I)
            SUMYS=SUMYS+D(I)*D(I)
            SUMXY=SUMXY+D(I)*T(I)
 870  CONTINUE
      BOTTOM=FLOAT(NPOINT)*SUMXS-SUMX*SUMX
      SLOPE=(FLOAT(NPOINT)*SUMXY-SUMX*SUMY)/BOTTOM
      YINT=(SUMY*SUMXS-SUMXY*SUMX)/BOTTOM
      DO 900 I=1,NPOINT

SUMRS=SUMRS+((SLOPE*T(I)+YINT)-D(I))*((SLOPE*T(I)+YINT)
      -D(I))
 900  CONTINUE
      WRITE(*,*) 'DO YOU WISH TO USE THE ESTIMATED ERRY?
YES=1 '
      READ(*,*)NANS
      IF(NANS.EQ.1) GOTO 910
      SIGMAY=SUMRS/(NPOINT-2)
      SIGMAY=SQRT(SIGMAY)
      ERRY=CT(NPOINT-2)*SIGMAY/SQRT(FLOAT(NPOINT))
      ERRS=ERRY*(SQRT(NPOINT/BOTTOM))
      RETURN
 910  EDMAX=ERRD(1)
      DO 930 I=2,NPOINT
 930  EDMAX=MAX(ERRD(I),EDMAX)
      ERRY=EDMAX
      ERRS=ERRY*SQRT(FLOAT(NPOINT)/BOTTOM)
      RETURN
 100  WRITE(*,*)' ****ZERO INTERCEPT LEAST SQUARES**** '
      SUMXY=0
      YINT=0.0
      SUMXS=0
      SUMRS=0
      DO 200 I=1,NPOINT
      SUMXY=SUMXY+D(I)*T(I)
      SUMXS=SUMXS+T(I)*T(I)
      SLOPE=SUMXY/SUMXS
      SUMRS=SUMRS+(SLOPE*T(I)-D(I))*(SLOPE*T(I)-D(I))
```

```
 200  CONTINUE
      WRITE(*,*)' DO YOU WISH TO USE ESTIMATED ERRY? YES=1 '
      READ(*,*)NANS
      IF (NANS.EQ.1) GOTO 300
      SIGMAY=SUMRS/FLOAT(NPOINT-1)
      SIGMAY=SQRT(SIGMAY)
      ERRY=CT(NPOINT-1)*SIGMAY/SQRT(FLOAT(NPOINT))
      WRITE(*,*)'ERRY IS '
      WRITE(*,*)ERRY
      ERRS=ERRY/SQRT(SUMXS)
      RETURN
 300  WRITE(*,*)'  DETERMINING THE BARATRON FACTOR? YES=1 '
      READ(*,*)NANS
      IF (NANS.EQ.1) GOTO 500
      EDMAX=ERRD(1)
      DO 400 I=2,NPOINT
 400  EDMAX=MAX(ERRD(I),EDMAX)
      ERRY=EDMAX
      ERRS=ERRY/SQRT(SUMXS)
      RETURN
 500  WRITE(*,*)'DEFAULT ERROR IN BARATRON IS 2E-6.
CHANGE=Y'
 88   FORMAT(A)
      READ(*,88)YESNO
      IF(YESNO.EQ.'Y')THEN
           WRITE(*,*)' INPUT THE DESIRED MULTIPLIER OF ERROR
IN CIN '
           READ(*,*)ERRY
           GOTO 515
      ENDIF
      ERRY=2E-6
C DEFAULT ERROR IN BARATRON READING IS ESTIMATED AS 2E-6
TORR
 515  ERRS=ERRY/SQRT(SUMXS)
      RETURN
      END
      SUBROUTINE CNIC(NTIM,TEMP,ETEMP,XMAX,EXMAX)
C THIS SUBROUTINE MAKES BASELINE CORRECTION AND FINDS ERROR
BARS OF Y VALUES FOR BOTH ZERO AND NONZERO INTERCEPT LLSQ
CALC.
      DIMENSION  TEMP(100),ETEMP(100)
      CHARACTER*1 YESNO
      WRITE(*,*)'DEFAULT ERROR MULTIPLIER IN CIN IS 0.1
CHANGE=Y'
      READ(*,88)YESNO
      IF(YESNO.EQ.'Y')THEN
           WRITE(*,*)' INPUT THE DESIRED MULTIPLIER OF ERROR
IN CIN '
           READ(*,*)ECIN
           GOTO 915
      ENDIF
      ECIN=0.1
```

```
 915  DO 500 I=1,NTIM
 500  ETEMP(I)=ECIN*TEMP(I)
      XMIN=TEMP(1)
      DO 600 I=2,NTIM
 600  XMIN=MIN(TEMP(I),XMIN)
      EXMIN=ECIN*XMIN
      XMAX=TEMP(1)
      DO 625 I=2,NTIM
 625  XMAX=MAX(TEMP(I),XMAX)
      EXMAX=ECIN*XMAX
      DO 700 I=1,NTIM
 700  TEMP(I)=TEMP(I)-XMIN
      DO 750 I=1,NTIM
      ETEMP(I)=SQRT(ETEMP(I)*ETEMP(I)+EXMIN*EXMIN)
      WRITE(*,*)I
      WRITE(*,*)TEMP(I),ETEMP(I)
 750  CONTINUE
      WRITE(*,*)'LLSQ CALC:  NON-ZERO INTERCEPT=1   ZERO=0'
      READ(*,*)NANS
      IF(NANS.EQ.1) GOTO 950
      XMAX=XMAX-XMIN
      EXMAX=SQRT(EXMAX*EXMAX+EXMIN*EXMIN)
      DO 900 I=1,(NTIM-1)
900
ETEMP(I)=SQRT(ETEMP(I)*ETEMP(I)/(TEMP(I)*TEMP(I))+EXMAX*
         &EXMAX/(XMAX*XMAX))*TEMP(I)
      DO 910 I=1,(NTIM-1)
 910  TEMP(I)=TEMP(I)/XMAX
 950  DO 960 I=1,(NTIM-1)
 960  ETEMP(I)=ETEMP(I)/TEMP(I)
      DO 970 I=1,(NTIM-1)
 970  TEMP(I)=LOG(TEMP(I))
 88   FORMAT(A)
      RETURN
      END

      SUBROUTINE GRAF2D(XR,YR,NDP)
C General plotting routine for cga adaptor.
C Must be linked with GRAF.OBJ which contains the assembly
language
C subroutines WRITDOT, and SETDIS.
C Written by Cliff Watson 9-17-1987.
      DIMENSION XR(1024),YR(1024)
      CHARACTER YESNO*1
      COMMON /SCALE/ XMIN,XMAX,XS,YMIN,YMAX,YS
      YMAX = YR(1)
      YMIN = YR(1)
      XMIN = XR(1)
      XMAX = XR(1)
C                                                    FIND XAW
AND MIN VALUES
      DO 10 I = 1,NDP
```

```
      IF (XR(I) .GT. XMAX) XMAX = XR(I)
      IF (XR(I) .LT. XMIN) XMIN = XR(I)
      IF (YR(I) .LT. YMIN) YMIN = YR(I)
      IF (YR(I) .GT. YMAX) YMAX = YR(I)
 10   CONTINUE
      WRITE(*,*)XMAX,XMIN,YMAX,YMIN
      PAUSE
C
    SET SCALE
      XS = 639 / (XMAX - XMIN)
      YS = 199 / (YMAX - YMIN)
C     ENTER GRAPHICS MODE
C                                        SET DISPLAY TO HIGH
RESOLUTION GRAPHICS
      CALL SETDIS(6)
      CALL BOX(0,0,639,199)
C
    PLOT DATA
      DO 20 I = 1,NDP
         IX = (XR(I) - XMIN) * XS
         IY = (YR(I) - YMIN) * YS
         CALL PSET(IX,IY,1,IERR)
         CALL BOX(IX-5,IY-5,IX+5,IY+5)
 20   CONTINUE
C                                                          PAUSE
TO DISPLAY PLOT
      READ(*,'(A)') YESNO
C                                                            SET
DISPLAY TO TEXT
      CALL SETDIS(2)
      RETURN
      END
CCCCCCCCCCCCCCCCCCCCCCCCCCCCCCCCCCCCCCCCCCCCCCCCCCCCCCCCCCCCCCCCCCC

       SUBROUTINE PSET(IX,IY,ICOLOR,IERR)

C Subroutine to set pixel on high resolution graphics
screen.
C x = 0,639;  y = 0,199
      IERR = 0

      IF((IX.LT.0).OR.(IX.GT.639)) IERR = 1

      IF((IY.LT.0).OR.(IY.GT.199)) IERR = 1

      IF ((ICOLOR.LT.-1).OR.(ICOLOR.GT.1)) IERR = 1

      IF(IERR.EQ.1) GO TO 100

      INVY = 199 - IY
```

```
      CALL WRIDOT(IX,INVY,ICOLOR)
 100  CONTINUE
      RETURN
      END
CCCCCCCCCCCCCCCCCCCCCCCCCCCCCCCCCCCCCCCCCCCCCCCCCCCCCCCCCCCCCCCCCCCC
      SUBROUTINE LRL(IXMIN,IXMAX,IY,IERR)
C Subroutine to draw horizontal line
      DO 100 I = IXMIN,IXMAX
        CALL PSET(I,IY,1,IERR)
 100  CONTINUE
      RETURN
      END
CCCCCCCCCCCCCCCCCCCCCCCCCCCCCCCCCCCCCCCCCCCCCCCCCCCCCCCCCCCCCCCCCCCC
      SUBROUTINE LUD(IYBOT,IYTOP,IX,IERR)
C Subroutine to draw vertical line
      DO 100 I = IYBOT,IYTOP
        CALL PSET(IX,I,1,IERR)
 100  CONTINUE
      RETURN
      END
CCCCCCCCCCCCCCCCCCCCCCCCCCCCCCCCCCCCCCCCCCCCCCCCCCCCCCCCCCCCCCCCCCCC
      SUBROUTINE BOX(IXMIN,IYMIN,IXMAX,IYMAX)
C Subroutine to draw box
C Draw top of box
      CALL LRL(IXMIN,IXMAX,IYMAX,IERR)
C Draw bottom
```

```
      CALL LRL(IXMIN,IXMAX,IYMIN,IERR)
C Draw left side
      CALL LUD(IYMIN,IYMAX,IXMIN,IERR)
C Draw right side
      CALL LUD(IYMIN,IYMAX,IXMAX,IERR)
      RETURN
      END
```

APPENDIX II

ANALYTICAL EXPRESSIONS FOR KINETIC MODELING IN CHAPTER 5

A. Kinetic Differential Rate Equations for the Scheme Shown in Figure 5.3.

$$I_{C_3H_3^+} = I^o_{C_3H_3^+} + I^o_{\ell\text{-}C_3H_3^+}\left[1 + \beta\phi/(10\theta_1)\right]\left[\exp(\theta_1 t) - 1\right]$$

$$I_{C_3H_2D^+} = 3I^o_{\ell\text{-}C_3H_3^+}\left[\exp(\theta_2 t) - \exp(\theta_1 t)\right] - \frac{3}{10}\beta\phi I^o_{\ell\text{-}C_3H_3^+}\{[\exp(\theta_1 t) - 1]/\theta_1 - 3[\exp(\theta_2 t) - 1]/\theta_2\}$$

$$I_{C_3HD_2^+} = 3I^o_{\ell\text{-}C_3H_3^+}[\exp(\theta_1 t) - 2\exp(\theta_2 t) + \exp(\theta_3 t)] + \frac{3}{10}\beta\phi I^o_{\ell\text{-}C_3H_3^+}\{[\exp(\theta_1 t) - 1]/\theta_1 - 6[\exp(\theta_2 t) - 1]/\theta_2 + 6[\exp(\theta_3 t) - 1]/\theta_3\}$$

$$I_{C_3D_3^+} = I^o_{\ell\text{-}C_3H_3^+}[3\exp(\theta_2 t) + \exp(\theta_4 t) - \exp(\theta_1 t) - 3\exp(\theta_3 t)] - \beta\phi I^o_{\ell\text{-}C_3H_3^+}\{[\exp(\theta_1 t) - 1]/(10\theta_1) - 9[\exp(\theta_2 t) - 1]/(10\theta_2) + 9[\exp(\theta_2 t) - 1]/(5\theta_3) - [\exp(\theta_4 t) - 1]/\theta_4\},$$

in which $\beta = k_c/k_\ell$, $\phi = k_\ell k_f P_{C_2D_2}/(k_\ell + k_c)$, $\theta_1 = k_\ell\phi/10 - k_f P_{C_2D_2} - k_p P_{C_3H_3I}$, $\theta_2 = 3k_\ell\phi/10 - k_f P_{C_2D_2} - k_p P_{C_3H_3I}$, $\theta_3 = 3k_\ell\phi/5 - k_f P_{C_2D_2} - k_p P_{C_3H_3I}$, and $\theta_4 = k_\ell\phi - k_f P_{C_2D_2} - k_p P_{C_3H_3I}$. The fitting parameters for this model are $I^\circ_{\ell\text{-}C_3H_3^+}$, β, $k_f P_{C_2D_2}$, and $k_p P_{C_3H_3I}$. $I^\circ_{C_3H_3^+}$ is fixed at its experimental value if the initial point is at t=0; otherwise it is also a fitting parameter.

B. Kinetic Differential Rate Equations for the Scheme Shown in Figure 5.7.

$$dI_{\ell\text{-}C_3H_3^+}/dt = \theta I_{\ell\text{-}C_3H_3^+}$$

$$dI_{c\text{-}C_3H_3^+}/dt = \beta I_{\ell\text{-}C_3H_3^+}/(10F^2)$$

$$dI_{\ell\text{-}HDC_3H^+}/dt = -(F^2k_f' + k_p')\, I_{\ell\text{-}HDC_3H^+} + \phi_2(I_{\ell\text{-}HDC_3H^+} + FI_{\ell\text{-}H_2C_3D^+})/(5F^2) + 2\phi_1 I_{\ell\text{-}C_3H_3^+}/(5F)$$

$$dI_{\ell\text{-}H_2C_3D^+}/dt = -F(F^2k_f' + k_p')\, I_{\ell\text{-}H_2C_3D^+} + \phi_2 (I_{\ell\text{-}HDC_3H^+} + FI_{\ell\text{-}H_2C_3D^+})/(10F^3) + \phi_1 I_{\ell\text{-}C_3H_3^+}/(5F^2)$$

$$dI_{c\text{-}C_3H_2D^+}/dt = 3\beta[\phi_2(I_{\ell\text{-}HDC_3H^+} + FI_{\ell\text{-}H_2C_3D^+})/(2F) + \phi_1 I_{\ell\text{-}C_3H_3^+}]/(5F)$$

$$dI_{\ell\text{-}HDC_3D^+}/dt = -F(F^2k_f' + k_p')I_{\ell\text{-}HDC_3D^+} + 2\phi_3(FI_{\ell\text{-}HDC_3D^+} +$$

$$I_{\ell\text{-}D_2C_3H^+})/(5F^3) + 2\phi_2(I_{\ell\text{-}HDC_3H^+} +$$

$$FI_{\ell\text{-}H_2C_3D^+})/(5F^2) + \phi_1 I_{\ell\text{-}C_3H_3^+}/(5F)$$

$$dI_{\ell\text{-}D_2C_3H^+}/dt = -(F^2k_f' + k_p')I_{\ell\text{-}D_2C_3H^+} + \phi_3(FI_{\ell\text{-}HDC_3D^+} +$$

$$I_{\ell\text{-}D_2C_3H^+})/(5F^2) + \phi_2(I_{\ell\text{-}HDC_3H^+} +$$

$$FI_{\ell\text{-}H_2C_3D^+})/(5F) + \phi_1 I_{\ell\text{-}C_3H_3^+}/10$$

$$dI_{c\text{-}C_3HD_2^+}/dt = 3\beta[\phi_3(FI_{\ell\text{-}HDC_3D^+} + I_{\ell\text{-}D_2C_3H^+})/F^2 + \phi_2(I_{\ell\text{-}HDC_3H^+}$$

$$+ FI_{\ell\text{-}H_2C_3D^+})/F + \phi_1 I_{\ell\text{-}C_3H_3^+}/2]/5$$

$$dI_{\ell\text{-}C_3D_2^+}/dt = [\phi_4/F^2 - F(F^2k_f' + k_p')]I_{\ell\text{-}C_3D_3^+} + 2\phi_3(FI_{\ell\text{-}HDC_3D^+}$$

$$+ I_{\ell\text{-}D_2C_3H^+})/(5F^2) + \phi_2(I_{\ell\text{-}HDC_3H^+} + FI_{\ell\text{-}H_2C_3D^+})/(10F)$$

$$dI_{c\text{-}C_3D_3^+}/dt = \beta[\phi_4 I_{\ell\text{-}C_3D_3^+}/F^2 + 2\phi_3(FI_{\ell\text{-}HDC_3D^+} +$$

$$I_{\ell\text{-}D_2C_3H^+})/(5F) + \phi_2(I_{\ell\text{-}HDC_3H^+} + FI_{\ell\text{-}H_2C_3D^+})/10,$$

in which $\theta = \phi_1/(10F^2) - F^2k_f' - k_p'$, $k_f' = k_f P_{C_2D_2}$, $k_p' = k_p P_{C_3H_3I}$, $\phi_1 = F^2k_f'/(\lambda_1 + \beta\lambda_2)$, $\phi_2 = F^2k_f'/(\lambda_3 + \beta\lambda_1)$, $\phi_3 = F^2k_f'/(\lambda_4 + \beta\lambda_5)$, $\phi_4 = F^6k_f'/(1 + F\beta)$, and the λ's are given as:

$$\lambda_1 = (1 + 6/F + 3/F^2)/10$$

$$\lambda_2 = (3 + 6/F + 1/F^2)/10$$

$$\lambda_3 = \lambda_2/F$$

$$\lambda_4 = (3 + 2/F)/5F^2)$$

$$\lambda_5 = (2 + 3/F)/(5F).$$

The fitting parameters for this model are $I^o_{\ell\text{-}C_3H_3^+}$, β, k_f', k_p', and F. $I^o_{C_3H_3^+}$ is fixed if the initial point is at t=0; otherwise it is also a fitting parameter.

C. Kinetic Differential Rate Equations for the Scheme Shown in Figure 5.10.

$$I_{C_3H_3^+} = I^o_{C_3H_3^+} + I^o_{\ell\text{-}C_3H_3^+}[1 + k_{-31}\phi_1/\theta_1][\exp(\theta_1 t) - 1]$$

$$I_{C_5H_3^+} = k_{-11}\phi_1 I^o_{\ell\text{-}C_3H_3^+}[\exp(\theta_1 t) - \exp(\theta_2 t)]/\theta_{12}$$

$$I_{C_7H_3^+} = k_{-11}k_{-21}\phi_1\phi_2 I^{\circ}_{\ell\text{-}C_3H_3^+}[\exp(\theta_1 t)/\theta_{13} - \exp(\theta_2 t)/\theta_{23} + (1/\theta_{23} - 1/\theta_{13})\exp(\theta_3 t)]/\theta_{12}$$

$$I_{C_9H_5^+(s)} = k_{-11}k_{s1}\phi_1\phi_2 I^{\circ}_{\ell\text{-}C_3H_3^+}\{[\exp(\theta_1 t) - 1]/\theta_1 - [\exp(\theta_2 t) - 1]/\theta_2\}/\theta_{12}$$

$$I_{C_{11}H_5^+(s)} = k_{-11}k_{-21}k_{s2}\phi_1\phi_2\phi_3 I^{\circ}_{\ell\text{-}C_3H_3^+}\{[\exp(\theta_1 t) - 1]/(\theta_1\theta_{13}) - [\exp(\theta_2 t) - 1]/(\theta_2\theta_{23}) - (1/\theta_{23} - 1/\theta_{13})[\exp(\theta_3 t) - 1]/\theta_3\}/\theta_{12},$$

$$I_{C_8H_6^+} = k_{-11}k'_{p2}\theta_1 I^{\circ}_{\ell\text{-}C_3H_3^+}[\exp(\theta_1 t)/\theta'_1 - \exp(\theta_2 t)/\theta'_2 + (1/\theta'_2 - 1/\theta'_1)\exp(-k_2 t)]/\theta_{12},$$

in which $\phi_1 = k_{f1}P_{C_4H_2}/(k_{-11} + k_{-12} + k_{-13})$, $\phi_2 = k_{f2}P_{C_4H_2}/(k_{-21} + k_{-22} + k_{s1})$, $\phi_3 = k_{f3}P_{C_4H_2}/(k_{-31} + k_{-32} + k_{s2})$; $-\theta_1$, $-\theta_2$, and $-\theta_3$ are parameters (1), (2), and (3), in that order, in equations (a), $\theta_{12} = \theta_1 - \theta_2$, $\theta_{13} = \theta_1 - \theta_3$, $\theta_{23} = \theta_2 - \theta_3$, $\theta_1 = \theta_1 + k_d$, and $\theta_2' = \theta_2 + k_d$. The fitting parameters are θ_1, θ_2, θ_3, $I^{\circ}_{\ell\text{-}C_3H_3^+}(1 + k_{-31}\phi_1/\theta_1)$, $k_{-11}\phi_1 I^{\circ}_{\ell\text{-}C_3H_3^+}/\theta_{12}$, $k_{s2}\phi_3$, $k_{-21}\phi_2$, $k_{s1}\phi_2$, and k_d. It can be seen that $k'_{p2} = -\theta_1 - k_{-21}\phi_2 - k_{s1}\phi_2$, in which $k'_{p2} = k_{p2}P_{C_3H_3I}$.

BIBLIOGRAPHY

Abbaund, J. L. M.; Hehre, W. J.; Taft, R. W. J. Am. Chem. Soc., 1976, 98, 6072-3.

Andrews, L.; Keelan, B. W. J. Am. Chem. Soc., 1981, 103, 99.

Anicich, V. G.; Huntress, Jr. W. T.; McEvan, M. J. J. Phys. Chem., 1986, 90, 2446.

Annino, R.; Driver, R. "Scientific and Engineering Applications with Personal Computers," John Wiley and Sons, Inc.: New York, 1986.

Ausloos, P. J. Am. Chem. Soc., 1982, 104, 5259.

Ausloos, P.; Jackson, J-A. A.; Lias, S. G. Int. J. Mass Spectrom. Ion Phys., 1980, 33, 269-83.

Ausloos, P. J.; Lias, S. G. J. Am. Chem. Soc. 1981, 103, 6505.

Baer, T.; Willett, G. D.; Smith, D.; Phillips, J. S. J. Chem. Physics, 1979, 62, 2186.

Barker, R. A.; Ridge, D. P. J. Chem. Phys. 1976, 64, 4411.

Bartmess, J.E., J. Am. Chem. Soc., 1982, 104, 335.

Baykut, G.; Eyler, J. R. Trends Anal. Chem. 1986, 5, 44.

Baykut, G.; Brill, F. W.; Eyler, J. R. Combust. Sci. Technol. 1986, 45, 233.

Bittner, J. D.; Howard, J. B. in "Particulate Carbon Formation during Combustion," Siegla, D.C.; Smith, G.W., Eds.; Plenum: New York, 1981a, 109.

Bittner, J. D.; Howard, J. B. Symp. (Int.) Combust. [Proc.], 18th 1981b, 1105.

Bombach, R.; Dannacher, J.; Stadelmann, JP. J. Am. Chem. Soc., 1983, 105, 4205-11.

Bombach, R.; Dannacher, J.; Stadelmann, JP. Chem. Phys. Lett., 1983, 95, 259-61.

Bonne, U.; Homann, K. H.; Wagner, H. Gg. Symp. (Int.) Combust. [Proc.], 10th 1965, 503.

Borden, M. J.; Haddon, R. C. J. Am. Chem. Soc., 1979, 101, 3771.

Bowers, M. T.; Laudenslager, J. B. J. Chem. Phys. 1972, 56, 4711.

Brill, F. W., Ph.D. Dissertation, Univ. of Florida, 1983.

Brill, F. W.; Eyler, J. R. J. Phys. Chem., 1981, 85, 1091.

Buckley, T. J., Ph.D. Dissertation, Univ. of Florida, 1982.

Bursey, J.T.; Bursey, M.M.; Kingston, D.G.I., Chem. Rev., 1973, 73, 191.

Bursey, M.M.; Hoffman,M.K.; Benezra, S.A., J. Chem. Soc. D, 1971, 1417.

Cabannes, F. J. Phys. Radium 1956, 17, 492-496.

Calcote, H. F. Symp. (Int.) Combust. [Proc.], 8th 1962, 184.

Calcote, H. F. Symp. (Int.) Combust. [Proc.], 9th 1963, 622.

Calcote, H. F. in "Ion-Molecule Reactions," J. L. Franklin, Ed.; Plenum: New York, 1972, 2, 673.

Calcote, H. F. Combust. and Flame 1981, 42, 215.

Chesnavich, W. J.; Bowers, M. T. J. Am. Chem. Soc. 1976, 97, 892.

Chesnavich, W. J.; Bowers, M. T. J. Am. Chem. Soc. 1977, 99, 1705.

Comisarow, M. B. Analyt. Chim. Acta 1985, 178, 1.

Comisarow, M. B.; Grassi, V.; Parisod, G. Chem. Phys. Let., 1978, 57, 413.

Comisarow, M. B.; Marshall, A. G. Chem. Phys. Lett. 1974a, 25, 282-283.

Comisarow, M. B.; Marshall, A. G. Chem. Phys. Lett. 1974b, 26, 489-490.

Comisarow, M. B.; Marshall, A. G. Can. J. Chem. 1974c, 52, 1997-1999.

Comisarow, M. B.; Marshall, A. G. J. Chem. Phys. 1975, 62, 293-295.

Cone, C.; Dewar, M. J. S.; Landman, D. J. Am. Chem. Soc., 1977, 99, 372-6.

Cooks, R. G.; Beynon, J. H.; Bertrand, M.; Hoffman, M. K. Org. Mass Spectrom., 1973, 7, 1303-12.

Cooley, J. W.; Tukey, J. W. Math Comp. 1975, 19, 9.

Cullis, C. F. in "Petroleum Derived Carbons," M. L. Deviney; T. M. O'Grady, Eds.; Amer. Chem. Soc., Symp. Ser. Washington, DC. 1976, 21, 348.

D'Alessio, A.; Di-Lorenzo, A.; Borghese, A.; Beretta, F.; Massi, S. Symp. (Int.) Combust. [Proc], 16th 1977, 695.

Dannacher, J.; Heilbronner, E.; Stadelmann, J.-P.; Vogt, J. Helvetica Chimica Acta, 1979, 62, 2186.

Davidson, R. A.; Skell, P. S. J. Am. Chem. Soc., 1973, 95, 6843.

Derrick, P. J. Mass Spec. Rev., 1983, 2, 285.

Dewar, M. J.; Haddon, R. C. J. Am. Chem. Soc., 1973, 95, 5836.

Dewar, M. J. S.; Landman, D. J. Am. Chem. Soc., 1977, 99, 2446-53.

DiLorenzo, A.; D'Alessio, A.; Cincotti, V.; Massi, S.; Menna, P.; Venitozzi, C. Symp. (Int.) Combust. [Proc.], 18th 1981, 485.

Dorman, F. H. J. Chem. Phys., 1965, 43, 3507.

Dreuth, W.; Kwart, H. "Kinetics Applied to Organic Reactions", Marcel Dekker, Inc., 1980.

Dugan, J. W.; Magee, J. L. NASA Tech. Note, NASA TN-D-3229, 1966.

Dugan, J. W.; Magee, J. L. J. Chem. Phys. 1967, 47, 3103.

Dunbar, R. C.; Fu, E. W. J. Am. Chem Soc., 1973, 95, 2716.

Dunbar, R. C.; J. Am. Chem. Soc., 1975, 97, 1382-4.

Dunbar, R.C.; Klein, R., J. Am. Chem. Soc., 1977, 99, 3744.

Elder, F.A.; Parr, A.C., J. Chem. Phys., 1969, 50, 1027.

Evans, M. C.; Polanyi, M. Trans. Faraday Soc., 1935, 31, 875.

Eyler, J. R. in "Chemistry of Combustion Processes," American Chemical Symposium Series, Sloane, T. M. Ed.: Washington, D.C., 1984, 49-67.

Eyring, H. J. Chem. Phys., 1935, 3, 107.

Forst, W. "Theory of Unimolecular Reactions," Academic Press: New York.

Frenklach, M.; Clary, D. W.; Gardiner, W. C., Jr.; Stein, S. E. in "Twentieth Symposium (Int.) on Combustion," The Combustion Institute: Pittsburgh, 1985, p.87.

Futrell, J. H.; Tiernan, T. O. in "Fundamental Process in Radiation Chemistry," (P. Ausloos, ed.) Wiley (Interscience): New York, 1968, p. 171.

Gajewski, J.J.; Gortva, A. M.; J. Am. Chem. Soc., 1982, 104, 334.

Gaydon, A. G.; Wolfhard, H. G. "Flames," Third Edition, Chapman and Hall, London 1970.

Gioumousis, G.; Stevenson, D. P. J. Chem. Phys. 1958, 29, 294.

Glassman, I. Technical Meeting, Eastern Section of the Combust. Inst.: Princeton Univ. Princeton, NJ. 1980.

Goodings,J. M.; Bohme, D. K.; Ng, C-W. Combust. Flame 1979, 36, 27.

Graham, S. C.; Homer, J. B.; Rosenfeld, J. L. J. Proc. Roy. Soc. London, 1975, A344, 259-285.

Griffiths, P. L. in "Transform Techniques in Chemistry," Plenum Press: New York, 1978.

Gross, M. L.; Norbeck, J. J. Chem. Phys. 1971, 54, 3651.

Gross, M. L.; Rempel, D. L. Science 1984, 226, 261.

Grotemeyer, J.; Grueitzmacher, H. F. Curr. Top. Mass Spectrom. Chem. Kinet., Proc. Symp., 1981, Beynon, J. H.; McGlashan, M. L., Eds.; Heyden: London, UK, 1982, pp.29-59.

Harrison, A. G.; Haynes, P.; McLean, S.; Meyer, F. J. Am. Chem. Soc., 1965, 87, 5099.

Hehre, W. J.; Schleyer, P. v. R. J. Am. Chem. Soc., 1973, 95, 5837.

Henglein, A. in "Molecular Beams and Reaction Kinetics," (C. Schlier, ed.), Academic Press: New York, 1970.

Herod, A. A.; Harrison, A. G. Int. J. Mass. Spectrom. Ion Phys., 1970, 4, 415.

Holmes, J. L.; Lossing, F. P. Can. J. Chem., 1978, 57, 249.

Homann, K. H. Combust. Flame, 1967, 11, 265-287.

Homann, K. H.; Wagner, H. Gg. Symp. (Int.) Combust. [Proc], 11th 1967, 371.

Homann, K. H.; Wagner, H. G. Proc. Roy. Soc. London, 1968, A307, 141.

Jackson, J-A. A. Diss. Abstr. Int. B , 1977, 38, 2691.

Jackson, J-A. A.; Lias, S. G.; Ausloos, P. J. Am. Chem. Soc., 1977, 99, 7515-21.

Jarrold, M. F.; Wagner-Redeker, W.; Illies, A. J.; Kirchner, N. J.; Bowers, M. T. Int. J. Mass Spectrom. Ion Phys., 1984, 58, 63.

Jensen, D. E. Proc. Roy. Soc. London, 1974, A338, 375-396.

Johlman, C. L.; White, R. L.; Wilkins, C. L. Mass Spectrom. Rev., 1983, 2, 389.

Keck, J. C. J. Chem. Phys. 1958, 29, 410.

Kent, J. H.; Jander, H.; Wagner, H. Gg. Symp. (Int.) Combust. [Proc.], 18th, 1981, 1117.

Koeppel, C.; Dymerski, P. P.; Bockhoff, F. M.; McLafferty, F. W. Adv. Mass Spectrom., 1978, 7A, 295-6.

Kollmar, H.; Smith, H. O.; Schleyer, P. v. R. J. Am. Chem. Soc., 1973, 95, 5834.

Knewstubb, P. F.; Sugden, T. M. Symp. (Int.) Combust. [Proc.], 7th 1959, p.247.

Knight, J.S.; Freeman, C.G.; McEwan, M.J.; Anicich, V.G.; Huntress, W.T.,Jr., J. Phys. Chem., 1987, 91, 3898.

Lahaye, J.; Prado, G. in "Chemistry and Physics of Carbon," P. L. Walker, Jr., Eds.; Marcel Dekker: New York 1978, 14, 167.

Lampe, F. W.; Field, F. H. Tetrahedron, 1959, 7, 189.

Langevin, P. M. Ann. Chim. Phys. 1905, 5, 245.

Laude, Jr., D. A.; Johlman, C. L.; Brown, R. S.; Weil, D. A.; Wilkins, C. L. Mass Spectrom. Rev. 1986, 5, 107.

Lawrence, E. O.; Livingston, M. S. Phys. Rev. 1932, 40, 19.

Le Breton, P. R.; Williamson, A. D.; Beauchamp, J. L.; Huntress, W. T. J. Chem. Phys. 1975, 62, 1623.

Leusen,K.; McLafferty, F.W.; Serina, D.M., J. Am. Chem. Soc., 1973, 95, 6332.

Light, J. C. Discuss. Faraday Soc. 1967, 44, 14.

Lossing, F. P. Can. J. Chem. 1972, 50, 3973.

Lossing, F. P.; Traeger, J. C. J. Am. Chem. Soc., 1975, 97, 1579.

March, J. "Advanced Organic Chemistry, Reactions, Mechanisms and Structure," 1977, 2nd Ed.; Plenum: New York, 177.

Marcus, R. A.; Rice, O. K. J. Phys. Colloid Chem. 1951, 55, 894.

Marshall, A. G. (Ed.), in "Fourier, Hadamard and Hilbert Transforms in Chemistry," Plenum Press: New York, 1982.

Marshall, A. G. Accounts of Chemical Research, 1985, 18, 316.

McCreary, D. A.; Freiser, B. S. J. Am. Chem. Soc., 1978, 100, 2902.

McDaniel, E. W. "Collision Phenomena in Ionized Gases," Wiley: New York, 1964.

McLafferty, F. W.; Bockhoff, F. M. J. Am. Chem. Soc., 1979, 101, 1783-6.

McLafferty, F. W.; Winkler, J. J. Am. Chem. Soc., 1974, 96, 5182-9.

McLoughlin, R. G.; Morrison, J. D.; Traeger, J. C. Org. Mass Spectrom., 1979, 14, 104-8.

Mead, P. T.; Douchi, K. F.; Traeger, J. C.; Christie, J. R.; Derrick, P. J. J. am. Chem. Soc., 1980, 102, 3364.

Melander, L. "Isotope Effects on Reaction Rates," Ronald Press: New York, 1960.

Melander, L.; Saunders, W. H., Jr. "Reaction Rates of Isotopic Molecules," John Wiley and Sons: New York, 1980.

Michaud, P.; Delfau, J. L.; Barrasin, A. Symp. (Int.) Combust. [Proc.], 18th 1981, 443.

Miller, W. H. J. Chem. Phys. 1974, 61, 1823.

Miller, W. H. J. Chem. Phys. 1976, 65, 2216.

Moran, T. F.; Hamill, W. H. J. Chem. Phys. 1963, 39, 1413.

Occolowitz, J. L.; White, G. L. Aust. J. Chem., 1968, 21, 997.

Olson, D. B.; Calcote, H. F. In "Particulate carbon Formation during Combustion," Siegla, D. C.; Smith, G. W. Eds.; Plenum: New York, 1981a, 177.

Olson, D. B.; Calcote, H. F. Symp. (Int.), Combust. [Proc.], 18th 1981b, 453.

Olson, D. B.; Keil, D. G.; Calcote, H. F. Report of a Workshop on the Mechanism of Soot Formation, June 14-15, 1984, sponsored by U.S. Army Research Office and NASA-Lewis Research Center.

Palmer, H. B.; Cullis, C. F. in "Chemistry and Physics of Carbon," P. L. Walker, Jr., Eds., Marcel Dekker: New York, 1965, 1, 265.

Pechukas, P.; McLafferty, F. J. J. Chem. Phys. 1972, 58, 1622.

Pelzer, H.; Wigner, E. Z. Phys. Chem., Abt. 1932, B 15, 445.

Pottie, R. F.; Lossing, F. P. J. Am. Chem. Soc. 1963, 85, 269.

Radom, L.; Hariharan, P. C.; Pople, J. A.; Schleyer, P. v. R. J. Am. Chem. Soc. 1976, 98, 10.

Rosenstock, H. M.; Wallenstein, M. B.; Wahrhaftig, A. L.; Eyring, H. Proc. Natl. Acad. Sci. U.S.A. 1952, 38, 667.

Sagi, N.; Yamamoto, Y.; Nagaoka, K.; Takamuku, S.; Sakurai, H. Bull. Chem. Soc. Jap., 1974, 47, 1387-92.

Sharma, D. K. S.; Kebarle, P. Can. J. Chem., 1981, 59, 1592.

Shen, J.; Dunbar, R. C.; Olah, G. A. J. Am. Chem. Soc., 1974, 96, 6227.

Sieck, W.; Ausloos, P. J. Res. Natl. Bur. Stand. U.S.A. 1972, 76, 253.

Smith, E. C. W. Proc. Roy. Soc. London 1940, A174, 110-125.

Smith, D.; Adams, N. G. Int. J. Mass Spectrom. Ion Phys., 1987, 76, 307.

Smyth, K. C.; Lias, S. G.; Ausloos, P. Combust. Sci. and Tech., 1982, 28, 147.

Smyth, K. C.; Mallard, W. G. Combust. Sci. Technol. 1981, 26, 35.

Snow, A. W. J. Macrom. Sci., 1985, A22, 1429.

Stein, S. E. J. Phys. Chem., 1978, 82, 566-571.

Stohrer, W. D.; Hoffman, R. J. Am. Chem. Soc., 1972, 94, 1661.

Streitweiser Jr.,A.; Jagov, R. H.; Fahey, R.C.; Suzuki, S. J. Am. Chem. Soc., 1958, 80, 2326.

Su, T.; Bowers, M. T. Int. J. Mass Spectrom. Ion Phys. 10, 1973, 347.

Su, T.; Bowers, M. T. Int. J. Mass Spectrom. Ion Phys. 17, 1975, 309.

Su, T.; Su, E. C. F.; Bowers, M. T. J. Chem. Phys. 1978, 69, 2243.

Takamuku, S.; Nakamura, K.; Nagaoka, K.; Sakurai, H. Chem. Lett., 1973, 12, 1303-6.

Takamuku, S.; Sagi, N.; Nagaoka, K.; Sakurai, H. J. Am. Chem. Soc., 1972, 94, 6217-18.

Thomas, A. Symp. (Int.) Combust. [Proc.], 10th 1965, 511.

Thrush, B.A.; Zwolenik, J.J., Discuss. Faraday Soc., 1963, 35, 196.

Traeger, J. C.; McLoughlin, R. G. J. Am. Chem. Soc., 1977, 99, 7351-2.

Traeger, J. C.; McLoughin, R. G. Int. J. Mass Spectrom. Ion Phys., 1978, 27, 319-33.

Tumas, W.; Foster, R. F.; Pellerite, M. J.; Brauman, J. R. J. Am. Chem. Soc., 1987, 109, 961.

Vinckier, C.; Gardner, M. P.; Bayes, K. D. Symp. (Int.) Combust. [Proc.], 16th 1977, 881.

Warneck, P. Ber. Bunsen-Ges. Phys. Chem. 1972, 76, 421.

Winkler, J.; McLafferty, F. W. J. Am. Chem. Soc., 1973, 95, 7533.

Yamamoto, Y.; Takamuku, S.; Sakurai,H. J. Am. Chem. Soc., 1969, 91, 7192-4.

Yaroslavtsev, V. T.; Abakumov, G. A.; Simonov, A. P. Kuantovaya Electron., 1984, 11, 752-6.

BIOGRAPHICAL SKETCH

Up until 1982, Feza Öztürk's educational background originated in Turkey. She received a Bachelor of Science degree in chemistry in 1976 and Master of Science degree in 1977 from Ege University in Izmir. After teaching for five years at the same university, she came to the United States and started the Ph.D program at the University of Florida in Gainesville in 1982. Three years later, she began working in Dr. John Eyler's lab in the area of gas-phase ion/molecule reactions. She completed her graduate studies during the summer of 1988.

I certify that I have read this study and that in my opinion it conforms to acceptable standards of scholarly presentation and is fully adequate, in scope and quality, as a dissertation for the degree of Doctor of Philosophy.

John R. Eyler, Chairman
Professor of Chemistry

I certify that I have read this study and that in my opinion it conforms to acceptable standards of scholarly presentation and is fully adequate, in scope and quality, as a dissertation for the degree of Doctor of Philosophy.

William Jr. Weltner
Professor of Chemistry

I certify that I have read this study and that in my opinion it conforms to acceptable standards of scholarly presentation and is fully adequate, in scope and quality, as a dissertation for the degree of Doctor of Philosophy.

Willis B. Person
Professor of Chemistry

I certify that I have read this study and that in my opinion it conforms to acceptable standards of scholarly presentation and is fully adequate, in scope and quality, as a dissertation for the degree of Doctor of Philosophy.

Merle A. Battiste
Professor of Chemistry

I certify that I have read this study and that in my opinion it conforms to acceptable standards of scholarly presentation and is fully adequate, in scope and quality, as a dissertation for the degree of Doctor of Philosophy.

Charles L. Proctor
Associate Professor of
Mechanical Engineering

This dissertation was submitted to the Graduate Faculty of the Department of Chemistry in the College of Liberal Arts and Sciences and to the Graduate School and was accepted as partial fulfillment of the requirements for the degree of Doctor of Philosophy.

August, 1988

Dean, Graduate School